P-442-0078

FINAL REPORT

HUBBLE INDEPENDENT OPTICAL REVIEW PANEL

817
701 Bruce
82

Goddard Space Flight Center
Greenbelt, MD 20771

QC
385.2
.D47
F56
1991

P-442-0078

FINAL REPORT
HUBBLE INDEPENDENT OPTICAL REVIEW PANEL

Goddard Space Flight Center
Greenbelt, MD 20771

Final Report

Hubble Independent Optical Review Panel

Duncan T. Moore, Chairman
Director, Institute of Optics, University of Rochester

George N. Lawrence
Applied Optics Research

Daniel Schulte
Lockheed Optical Systems Design Laboratory

Dietrich Korsch
Korsch Optics

Marjorie Meinel
Scientist, Jet Propulsion Laboratory

Aden Meinel
Distinguished Scientist, Jet Propulsion Laboratory

Goddard Space Flight Center
Greenbelt, MD 20771

TABLE OF CONTENTS

HST INDEPENDENT OPTICAL REVIEW PANEL

Executive Summary

The Hubble Independent Optical Review Panel was established to determine the exact parameters of the as-built Hubble Space Telescope (HST). After over one year of meetings and analysis of large amounts of data, the panel has concluded that the conic constant of the primary mirror is the principal error in the optical system. The conic, which should have had a value of -1.0023 was in fact constructed with a value of -1.0139. As the Allen Committee concluded, the principal cause of the error was the measurement of the primary using a reflective null corrector which suffered from a number of assembly errors. The Allen Committee, in their report, provided a preliminary value of the conic constant of -1.0132.

Midway through the panel deliberations, NASA required the panel to provide a preliminary value for the conic constant to meet the WFPC II schedule. The panel submitted a value of -1.0135 in December, 1990. However, this panel, upon completion of a series of very comprehensive studies, has concluded that correct value should be -1.0139.

Three independent methods for determining the value of the conic constant were used. First a re-evaluation of all of the fossil data (Appendix III), including the as-built reflective null which suffered not only from the error identified in the Allen report (the spacing of the field lens to the mirror), but also another small error which contributed to the final performance of the reflective null. In addition to the reflective null, the refractive null data and inverse null data were also analyzed. It was also discovered that the Wide-Field (WF) and Planetary Cameras (PC) that were built had an additional error which further complicated the testing methods.

The second method called Image Metrology was based on a modified Hartmann Test which was used by Vaughan and Meinel (See Appendix IV). Using the diffraction from the pads on the mirror as an Arago (or inverse Hartmann) Test, the spherical aberration was determined.

The third test was phase retrieval (See Appendix V). In this method, the phase front is determined by analyzing the point spread function near the focal point and determining what phase front must have been present in order to achieve that point spread function. By far, the largest number of groups working on the problems of the Hubble Space Telescope were in the area of phase retrieval. A modification of this approach was a method entitled prescription retrieval (Redding, Shao, JPL). In this

method, the construction parameters are fitted as the independent variables rather than the phase front in the exit pupil.

Finally, there was a wavefront sensor built into each of three Fine Guidance Sensors (FGSs) that would have been able to analyze a wavefront error of up to about one wave. Unfortunately, the manufacturing error of the primary mirror was significantly larger than that value; and, therefore, the wave front sensor was not usable for quantifying the telescope error.

The evaluation of the error bar on the measured conic constant is very important. An error bar on the primary mirror conic constant of ± 0.0005 corresponds to RMS wavefront of $\lambda/50$ at a wavelength of 0.6328 micrometers. This is not quite to the specification originally set for the instrument. The panel feels confident that the error bar on the designated conic constant is within the ± 0.0005 value (two sigma) and in fact, many of the panel members felt that the error bar was probably as low as ± 0.0003. While with more extensive tests and other measurements, these numbers might be refined further, the panel felt that the time and expense involved in determining this is inappropriate.

The panel also looked at the possibility that the secondary mirror of the telescope was made incorrectly (See Appendix VII). The panel concluded that from the fossil data and from measurements on the backup secondary that the flight secondary mirror was made within specification.

History of the Panel

The panel first met on July 5, 1990. At that point, it was considered to be a one-day meeting in order to review the status of data that had been provided by Hughes Danbury Optical Systems, NASA, and other interested parties who had developed theories about the causes of the poor imagery of the Hubble Space Telescope. The panel, at that point, had no chairman and was considered an ad hoc committee to meet for a single one-day session. Later in that month, Charles Jones of NASA/MSFC asked Duncan T. Moore of The Institute of Optics (University of Rochester) to chair the Hubble Independent Optical Review Panel (HIORP). The members for the panel chosen by NASA were George N. Lawrence (University of Arizona), Dan Schulte (Lockheed), Paul Robb (Lockheed) (who later withdrew because of pressing responsibilities), Dietrich Korsch (Korsch Optics), and Aden and Marjorie Meinel (Jet Propulsion Laboratory). A number of other key people were added as advisors, specifically, John Mangus who had served on the Allen Committee and was a valuable resource for data; Dr. James Fienup of ERIM was our liaison to the phase retrieval teams; and the team at Optical Research Associates (specifically, William Wetherell and Mark Kahan) were charged by NASA to analyze all of the data in detail, using their software programs. Laurie Furey, Robert Basedow and Christ Ftaclas from Hughes Danbury Optical Systems and Dr. Chris Burrows of the Hubble Space Telescope Science Institute (ST ScI) provided input to the panel. In Appendix I, the agendas of all sessions are given. The first official meetings of this panel were attended by well over 200 people and as the meetings progressed through the next year, the attendance decreased as the problem became more well-defined and the panel reached its conclusions. Oversight and coordination of the last eight meetings was handled by Dr. H. John Wood, The NASA HST Optics Lead Engineer.

Background Issues

History of the Telescope

The history of the design and manufacturing of the Hubble Space Telescope was well documented in the Allen Committee report dated November 1990. In that report, the committee concluded that the conic constant was made incorrectly due to an error in the spacing of a lens in the reflective null.

The original system was a Ritchey-Chretien with two hyperbolic mirrors which were to be tested separately and assembled, but with no full-up tests. The specifications for the original instrument are given in Table 1 and the results of the Allen Committee are given in Table 2. Table 3 is the result of the HIORP deliberations. Table 4 gives the correct values for the Orthogonalized Zernike Polynomials in the case of 33% obscuration as is the case for HST. The Allen Committee was not specifically charged with quantifying the condition of the telescope. That was the responsibility of this panel. The charge of the Allen Committee was simply to determine approximately what happened, why it occurred, and to leave the details to a different team of scientists and engineers.

The HIORP conducted a series of meetings (See Appendix I) at which experts analyzing data from the HST and data from interferograms and null corrector measurements (fossil data) made before launch were presented. These data showed that two values of the primary mirror conic constant were being generated which were significantly different. The fossil data yielded a conic constant that was approximately -1.0133 and that of the phase retrieval data was -1.0142. The fossil data was being analyzed by two different teams, Optical Research Associates and HDOS. The philosophy of the panel was always to have two independent groups analyze the data. The phase retrieval data was being analyzed by no less than eight teams. All of the phase retrieval data from all groups was consistently higher (in absolute value) than that of the fossil data. There are a number of ways to account for this, but the most obvious one is that the secondary mirror was made incorrectly. The panel later concluded that was probably not the case and was left with a potentially difficult problem. The panel later discovered that there existed two other errors. The first was in the assembly of the reflective null corrector. The manufacturing error which had been previously identified by the Allen Committee was not the only manufacturing error in the reflective null. Other spacing errors were also contributing to the differences between the two measurements. In fact, the distance error of the field lens in the mirror was about 98% of the problem, but 2% of the error was contributed by the short radius of the upper mirror and its short spacing. They were such that the correct value of the fossil data should be

-1.0139. That still left the phase retrieval data systematically high relative to the fossil data. Unfortunately, almost all of the phase retrieval data that was analyzed was from one camera, namely PC-6. There were a limited number of data points from the faint object camera which yielded a number that was approximately -1.0138. Fortunately, the pre-launch interferograms from PC-6 were found, and it was discovered that the camera had been made within specification but had a small amount of residual aberration which was of a sign that would bring the phase retrieval data to a number that was closer to -1.0139. Fortunately, later data from the other cameras on WFPC confirmed this.

Analysis of the Secondary Mirror

One possible explanation for the difference between the phase retrieval and fossil data would have been that the secondary mirror was also made incorrectly. In the phase retrieval analysis, the defects of both the primary and secondary mirror (as well as the cameras) would have been included in the calculations while the fossil data was only that of the primary mirror. The panel decided on three courses to try to determine whether the secondary was made incorrectly. The first way was to review all of the fossil data on the secondary, i.e., the interferograms. The second was to test the backup secondary which had been manufactured at the same time. Finally, if there were an error in the secondary mirror, one would expect a field-dependent coma to be present.

In reviewing the interferograms, it was concluded that the interferograms appeared to be correct. While some residual errors in the secondary existed, they were of an order of magnitude less than would be necessary for any error to be present in the phase retrieval data.

The back-up secondary mirror was tested by the Hindle Sphere Test at the University of Arizona during the first quarter of 1991. The results of those tests showed that no gross errors were present. The accuracy to which the tests could be performed was not sufficient to absolutely say that it was made correctly, but was sufficient to eliminate any large errors. Further, it was concluded by the panel that any further tests on the backup secondary would not be prudent since there was no guarantee that the secondary that was on-orbit and one that was here on earth were identical. (See Appendix VII)

If the secondary mirror were made with the wrong conic constant, it would introduce spherical aberration. Because the aperture stop is at the primary mirror, not the secondary, this would induce coma into the optical system. One would therefore expect images that were far off axis to show a comatic pattern. This type of coma could be differentiated from the coma that is present when optical system is not rotationally symmetric, i.e.,

when the secondary mirror and the primary mirrors do not share the same optical axis. In the case of a tilted system, a non-field dependent coma is introduced. It was possible to measure the field dependent coma since there were two cameras at two different field positions. No field dependent coma was observed.

The conclusion of the panel, after looking at a large number of images, was that if there is any error in the secondary mirror, it is very small and is masked by the large amount of other aberrations present in the optical system. The panel therefore, has assumed that the secondary mirror was made to specification and only with a refinement of the optical instrumentations on-orbit would any possible error on the secondary be found.

Summary of Testing Methods

The three principal methods for determining the condition of the Hubble Space Telescope were the fossil data, the image metrology, and phase retrieval. The details for each of these methods is described in the Appendices which were prepared under subcontract to NASA for this panel. The reports are included in their entirety and represent the findings of this panel. There are a large number of other reports that were provided to the panel which provide backup documentation for our findings. Copies of additional reports may be obtained from H. John Wood at NASA/GSFC.

Table 1. HST OTA Paraxial Design Parameters

Parameters	Value
Primary Mirror	
Radius, mm	11,040.0 (concave)
Conic constant	-1.0022985
Working aperture, mm	1,200.0
Secondary Mirror	
Radius, mm	1,358.0 (convex)
Conic constant	-1.49600
Spacings	
Back focal plane, mm behind primary vertex[a]	1,500.0
Derived first-order parameters	
Magnification	10.434569
System f/number	24.00125

[a]Location set by instrument package.

Table 2. HST OTA Paraxial As-Built Parameters - Allen Committee

Parameters	Value
Primary Mirror	
Radius, mm	11.041.70 (concave)
Conic constant	-1.013236[a]
Working aperture, mm	1,200.0
Secondary Mirror	
Radius, mm	1,358.065 (convex)
Conic constant	-1.49600
Spacings	
Back focal plane, mm behind primary vertex[b]	1,500.0
Primary-secondary separation, mm	4,906.888
Derived first-order parameters	
Magnification	10.43532
System f/number	24.00666

[a]Note: The primary mirror conic constant is the actual conic constant now on the mirror, due to the null corrector spacing error.

[b]Location set by instrument package.

Table 3. HIORP Specifications for HST

Parameters	Value
Primary Mirror	
Radius, mm	11.041.70 (concave)
Conic constant	-1.0139
Working aperture, mm	1,200.0
Secondary Mirror	
Radius, mm	1,358.065 (convex)
Conic constant	-1.4960
Spacings	
Back focal plane, mm behind primary vertex	1,500.128
Primary-secondary separation, mm	4,907.01
Derived first-order parameters	
Magnification	10.4
System f/number	24.0

Number	Normalization Factor	Polynomial
1	1.0000000D 00	
2	1.8992573D 00	$R \cos(\theta)$
3	1.8992573D 00	$R \sin(\theta)$
4	3.8874443D 00	$R^2 + -0.554450$
5	2.3137662D 00	$R^2 \cos(2\theta)$
6	2.3137662D 00	$R^2 \sin(2\theta)$
7	8.3345629D 00	$(R^3 + -0.673796\ R) \cos(\theta)$
8	8.3345629D 00	$(R^3 + -0.673796\ R) \sin(\theta)$
9	2.6701691D 00	$R^3 \cos(3\theta)$
10	2.6701691D 00	$R^3 \sin(3\theta)$
11	1.6895979D 01	$R^4 + -1.108900\ R^2 + 0.241243$
12	1.2033645D 01	$(R^4 + -1.108900\ R^2) \cos(2\theta)$
13	1.2033645D 01	$(R^4 + -1.108900\ R^2) \sin(2\theta)$
14	2.9851527D 00	$R^4 \cos(4\theta)$
15	2.9851527D 00	$R^4 \sin(4\theta)$
16	3.6321417D 01	$(R^5 + -1.230566\ R^3 + 0.323221\ R) \cos(\theta)$
17	3.6321417D 01	$(R^5 + -1.230566\ R^3 + 0.323221\ R) \sin(\theta)$
18	1.6372202D 01	$(R^5 + -0.800100\ R^3) \cos(3\theta)$
19	1.6372202D 01	$(R^5 + -0.800100\ R^3) \sin(3\theta)$
20	3.2700486D 00	$R^5 \cos(5\theta)$
21	3.2700486D 00	$R^5 \sin(5\theta)$
22	7.4782446D 01	$R^6 + -1.663350\ R^4 + 0.803136\ R^2 + -0.104406$
23	5.4696500D 01	$(R^6 + -1.340332\ R^4 + 0.405641\ R^2) \cos(2\theta)$
24	5.4696500D 01	$(R^6 + -1.340332\ R^4 + 0.405641\ R^2) \sin(2\theta)$
25	2.1196833D 01	$(R^6 + -0.833345\ R^4) \cos(4\theta)$
26	2.1196833D 01	$(R^6 + -0.833345\ R^4) \sin(4\theta)$
27	3.5320536D 00	$R^6 \cos(6\theta)$
28	3.5320536D 00	$R^6 \sin(6\theta)$
29	1.6007455D 02	$(R^7 + -1.781299\ R^5 + 0.948280\ R^3 + -0.142530\ R) \cos(\theta)$
30	1.6007455D 02	$(R^7 + -1.781299\ R^5 + 0.948280\ R^3 + -0.142530\ R) \sin(\theta)$
31	7.9942692D 01	$(R^7 + -1.429930\ R^5 + 0.477328\ R^3) \cos(3\theta)$

Table 4
Zernike Polynomials Orthogonalized over an Annular Aperture
Radius of Cental Obscuration 0.3300

APPENDIX I
PANEL AND AGENDAS

Independent Optical Review Panel

Charter

This panel is formed to support the HST Project Office in the following areas:

I. Review approach for characterizing the OTA optical aberrations required for the design of Advanced Scientific Instruments (ASI), whether obtained from orbital evaluation of OTA optical performance or from the identification of OTA development errors. This review should include assessing the technical adequacy of specifications; techniques proposed for obtaining data; anticipated accuracy and residual uncertainties; and quality of the final data products.

II. Review analyses and/or test results used to identify OTA primary optics development/manufacturing error.

III. Assess the validity of proposed concepts for enhancing the HST optical performance, such as, entrance aperture apodization.

Duncan Moore
Professor, Institute of Optics
University of Rochester

Paul Robb
Manager, Optical Sciences Lab
Lockheed Palo Alto Research Labs

Aden and Marjorie Meinel
Distinguished Scientists
JPL

George Lawrence
Professor, Optical Sciences Center
University of Arizona

Daniel Schulte
Senior Staff Scientist, Optical Design
Lockheed Palo Alto Research Labs

Dietrich Korsch
Optical Science Consultant
Korsch Optics

** TOTAL PAGE.07 **

HST INDEPENDENT OPTICAL ASSESSMENT PANEL

THURSDAY JULY 5, 1990

09:00 A	INTRODUCTION	C. JONES
	o PURPOSE OF MEETING	
	o HST OPTICAL STATUS OVERVIEW	
	o PANEL CHARTER, ORGANIZATION	
	o PANEL FINDINGS, DISSEMINATION	
	o SCHEDULE/AGENDA	
09:30	LOGISTICS & ADMINISTRATIVE DETAILS	B. BROWN
09:45	PANEL CAUCUS	
10:00	OTA OPTICAL OVERVIEW	B. BASEDOW
10:15	WF/PC OPTICAL OVERVIEW	S. FABER
10:30	WF/PC DEFOCUSED IMAGE ANALYSIS	J. HOLTZMAN
11:00	WF/PC OTA IMAGE MODELLING	C. BURROWS, R. LYONS
11:15	WAVEFRONT SENSOR OVERVIEW	B. BASEDOW

HST INDEPENDENT OPTICAL ASSESSMENT PANEL

THURSDAY JULY 5, 1990

12:00	WFS OPD MEASUREMENTS	B. BASEDOW
12:30 P	WORKING LUNCH	
12:45	WFS VISIBILITY ANALYSIS	B. CROUT
1:00	FOC IMAGE ANALYSIS	C. BURROWS, R. LYONS
1:20	OPTICAL BACKUP (ALIGNMENT) ALGORITHM	R. LYONS, C. BURROWS
2:00	WF/PC SIMULATOR RESULTS	W. FASTIE
2:15	FGS S-CURVE ANALYSIS	C. BURROWS
2:30	PRESENTATIONS BY PANEL MEMBERS	
3:00	PANEL DISCRETIONARY TIME	
4:00	OPTIONAL TOUR OF HST STOCC	

HST INDEPENDENT OPTICAL ASSESSMENT PANEL

FRIDAY JULY 6, 1990

08:00 A	TECHNICAL FOLLOW-UP AT DISCRETION OF PANEL
10:00	DRAFTING OF PANEL FINDINGS
12:00	ADJOURN

HST INDEPENDENT OPTICAL ASSESSMENT PANEL

CHARTER

REVIEW THE CURRENT HST OPTICAL ALIGNMENT AND IMAGING DATA IN ORDER TO:

1. ASSESS THE IMAGE AND WAVEFRONT QUALITY

2. CHARACTERIZE THE OPTICAL ABERRATIONS

3. DETERMINE THE LIKELY SOURCE OF ERRORS
   (CAMERAS, TELESCOPE, PRIMARY MIRROR, SECONDARY MIRROR)

4. PROVIDE WRITTEN SUMMARY OF FINDINGS

2ND MEETING OF THE
HST INDEPENDENT OPTICAL REVIEW PANEL

AGENDA

TUESDAY, JULY 31, 1990

8:45		EXECUTIVE SESSION OF INDEPENDENT OPTICAL REVIEW PANEL	MOORE
9:00	I.	INTRODUCTION o PURPOSE OF MEETING o AGENDA, MEETING PROCESS o PANEL CHARTER, TASKS	JONES/ ROTHENBERG
9:15	II.	HST STATUS & NEAR TERM PLAN o OTA ALIGNMENT o OTA CHARACTERIZATION o BEST FOCUS SETTING o PCS ENHANCEMENT o SAMPLE SCIENCE PROGRAM o WF/PC II SCHEDULE	ROTHENBERG
9:35	III.	SCIENCE PERSPECTIVE	BOGGESS
9:45		BREAK	
10:00	IV.	OTA ALIGNMENT STATUS o SEQUENCE OF EVENTS o WFS DATA & RESULTS o IMAGE DATA & RESULTS o FGS DATA & RESULTS	BASEDOW
10:45	V.	OTA CHARACTERIZATION REQUIREMENTS/ACCURACY o LEVEL III WFE BUDGET o LEVEL I SPECIFICATIONS o OTHER CONSIDERATIONS o OTA TO SI ICD MODIFICATIONS	BASEDOW
11:05	VI.	OTA CHARACTERIZATION CORE TEST PLAN o BIG SWEEP FOCUS RUN - OPERATIONAL DESCRIPTION - TECHNICAL DETAILS o DATA EVALUATION - WFS DATA - IMAGE EVALUATION o SPHERICAL ABERRATION SIGN DETERMINATION o PM/SM ERROR DISCRIMINATORS	BASEDOW
12:00		WORKING LUNCH	
12:15	VII.	BEST FOCUS DETERMINATION	BURROWS
12:30	VIII.	INPUT FROM WF/PC II DEV. TEAM	TRAUGER
1:00	IX.	INPUT FROM HST SI DEV. WORKING GROUP	CHENG
1:30	X.	INPUT FROM IMAGE PROCESSING WORKING GROUP	HUNT
2:00		EXECUTIVE SESSION OF INDEPENDENT OPTICAL REVIEW PANEL o ASSESS ADEQUACY OF OTA CHARACTERIZATION CORE TEST PLAN o ASSESS AND PRIORITIZE REQUIREMENTS FOR ADDITIONAL TESTS OR ANALYSES	MOORE

HST INDEPENDENT OPTICAL REVIEW PANEL

THIRD MEETING
August 29 and 30, 1990
Columbia Maryland

First Day

Presentation of Results from the Core Program and Allen Committee

09:00 INTRODUCTION - EXECUTIVE SESSION: Duncan Moore / Inst of Optics

Rules:

a) How things have changed since last time: H. John Wood / GSFC
b) Time allotted to each speaker is 30 minutes with 15 minutes Q&A
c) Time for the lunch break will be determined by the chairman

Charge to the Panel:

a) Evaluation of the data presented
b) Recommendations to the HST project manager:
   1) Nature of the aberrations present - with assessment of the reliability of the aberrations detected
   2) Magnitude of the aberration - assessment of the accuracy of the data analyses
   3) Sign of the aberrations
   4) Future characterization needs to be presented tomorrow

09:45 OPEN SESSION - PRESENTATIONS

Status of Project: Rothenberg / GSFC (15 Minutes)

Allen Committee Report: Mangus / GSFC (30+15)

Overall wavefront characterizations: Blind test and Mini-sweep
Analysts (30+15 each):

Jim Fienup / IPWG
Chris Burrows / STScI
Rick Lyon / HDOS
Sandra Faber / WF/PC
Art Vaughn / WF/PC II / JPL

Actuators and other issues: Charlie Jones / MSFC (30+15)

EXECUTIVE SESSION & SIMULTANEOUS MEETING OF THE PRESENTERS AND INTERESTED PARTIES
The analysts are asked stay available during the executive session

05:00 - END OF THE FIRST DAY

HJW: Draft 90.8.25

SECOND DAY

FOLLOW - ON CHARACTERIZATION ACTIVITIES

Open discussion led by Duncan Moore

08:00 DISCUSSION

Does the present Core program satisfy all the New Instruments needs?

A. Presentation of a draft matrix: H. John Wood

Type of Image Analysis
vs.
Parameters

B. Input from Current and New Instrument Teams:
NCMOS & STIS:Woodruff
WF/PC II: Rochblatt
FGS issues: Faber

C. Wavefront quality of the HST secondary:
Shannon / Meinel

D. Predicting the upgraded HST images:
Meinel

E. Written recommendations on future needs from the analysts:

Lunch

EXECUTIVE SESSION

The Panel on future characterization needs

Draft of recommendations to the Project

HJW: Draft 90.8.25

HST INDEPENDENT OPTICAL REVIEW PANEL

FOURTH MEETING
September 26 and 27, 1990
Columbia Maryland

AGENDA - First Day

09:00 INTRODUCTION & REVIEW OF MONTHS ACTIVITIES: Executive Session
During the Executive Session in the auditorium will be shown:
a movie of WF/PC jitter; FOC image-fit blink and FOC mini sweep

09:30 PRESENTATIONS: Open Session

Simulsecondarius GHRS and FOC observation - progress report 5 min	J. Wood
Report on PM, SM and null Testing 10+5 m	C. Jones
Report on Focus and Other Requirements of Other Current Scientific Instruments (GHRS, FOS, etc.) 10+5 m	Ed Cheung
Sign and Magnitude of the Spherical Aberration 6 ways (x 5 m ea.)	J. Wood et al.
Analysis of Telescope Parameters (Vertices, Focal Point) 10+5 m	C. Burrows
Phase Retrieval Analysis by 5 teams (x 15 m ea.) -DISCUSSION- chair:	J. Holtzman

12:00 Lunch

Report on Allen Committee Studies of Interest to the Panel I 30+10 m	R. Shannon
Report on Allen Committee Studies of Interest to the Panel II 30+10 m	W. Wetherell
Pictures of SA on OTA, null / PM and caustic 10+5 m	D. Schulte ← A. Vaughn
Optical Models of OTA + WF/PC 10+5 m	GSFC Optics
Characterization of Pupil Function 10+5 m	J. Mangus
FGS and Spacecraft Jitter I 10+15 m	Ed Nelan
FGS and Spacecraft Jitter II 10+15 m	Darrell Story
FGS and WFS Optical Analysis 15+10 m	R. Basedow

17:00 Summary & End of Open Sessions 10 m D. Moore

Tomorrow 27th - Executive Session Only

Presenters should prepare for distribution at the meeting 10 copies of a four-page summary report which describes the detailed error analysis. The presentation should consist of only a brief overview and the conclusions.

HJW:90.09.26

as Corrected by

FINAL AGENDA FOR HIORP V

October 31 - November 1, 1990
Columbia, Maryland

All speakers are asked to identify themselves and their work with a cover sheet and then initials a date on each viewgraph sheet. Please limit your presentation to 5 viewgraphs with details in a 4 page write-up. Please bring with you your viewgraphs and 15 copies of the viewgraphs and written material to be handed to the panel before your presentation.

FIRST DAY OPEN SESSION 9AM - 5PM

09:00 Executive session : Introduction and monthly review - J. Wood

09:30 Open session :

Late breaking news on OTA collimation testing - J. Wood (5 minutes)

Fossil testing and secondary mirror testing - C. Jones / by J. Wood (5)

Status of the Jitter Fix - J. Olivier / G. Nurre / by J. Wood (5)

Astrometry and the effect of the current FGS situation - W. H. Jefferies (30 + 10)

Wave Front Sensors and Fine Guidance Sensors: New Results - C. Ftaclas (30 + 10)

Assessment of zonal error effects - A. Vaughan / D. Rodgers (20+ 5)

Fresnel Diffraction - G. Lawrence / J. Fienup (5 + 5)

Final report of the HST Strategy Panel - R. Brown (15 + 5)

Lunch 12:00

Phase retrieval report: results from the 5 groups: quality and quantity of data available - J. Holtzman (50 + 10)

HARP 1a proposal : degree of success - K. Leschley (20 + 5)

New developments in the GSFC / HDOS Phase retrieval results - R. Lyon (10+5)

Some overall checks on the consistency of the present values of the conic constant - A. Meinel (20+20)

Optical design models of the OTA and Cameras - M. Wilson / C. Burrows (20+5)

A physical model of the focal plane assembly - D. Skillman / J. Decker (10+5)

A proposed corrector for the WF/PC - Margolis / Makowsky (20 + 10)

EXECUTIVE SESSION TERMINATED LATE ON 90.10.31

HJW: 90.11.25

FINAL AGENDA FOR HIORP VI

November 28 & 29, 1990
Columbia, Maryland

All speakers are asked to identify themselves and their work with a cover sheet and then initials and date on each viewgraph sheet. Please limit your presentation to 5 viewgraphs with details in a 4 page write-up. Please bring with you your viewgraphs and 15 copies of the viewgraphs and written material to be handed to the panel before your presentation.

FIRST DAY OPEN SESSION 9AM - 5PM

09:00 Executive session : Introduction and monthly review - J. Wood

09:30 Open session :

Recent WF/PC Imagery - J. Westphal (20 + 5)

Report of the Allen Committee - J. Mangus (20 + 5)

Fossil Testing - C. Jones / D. Johnston (30 + 5)

Sensitivity Analysis of the Reflective Null - L. Furey (20 + 5)

Progress on Code V OTA Model - W. Wetherell (10 + 5)

FGS Test Results and PC Breathing - E. Nelan (20 + 5)

12:30 **Lunch**

Phase Retrieval Report: Status of the Image Supply: - J. Holtzman (20 + 5)

Phase Retrieval Results at the Institute - C. Burrows (20 + 5)

Phase Retrieval Results at ERIM - J. Fienup (20 + 5)

Phase Retrieval Results at Goddard - R. Lyon / P. Miller (20 + 5)

Results of the First HARP Conference - R. Korechoff (20 + 5)

WF/PCII Team Optical Studies - A. Vaughan (20 + 5)

Overview of the Results on the OTA Prescription - A. Meinel (20 + 5)

SECOND DAY EXECUTIVE SESSION 8AM - 12NOON

HJW: 11/27/90 7:00 PM

AGENDA FOR MINIORP

December 13, 1990
Goddard Space Flight Center
Building 16W Room N76-80 8:30 - 4:30

All speakers are asked to present their derived value of K1 with its associated error bar. Please bring a written justification and discussion of the sources of error for the K1 value you present. Assuming the archival values for K2, R1 and R2, what are the calculated value for the spacings:
PM to SM and PM to focal plane?
Give data for:
Paraxial focus, Marginal focus, Circle of Least Confusion & Minimum Wavefront Error

Morning Session Informal Discussion & Presentations 08:30 - 12:00

Line of Sight Scans taken with the FGS's on days 149 and 150 P. Bely / STScI

I. PC/OTA Effects on Effective Focal Length

D. Schulte / LPARL: Design vs As-built ray trace through OTA + PC (30)

M. Wilson / GSFC: OTA intervertex distance (30)

II. Direct Image Measurements

A. Vaughan / JPL: Mini Hartmann test using PM Pads or Radial Profiles (30)

A. & M. Meinel / JPL: Pads, Rims and Az - Avg Radial Intensity (30)

Lunch 12:00 - 1:00
Afternoon Presentations 1:00 - 4:30

III. Phase Retrieval from PC and FOC Imagery

C. Burrows / STScI: (30)

R. Lyon & P. Miller / HDOS: (30)

IV. Field Lens Position Error (FLPE)

C. Jones / MSFC: The complete set of ±10μ accuracy measurements at Danbury (30)

L. Furey HDOS: The HDOS proprietary code calculations of K1 from FLPE (30)

W. Wetherell / ORA: The Code V calculations of K1 from FLPE (30)

V. Summary and Discussion

D. Moore / HIORP, A. Meinel / JPL and D. Rodgers / JPL: (30)

HJW: 90.12.18

Handed out at MINI ORP

December 13, 1990

TO: J. Rothenberg / 440

FROM: J. Wood / 717.3

SUBJECT: SWG Agreement on Focus

The issue of present and future focus of the HST was thoroughly discussed at yesterday's meeting of the Science Working Group.

At a separate meeting of representatives from the instrument teams, the following compromise focus position was agreed upon.

> "The HST shall operate at a focal position which maximises the encircled energy in 0.1 arc sec radius in the FOC f/96 camera at 486 nanometers wavelength."

It was recognised that optimum UV performance of the FOC and GHRS would require a focus 1mm shorter than this while the WF/PC would prefer a focus 3mm longer for optimum IR work.

This information can be transmitted to the WF/PC II team for their Rx correction to their cameras.

Regards, J. Wood

cc: A. Barr / 440
J. Osantowski / 717
J. Mangus / 600
F. Cepollina / 408

Handed out at MINIORP

Focus Meeting @ SWG
90.12.12

Kenneth Carpenter	GHRS IDT
Richard Harms	FOS IDT
Bill Sparks	Foc
Ed NELAN	**AST**
Duccio MACCHETTO	FOC
Dan Schroeder	Tel Sc / HSP
Ed Groth	Princeton / WFPC
A. John Wood	NASA / GSFC

Max EE in FOC f/96 @ 486 nm
compromises GHRS u v
" PC

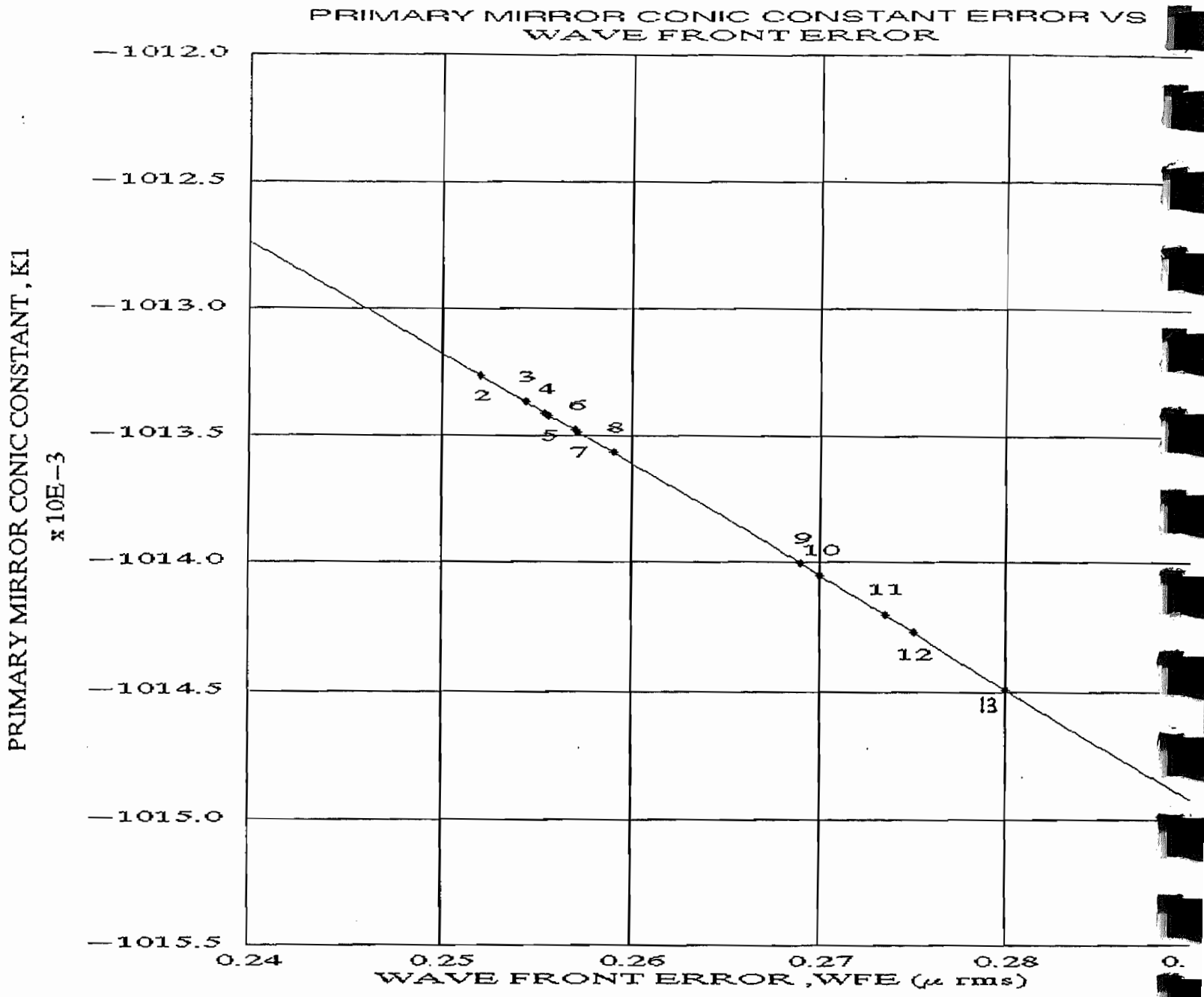

	DATA SOURCE	CONIC CONSTANT		UNCERTAINTY	WFE (μ rms)
~~1~~	~~Reflective Null, RNC @ 1.292mm~~	~~-1.013234~~	~~±~~	~~0.00090~~	~~-0.2514~~
2	Refractive Null, RvNC	-1.013262	±	0.00080	-0.2520
3	Reflective Null, RNC @ 1.308mm	-1.013365	±	0.00009	-0.2544
4	MIENELS, PAD LOCATION	-1.013410			
5	MIENELS, RIM IMAGE	-1.013420			
6	VAUGHN, PAD LOCATION	-1.013480			
7	FUREY: FLPE 1.3085 mm	-1.013485			
8	LYONS : HDOS-FOC	-1.013581	±	0.00033	-0.2593
9	LYONS : HDOS-PC	-1.014007	±	0.00035	-0.2690
10	SHAO : JPL-PC	-1.014051	±		-0.2700
11	FABER/HOLTZMANN : WF/PC-PC	-1.014200	±		-0.2734
12	FIENUP : ERIM - PC	-1.014270	±		-0.2750
13	BURROWS : HST Sci Inst-PC	-1.014490	±		-0.2800

Summary of the data at the Miniorp.

December 13, 1990

TO: J. Rothenberg / 440

FROM: J. Wood / 717.3

SUBJECT: MINIORP Agreement on Primary Mirror Conic Constant

In a meeting on 13 December 1990, a panel of scientists and engineers reviewed all of the on-orbit and fossil data on the HST primary mirror conic constant that is available today. A list of the attendees at that meeting is attached as well as a copy of the agenda.

The panel agreed on a single value of the conic constant which they could recommend to the JPL team building the WF/PC II instrument:

$$K = -1.01350$$

The panel recommends that JPL begin making the WF mirrors first using the above value. The WF cameras are much less sensitive to small uncertainties in the value of K than are the PC cameras. This will leave extra time for further refinement of the value for K.

Meanwhile further studies of the data were requested by the panel for reporting at the January 9 meeting of the HST Independent Optical Review Panel at BDM in Columbia MD.

This information can be transmitted to the WF/PC II team for their Rx correction to their cameras.

Regards,

encl: list of attendees at the MINIORP meeting
Agenda of MINIORP meeting

cc: A. Barr / 440
J. Osantowski / 717
J. Mangus / 600
F. Cepollina / 408

AGENDA FOR HIORP VII

February 6, 7 1991
Jet Propulsion Laboratory
Building 180, Room 101

Morning Session - Informal Open Discussions & Presentations 08:30 - 12:00

I. Introduction and Milestones since Last Meeting (20) - J. Wood / GSFC

II. PC/OTA Effects on Effective Focal Length (60)

D. Schulte / LPARL, W. Wetherell / ORA, M. Wilson / GSFC

III. Camera Internal Aberrations (60)

A. Vaughan / JPL, C. Burrows / STScI, J. Wood / GSFC

IV. Direct Image Measurements: Hartmann Pads, Diameters & Desorption (60)

A. Vaughan / JPL, D. Schroeder / Beloit, A. & M. Meinel / JPL

Lunch 12:00 - 1:00

Afternoon Session - Informal Open Discussions & Presentations 1:00 - 4:30

V. Phase Retrieval from PC and FOC Imagery (60)

Jim Fienup / ERIM C. Burrows / STScI R. Lyon & P. Miller / HDOS

HARP Summary Report by R. Korechoff

VI. Field Lens Position Error (FLPE) and Other Metrology at HDOS (60)

C. Jones / MSFC L. Furey HDOS W. Wetherell / ORA H. Garrett / JPL

VII. Hindle Test of the HST Clone Secondary Mirror (30)

G. Lawrence for R. Parks / Optical Sciences Center

VIII. Summary and Discussion (60)

D. Moore / Inst. of Optics, Members of the Panel, Advisors to the Panel

EXECUTIVE SESSION
February 7, 1991
08:00 - 12:00

HJW: 91.02.03

March 11, 1991

TO: Associate Director of Flight Projects for HST / J. Rothenberg / 440

FROM: OTA Systems Manager / J. Wood / 717.3

SUBJECT: As - Built Optical Parameters for the OTA of the HST

At the seventh HIORP meeting at JPL on February 7, 1991, a panel of scientists and engineers reviewed all of the on-orbit and fossil data on the HST primary mirror PM conic constant that is available today.

The panel agreed to continued use of a single value of the conic constant:

K = - 1.0135 ±0.0007 (CODE-V expression for a concave hyperboloid)

use: K = - ((WFE / 0.6328) + 36.14) / 36.06 to convert from WFE in μ rms

The current value of the uncertainty of ±0.0007 encompasses a large fraction of the on-orbit and fossil data. It was agreed that further measurements on the fossils at Danbury and Goddard is required to reduce the uncertainty in the above number. With further measurements on the reflective and refractive null components, the uncertainty may be reduced to about ±0.0003. This number may be achieved by mid-August 1991 if no unforeseen delays are encountered.

The WF/PC interferometric data on the flight cameras indicated slight residual spherical aberration (SA) in the cameras. Measurements of the cameras remaining on the ground confirm the sign of the SA in the cameras.

The values of SA in the flight cameras range from ΔK = 0.0000 to -0.0011. This amount is enough to adjust the on-orbit WF/PC data to near-agreement with the conic constants derived from the RNC fossil data from HDOS. The FOC data by the phase retrieval group agrees with the fossil data and the interferograms of the FOC mirrors shows negligible SA in the FOC f/96 camera.

The PM radius is: R = 11041.7 ± 0.3 mm est. unc. PR-237B Table VI

The SM (S/N 001) radius is: R = 1358.065 ± 0.025 mm est. unc. PR-240C Table IV

The conic constant of the SM is : K = - 1.4960 ± 0.0001 est. unc. PR-240C Table IV
(CODE-V expression for a convex hyperboloid)

The primary mirror vertex to focus distance is: 1500.128 mm nominal PR-706 Table 1

The intervertex distance corresponding to maximum encircled energy in a circle with 0.1 arc sec radius in the FOC f/96 camera at 487nm wavelength is: 4907.010 ± 0.010 mm M. Wilson / GSFC
(= 13.5 ± 0.5 mm long from paraxial focus)

The operating position of the SM in 1991 after the February desorption move is: Df = - 555 μm, Dy = - 109.21 μm, Dz = + 281.15 μm, Ty = - 79.28 arc sec (about V2) and Tz = - 52.91 arc sec (about V3). Information from A. Nonnenmacher, HDOS .

Regards,

cc: A. Barr / 440, F. Cepollina / 442, M. Jurotich / 442, J. Mangus / 600, J. Osantowski / 717

FINAL AGENDA FOR HIORP VIII

March 21, 1991
BDM Corporation
Columbia Maryland

Morning Session - Informal Open Discussions & Presentations 08:00 - 12:30

I. Introduction and Milestones since Last Meeting (60)

Wood / GSFC

II. Camera Manufacturing Aberrations (30)

Korechoff / JPL Wood / GSFC

III. RNC INC and RvNC and Other Metrology at Danbury (20)

Johnston / MSFC Garrett / JPL

IV. Tolerance analyses on the Null Correctors (30)

Furey / HDOS Kahan / ORA

V. Induced Aberrations in the Cameras (30)

Shannon / U. of A. Kahan / ORA

VI. Phase Retrieval from PC and FOC Imagery (30)

Fienup / ERIM HARP Summary Report by Korechoff / JPL

VII. Additional Short Presentations (30)

Meinel / JPL Mangus / GSFC Bottema / Ball Schulte / LPARL

Lunch 12:00 - 12:30

(Portrait photography by Cara Loss Wood during lunch)

Afternoon Session - Executive session 12:30 - 2:30

VIII. Executive Summary and Discussion (120)

D. Moore / Inst. of Optics, Members of the Panel, Advisors to the Panel

HJW: 91.03.24

AGENDA FOR HIORP IX

July 2, 1991
BDM Corporation
Columbia Maryland

Morning Session - Informal Open Discussions & Presentations 08:00 - 12:00

I. Introduction and Milestones since Last Meeting (60)

Wood / GSFC

II. Camera Manufacturing Aberrations (60)

Korechoff / JPL, Wood / GSFC Wolfe / Kodak

III. Telescope Manufacturing Tolerances - Ground to Orbit (60)

All with something to say

IV. Tolerance analyses on the Null Correctors and the Final Word (60)

Furey HDOS Kahan / ORA

Lunch 12:00 - 13:00

Afternoon Session - Executive session 13:00 - 15:30

EXECUTIVE SESSION
13:30 - 15:30

D. Moore / Inst. of Optics, Members of the Panel, Advisors to the Panel

HJW: 91.07.01

HST INDEPENDENT OPTICAL REVIEW PANEL

Executive Committee

Duncan T. Moore (Chair)	Director, Inst. of Optics University of Rochester Rochester, NY 14627	716-275-5248 716-473-6745 (FAX)
George N. Lawrence	Applied Optics Research 4455 N. Osage Road Tucson, AZ 85718	602-299-1933 602-299-1375 (FAX)
Dan Schulte / Paul Robb	Lockheed Optical Systems Design Laboratory Palo Alto, CA 94304-1191	415-424-3554 415-354-5002 (FAX)
Dietrich Korsch	Korsch Optics Huntsville, AL 35803	205-881-1166 205-881-1166 (FAX)
Aden & Marjorie Meinel	Distinguished Scientists / JPL Jet Propulsion Laboratory / 385 Pasadena, CA 91109-8099	818-354-0963 JPL 818-393-6285 (FAX) 805-965-4762 HOME 805-963-0859 (FAX)

Advisors to the Panel

Charlie Jones	MSFC	205-544-3433 205-544-5864 (FAX)
John Mangus	GSFC	301-286-6055 301-286-9263 (FAX)
Bill Rosenberg	LMSC	415-424-3977 415-424-3994 (FAX)
Jim Fienup	ERIM	313-994-1200, x2500 313-994-0944 (FAX)
Murk Bottema	Died July 3, 1992	
Art Vaughan	JPL / WFPC II	818-354-1669 818-393-9088 (FAX)
Chris Burrows	STScI	301-338-4913 301-338-4767 (FAX)
H. John Wood	GSFC / Code 442	301-286-8278 / 1266 301-286-8680 (FAX)

HJW: 92.12.09

APPENDIX II

OFFICIAL PRESCRIPTION

As - Built Optical Parameters for the OTA of the HST

- The PM conic is: K = - 1.0139 ± 0.0003 (1 sigma) (CODE V expression for a concave hyperboloid)

- The PM radius is: R = 11041.7 ± 0.3 mm est. unc. PR-237B Table VI

- The SM (S/N 001) radius is: R = 1358.065 ± 0.025 mm est. unc. PR-240C Table IV

- The conic constant of the SM is : K = - 1.4960 ± 0.0001 est. unc. PR-240C Table IV
  (CODE V expression for a convex hyperboloid)

- The primary mirror vertex to focus distance is: 1500.128 mm nominal PR-706 Table 1

- The intervertex distance corresponding to maximum encircled energy in a circle with 0.1 arc sec radius in the FOC f/96 camera at 487nm wavelength is: 4907.01 ± 0.01 mm M. Wilson/GSFC (= 13 ± 1 mm long from paraxial focus)

- The operating position of the SM in 1991 after the February desorption move is:

  DV2 = + 281 µm DV3 = - 109 µm
  TV2 = - 79 arc sec (about V2) TV3 = - 53 arc sec (about V3).

  This is the "Day 323" position referred to in the SM move history file. Images in the WFPC and FOC show 1/15 wave rms coma at 486 nm wavelength at this position.

- The zero coma and zero astigmatism position (collimated) position as determined from data acquired by the WFPC and FOC in October/Novermber 1991 is:

  DV2 = +248 µm DV3 = +7 µm
  TV2 = - 79 asec TV3 = - 53 asec

  This shall be referred to as the "origin" relative to the launch position of the SM. It has no measurable coma or residual astigmatism in the cameras at the 1/40th wave level.

- The instrument teams reviewed the results of new focus sweep data on November 6, 1991 and agreed to keep the OTA focus at 12.2 mm long from the paraxial focus. That means that the paraxial focus in the caustic of the as-built OTA is 12.2 mm forward (+V1) of its previously defined position at station number 198.44 inches in V1.

- A decision was reached by the project on November 18, 1991 after review of a 5 points of light test run the weekend before. It was decided to operate HST at the day 323 tilts and decenters until the first servicing mission.

- A concensus was reached at the SMOV planning meeting November 24 agreeing to collimate the OTA during the first focus move of the OTA secondary mirror after the servicing mission.

HJW: 92.12.14

August 28, 1991

TO: HST Flight Systems and Servicing Project Optics Leads

FROM: HST Optics Lead Engineer/J. Wood/442/717.3

SUBJECT: HST Optical Prescription Derivation and Statistics

This memorandum discusses the data which was used to determine the currently adopted value for the primary mirror conic constant for the as - built HST.

The data is devided into two separate groups: "fossil" data from the measurement program on the reflective null corrector at Danbury and phase retrieval "pr" data derived from images from the cameras aboard HST.

FOSSIL DATA

After all the measurements were completed at Danbury, it was found that the radius of curvature of the upper null corrector mirror was measured short by 60μm from the nominal design value. This tended to compensate for the inter-mirror spacing error which was also measured short by 72μm. When all the parameters were available, a new value of the conic constant for the HST primary mirror was calculated by Bill Wetherell of ORA and independently by Laurie Furey of HDOS. Their numbers agreed closely with each other and also came within close agreement with the on-orbit PR data. The following values were presented to the HIORP IX meeting July 2, 1991.

L. Furey: $K = -1.01378 \pm 0.0003$ W. Wetherell: $K = -1.013756 \pm 0.0003$

PHASE RETRIEVAL

Various teams reported studies of selected FOC and HARP images. I will list here the results from those teams which provided final reports to NASA. Preliminary results from other teams were in general agreement with these data but were not considered finished for lack of a final report to the writer. Residual SA (ΔK) in the PC-6 camera has been measured from interferograms of the relays before launch and from differences between it and WF1 (with no measurable residual SA) on orbit. ΔK has been measured by Vaughan to be as small as + 0.0002 and by Korechoff to be as large as + 0.0011. I am using a Δ conic for the correction for spherical aberration in the PC-6 camera of $\Delta K = + 0.0005$ based on my judgement that the value of 0.0011 may be an over-estimate and that 0.0002 may be an underestimate. The numbers in parenthesis are the number of images used to derive the K value.

Team	Measured value	Corrected for camera SA
J. Fienup	PC-6 (few) = -1.0150 ± 0.0006	OTA alone = -1.0145
R. Lyon	FOC (7) = -1.0138 ± 0.0004	FOC (7) = -1.0138
R. Lyon	PC-6 (19) = -1.0143 ± 0.0005	OTA alone = -1.0138
Meinels	PC-6 (96) = -1.0143 ± 0.0002	OTA alone = -1.0138
Roddier	PC-6 (30) = -1.0151 ± 0.0002	OTA alone = -1.0146
Roddier	FOC (few) = -1.0131 N/A	FOC (few) = -1.0131
Vaughan	PC-6 (30) = -1.0147 ±0.0003	OTA alone = -1.0142
Vaughan	WF1 (few) = -1.014472 $^{+0.0004}_{-0.0002}$	WF1 (few) = -1.0145

AVERAGES

If one takes the arithmetical mean and computes the population standard deviation (sigma) for all of the right-hand column numbers for phase retrieval alone:

1) $K_{pr} = -1.0140375 \pm 0.00048$; n = 8

Similarly, the average of the two calculations based on the fossil data gives:

2) $K_f = -1.013768 \pm 0.00001$; n = 2

If one considers all ten K - values of equal weight and computes the arithmetical mean and population standard deviation:

3) $K_{all} = -1.0139836 \pm 0.00044$; n = 10

The straight average of 1) and 2) is:

4) $K_{avg} = -1.013902$

As a further test, I have attempted to assign various weights to the data based on factors ranging from numbers of images to dollar amounts spent. It was found that the *average value of K and its error bar* vary but little no matter which weighting scheme is used. Thus I have adopted the equal weights solution. It is clear that from the above discussion, the HIORP considered the fossil data of approximately equal weight to all of the diverse phase retrieval results they were considering.

Thus we are using a one sigma error bar on the derived conic constant when we quote the adopted value:

K = -1.0139 ± 0.0005 one sigma

#1 20-SEP-1991 14:11:22.33 MAIL
From: STSCIC::BURROWS "CHRIS X4913 RM 323"
To: c717::hjwood
CC: scivax::burrows,scivax::hartig,scivax::crocker,scivax::ford
Subj: OTA conic constant

MEMORANDUM

TO: H. John Wood, HST Optics Lead Engineer 442/717.3 20 Sept 1991
FROM: G. Hartig, C. Burrows and J. Crocker, STScI
RE: Determination of HST PM K value and associated error estimate.

Your August 28 memo to the HST Flight Systems and Servicing Project Optics Leads concluded with the statement that the HST primary mirror conic constant was best estimated at K=-1.0139+/-0.0005, with the error bar identified as being the one sigma uncertainty. This can be (and has been) interpreted as indicating that there is a >30% probability that K actually is outside the quoted error bar, and that COSTAR and WFPC-II may be unable to provide acceptable image correction over the range of probable K values. We believe that the derivation of this error bar is incorrect, and that the true uncertainty is considerably smaller.

We have checked with Art Vaughn and he believes that the PC6 correction should be 0.0011, in agreement with the JPL position that it is 0.001. He will be documenting this in the near future. Therefore, we believe that a correction of 0.001 should be applied to conic constants derived by phase retrieval from the PC6 data. This lowers considerably the mean K value in your analysis.

Applying the larger PC-6 correction, and making use of the estimated probable errors which you quote to compute the variance-weighted mean of the phase-retrieval (PR) data that you tabulate, we have

$$K = -1.01370 \pm 0.00011$$

This is nearly identical with the reflective null fossil data. The error estimates on both PR and fossil results are also about the same, and we could draw the conclusion from this analysis that, with 95% confidence, the true value of K satisfies

$$-1.0135 < K < -1.0139$$

However, the probable errors associated with the PR determinations of K are largely derived from goodness-of-fit and scatter estimates alone, neglecting systematic errors. Furthermore, it is incorrect to assume, as is implicit in this analysis, that the various PR determinations of K are independent. For these reasons, the true uncertainty in K is somewhat larger.

One of us (Burrows) has independently analyzed the on orbit data, carefully estimating the probable errors, including both statistical and systematic error sources. The results are depicted in Figure 1 (to be sent by mail), along with the fossil data determinations, and their errors, as estimated by L. Furey

(HDOS). A correction of .0010 due to PC-6 spherical aberration has been applied, as indicated by the arrow. The value of K derived from analysis of interferograms obtained with the refractive null corrector is clearly low with respect to the other determinations. The HIORP gave little weight to the refractive null data, since the corrector has not been remeasured and shown to be as specified, and other sources of systematic error are present but not included in the error bar shown. Fully discounting the refractive null data we obtain, from the remaining three determinations alone, a variance-weighted mean of

K=-1.01389 +/-0.00024

This agrees with the HIORP adopted value. The error estimate adopted by the HIORP then corresponds approximately to a 2-sigma uncertainty in this analysis.

We conclude that, at about the 95% confidence level, the actual value of K lies in the range -1.0134 to -1.0144. This range is well within the planned correction capability of COSTAR and WFPC II, if their optics are designed for K=-1.0139.

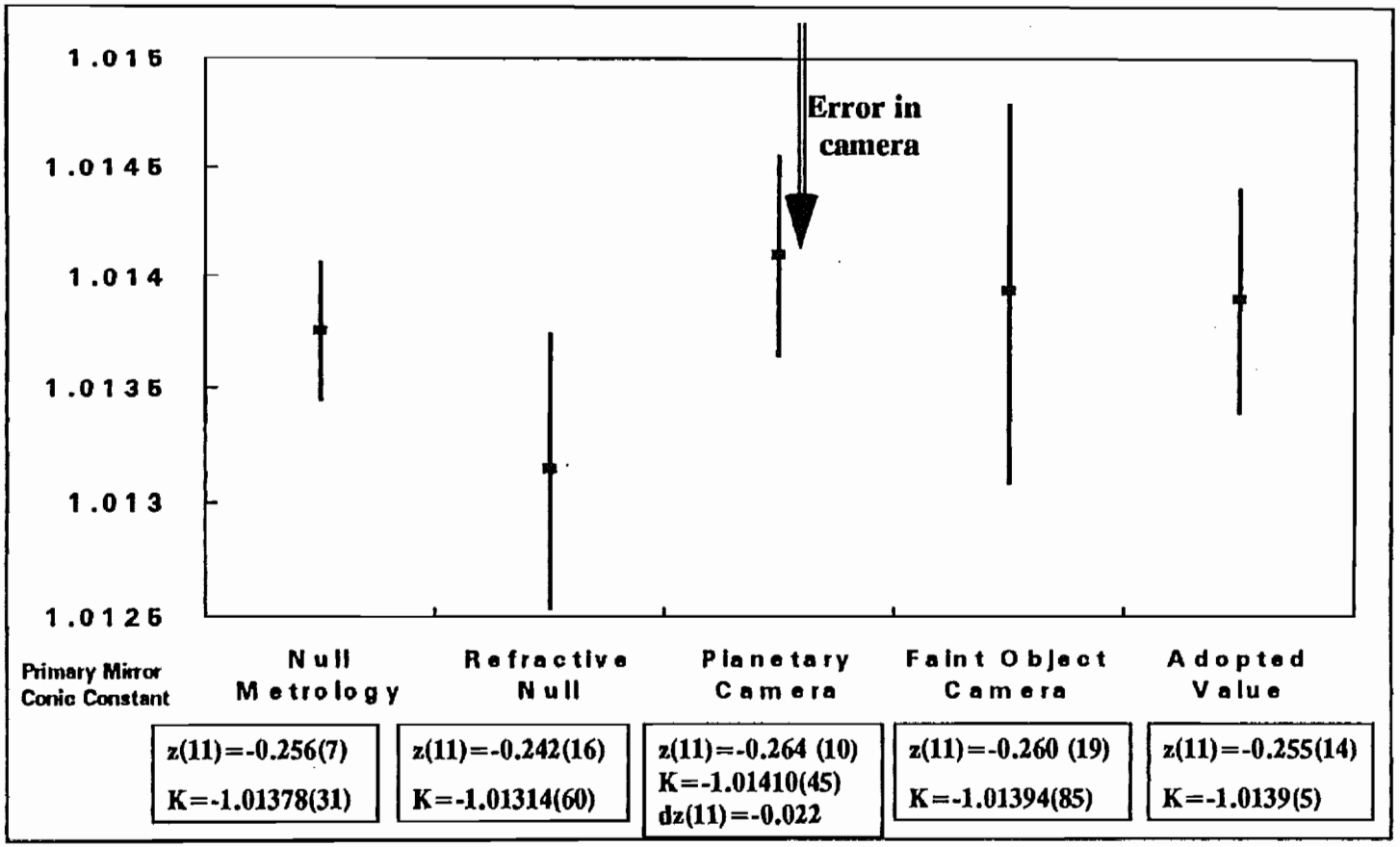

Figure 1. Estimates of the HST primary mirror conic constant.

Design File Memo: DFMEK #16

December 25, 1991

1992

TO: Bob Korechoff, Jet Propulsion Laboratory

FROM: Tom Wolfe (716-253-2640) T.F.W.

SUBJECT: Kodak Analysis of WF/PC-1 Flight Relay Interferograms

During May of 1991, Kodak was given WF/PC-1 flight relay data books which contained instant photography pictures of the original interferograms taken during the assembly of each relay camera head. The only exception being a missing data book for Wide Field Camera 4. A large number of these interferograms, which represent different stages of buildup, are contained in each data book. Some of these interferograms had the expected three struts associated with the SM spider, while others had a surprising four struts (see Figure 1). We were informed by the optics assembly personnel that a four strut spider was used during the early stages of assembly, which was later replaced by the flight spider containing only three struts. Therefore, some interferograms containing four struts should be expected when one examines these data books.

But there is another way that four struts could be observed. This phenomenon could be caused by the convex retroreflecting sphere being incorrectly placed at the rear conjugate location of a relay containing only three struts. Unless this retro sphere is precisely aligned, a catseye pupil could appear as shown in Figure 2. This test configuration will cause the wavefront to flip over upon itself, creating a false image of a fourth strut. In interferometry, a flipped wavefront tends to cancel all odd ordered aberration terms (coma; trefoil etc.), while leaving the even ordered terms

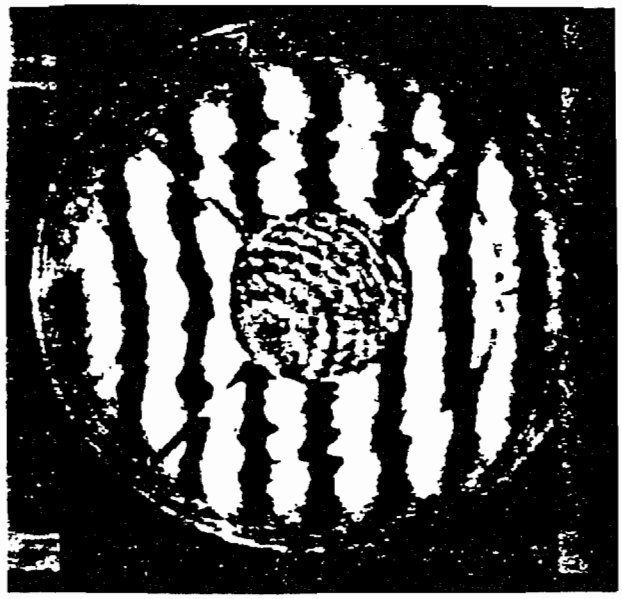

PC-7 with Three Struts

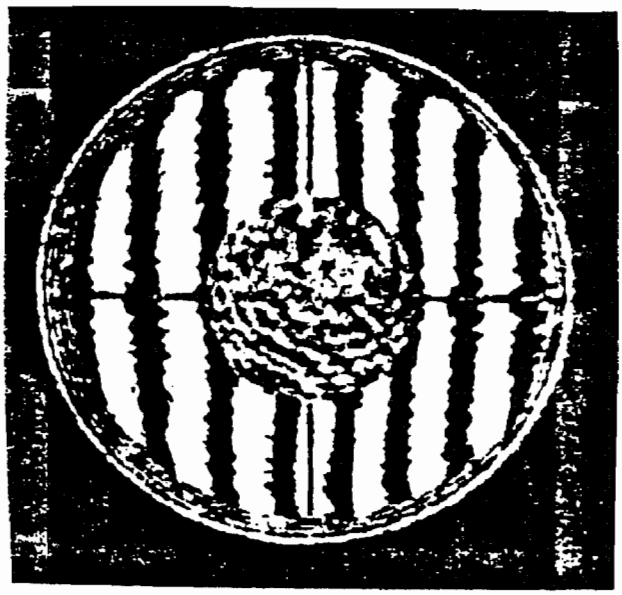

WFC-2 with Four Struts

Figure 1

(power, spherical etc.) unchanged. Since this analysis will concentrate only on the amount of residual Seidel spherical aberration (SA3) present in each flight relay, then the analysis of these flipped interferograms is still valid.

One problem encountered during the analysis was the lack of a sufficient number of fringe centers to be digitized. On average the number of fringes varied between 6 and 8 for each picture and thus provided only 250 to 370 data points over the clear aperture of each relay. Hence, the reported single-pass wavefront RMS values should be viewed as only a global contribution from third-order, primary aberrations and is not by any means a representation of the low-to-mid spatial frequency domain.

A further hinderance to the analysis was the poor edge definition encountered around both the central obstruction and the pupil's outer diameter, in most of the pictures throughout each data book. This was obviously due to the test configuration's inability to properly reimage either of these planes onto the Zygo's vidicon detector. Since there was a lack of any fiducials to properly scale each fringe pattern with respect to the physical pupil's size and shape, we were left with the only option of digitally "guessing" the diameter of the central obstruction in order to conform with the proper SM obscuration ratio for each camera. Therefore, a relatively sharp central obstruction was used as the criterion for choosing pictures from each relay's data book. This resulted in the selection of 3 to 7 candidate interferograms from a total of approximately 50 to 80 pictures per book. A sensitivity analysis was eventually performed to determine the uncertainty associated with digitally

"guessing" the diameter's of each central obstruction. They are:

SA3: + or - 0.05 waves p-v

conic: + or - 0.00008

RMS: + or - 0.01 waves p-v.

In fringe scanning interferometry, the polarity or sign of the wavefront aberrations are usually determined by knowing a priori the direction of the wedge between the reference surface and the wavefront under test. Since this information was never recorded on any of the pictures in the data books, I instead concentrated my attention on areas within the interferograms where the fringes crossed the struts. Upon careful examination of Figure 3, a characteristic diffraction "V" can be seen at each interface between a fringe and a perpendicular strut. Using a spare relay assembly, the exact same test configuration was repeated in the lab. The same diffraction "V" again manifested itself and clearly flipped it's direction as the wedge was reversed on the reference surface. This was verified for all focus settings of the Zygo interferometer. The test configuration was modified by moving the retro sphere to the rear conjugate position to flip the wavefront and thus produce an interferogram with four struts instead of three. In all cases, the diffraction "V" pointed in the direction of higher order fringes (as defined by the analysis software). Knowing the polarity of the spare relay's aberrations, I was able to discern the polarity of most of the flight relay interferograms. It should be noted that a negative spherical aberration indicates a wavefront with a trailing edge.

The software that was used to perform the analysis was FAST! V/AI,

version 3.03, manufactured by Phase Shift Technology, Inc. Figures 4 and 5 depict a typical output of a thermal-vacuum test for WFC-3 at 0°C. The starting interferogram is shown in Figure 3 and is thought to represent a flipped wavefront. Note the relatively small amount of coma present.

The following discussion centers primarily on the method of analysis used and the results for each individual camera relay.

Wide Field Camera 1, S/N 05

A total of three interferograms were analyzed; one with three struts dated 5/9/83, and two with four struts (flipped wavefront) dated 5/13/83. All three pictures were taken at 20°C. A range of 86.8% to 93% of the fringe apertures were scanned on different pictures to conform with a 43.3% SM obscuration ratio. The average Seidel S.A. was -0.09 waves p-v at 0.6328 microns, which is equivalent to a conic error of -0.00015 on the PM.

Wide Field Camera 2, S/N 06

A total of four interferograms were analyzed; two with four struts dated 9/14/81 and 6/11/82, and two with three struts dated 9/14/82 and 5/6/83. All four pictures were taken at 20°C. Because the first two pictures represent the relay in a prealignment condition (four struts), their results were quite different and thus were not included in the final average reported here. Approximately 90% of the fringe apertures were scanned on each picture to conform with a 43.3% SM obscuration ratio. The average Seidel S.A. was -0.31 waves p-v at 0.6328 microns, which is equivalent to a conic error of -0.00050 on the PM.

Wide Field Camera 3, S/N 03

A total of seven interferograms were analyzed; two with three struts dated 5/9/83, and five with four struts (flipped wavefront) taken during a thermal-vacuum test dating from 5/10/83 to 5/11/83. The first two pictures were taken at 20°C but the thermal-vacuum pictures ranged from -10°C to +40°C. A range of 89.6% to 93.3% of the fringe apertures were scanned to conform with a 43.3% SM obscuration ratio. The results of the thermal-vacuum test are shown in Figure 6. The amount of Seidel S.A. almost doubled when the relay was taken from 20°C to 10°C. Upon interpolation of the curve, approximately -0.78 waves p-v of Seidel S.A. exists at 8°C. But if we compare the amount of Seidel S.A. at 20°C during the thermal-vacuum test (-0.46 waves p-v) to the average Seidel S.A. of the first two pictures with only three struts (-0.42 waves p-v), we find that a bias of +0.04 waves p-v will need to be added to the thermal-vacuum data. This bias is assumed to be caused by the interpolation of a flipped, centrally-obstructed wavefront containing only even-ordered aberrations. Hence, the predicted amount of Seidel S.A. is -0.74 waves p-v (-0.78+0.04) at 8°C, which is equivalent to a conic error of -0.00122 on the PM.

Wide Field Camera 4, S/N 04

The interferogram data book could not be located for analysis.

Planetary Camera 5, S/N 08

A total of four interferograms were analyzed; two with four struts dated 10/12/81, and two with three struts dated 5/5/83. All four pictures were taken at 20°C. Because the first two pictures represent the

relay in a prealignment condition (four struts), their results are not included in the average reported here. 89.9% of the fringe apertures were scanned on the last two pictures to conform with a 42.1% SM obscuration ratio. Since the characteristic diffraction "V" was absent from these interferograms, it was impossible to assign the correct polarity to the spherical aberration and conic error. The average Seidel S.A. was (?)0.55 waves p-v at 0.6328 microns, which is equivalent to a conic error of (?)0.00090 on the PM.

Planetary Camera 6, S/N 06

A total of five interferograms were analyzed; two with three struts dated 5/5/83, and three with four struts (flipped wavefront) taken during a thermal-vacuum test dated 5/20/83. The first two pictures were taken at 20°C while the thermal-vacuum pictures ranged from -10°C to +20°C. A range of 85.3% to 87.7% of the fringe apertures were scanned to conform with a 42.1% SM obscuration ratio. The results of the thermal-vacuum test are shown in Figure 7. The amount of Seidel S.A. varied almost linearly with temperature, so a straight line was fit to the data points. After interpolation, it can be shown that -0.52 waves p-v of Seidel S.A. exists at 8°C. Again, if we compare the amount of Seidel S.A. at 20°C during the thermal-vacuum test (-0.45 waves p-v) to the average Seidel S.A. of the first two pictures with three struts (-0.53 waves p-v), we find that a bias of -0.08 waves p-v will need to be added to the thermal-vacuum data in which the wavefront has been flipped. Hence, the predicted amount of Seidel S.A. is -0.60 waves p-v (-0.52-0.08) at 8°C, which is equivalent to a conic error of -0.00098 on the PM.

Planetary Camera 7, S/N 05

A total of three interferograms were analyzed; one with three struts dated 5/6/83, and two with four struts (flipped wavefront) dated 5/18/83. All three pictures were taken at 20°C. Approximately 89% of the fringe apertures were scanned on each picture to conform with a 42.1% SM obscuration ratio. The average Seidel S.A. was +0.15 waves p-v at 0.6328 microns, which is equivalent to a conic error of +0.00025 on the PM.

Planetary Camera 8, S/N 04

A total of three interferograms were analyzed; one with three struts dated 5/6/83, and two with four struts (flipped wavefront) dated 5/16/83. All three pictures were taken at 20°C. A range of 79.3% to 89.3% of the fringe apertures were scanned to conform with a 42.1% SM obscuration ratio. The average Seidel S.A. was -0.42 waves p-v at 0.6328 microns which is equivalent to a conic error of -0.00069 on the PM.

A summary of the preceeding results, as well as the single-pass wavefront RMS values, are tabularized in Figure 8. The equivalent conic constant error is derived from the Seidel S.A. by the following relation:

PM conic error =(4*R^3*SA3*.6328)/Y^4

where R (PM rad of curv) =11040000 um and Y (PM pupil rad) =1200000 um.

Catseye Pupil

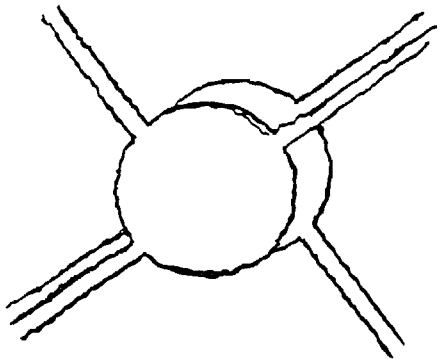

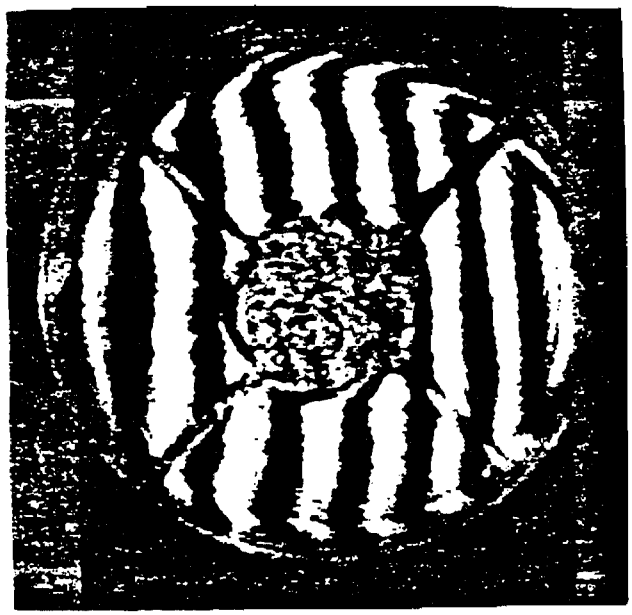

PC-7 with Four Struts
(flipped wavefront)

Figure 2

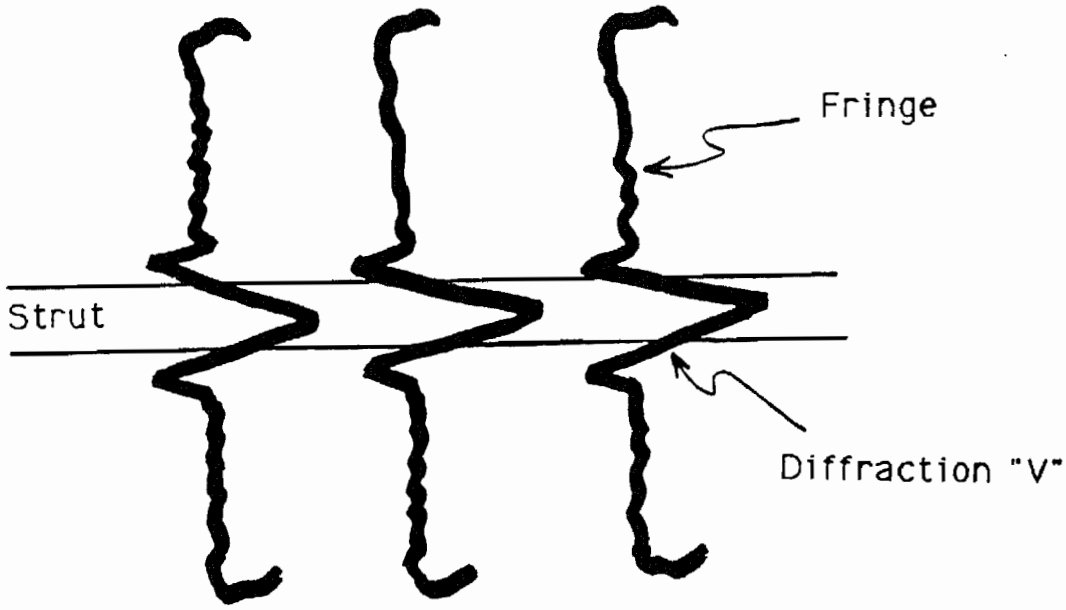

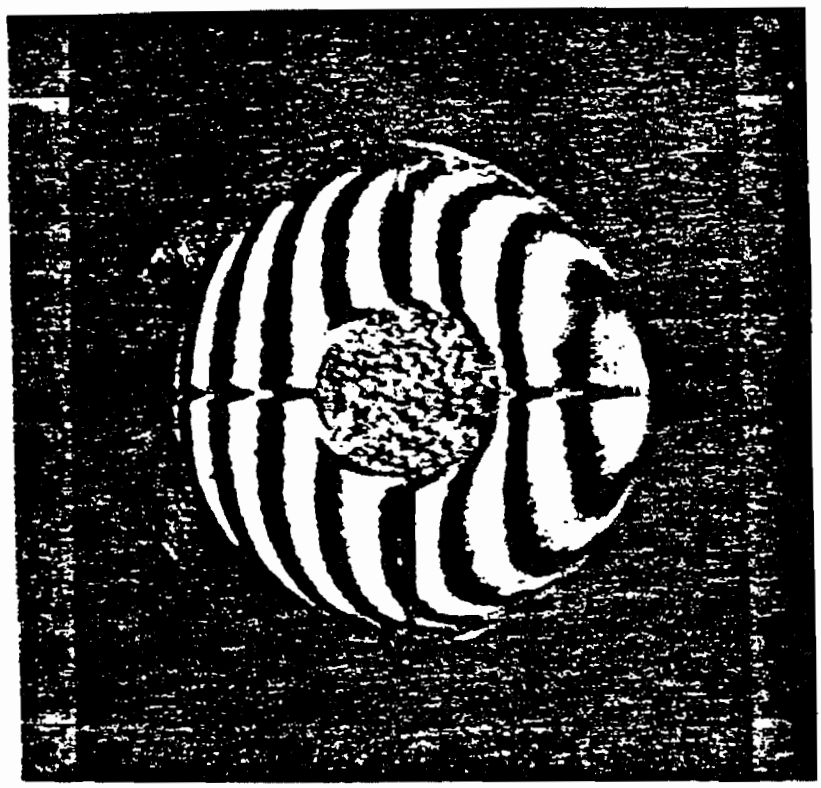

Example: Wide Field Camera 3

Figure 3

Example: Wide Field Camera 3

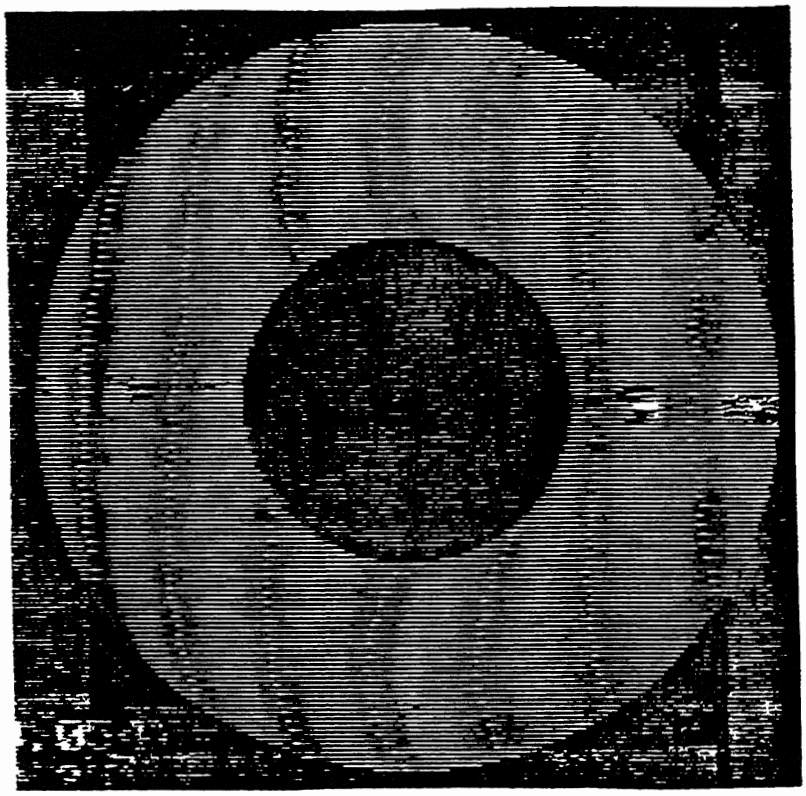

Digitized Fringe Pattern

Quality of Fit of Fringe Centers

Term	N	Rms fit	Zernike Polynomial Coefficients (in waves)					
Plane	2	0.105	1.823	-0.069				
Sphere	3	0.090	1.813	-0.068	-0.064			
4th Order	8	0.043	1.811	-0.065	0.005	-0.013	0.043	0.01
			-0.000	-0.133				

Figure 4

Example: Wide Field Camera 3

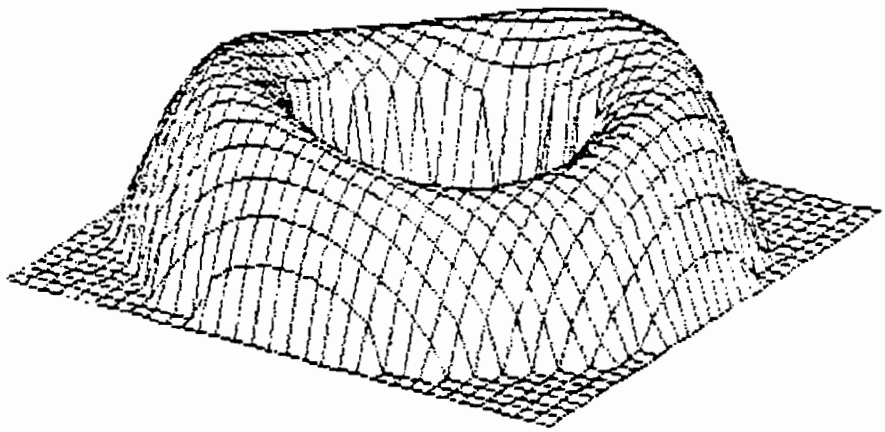

Single-Pass Phase Map

SEIDEL ABERRATION COEFFICIENTS FROM FRINGE CENTERS

Magnitude waves	Angle deg	Aberration
1.812	-2.1	TILT
0.009		FOCUS
0.090	53.3	ASTIGMATISM
0.032	-0.7	COMA
-0.798		SPHERICAL

	Wedge	Waveleng
TEST:	0.50	0.63
USER:	0.50	0.63

Terms Subtracted From Data
Piston Tilt Focus

Residual Wavefront Variations Evaluated at Fringe Centers (in waves)

Number of pts	Peak	Valley	P-V	RMS	Strehl Ratio
329	0.086	-0.166	0.252	0.054	0.891

Residual Wavefront Variations Over Uniform Grid (in waves)

Number of pts	Peak	Valley	P-V	RMS	Strehl Ratio
2352	0.122	-0.167	0.289	0.064	0.851

Figure 5

Wide Field Camera-3 Data (5/10,11/83)

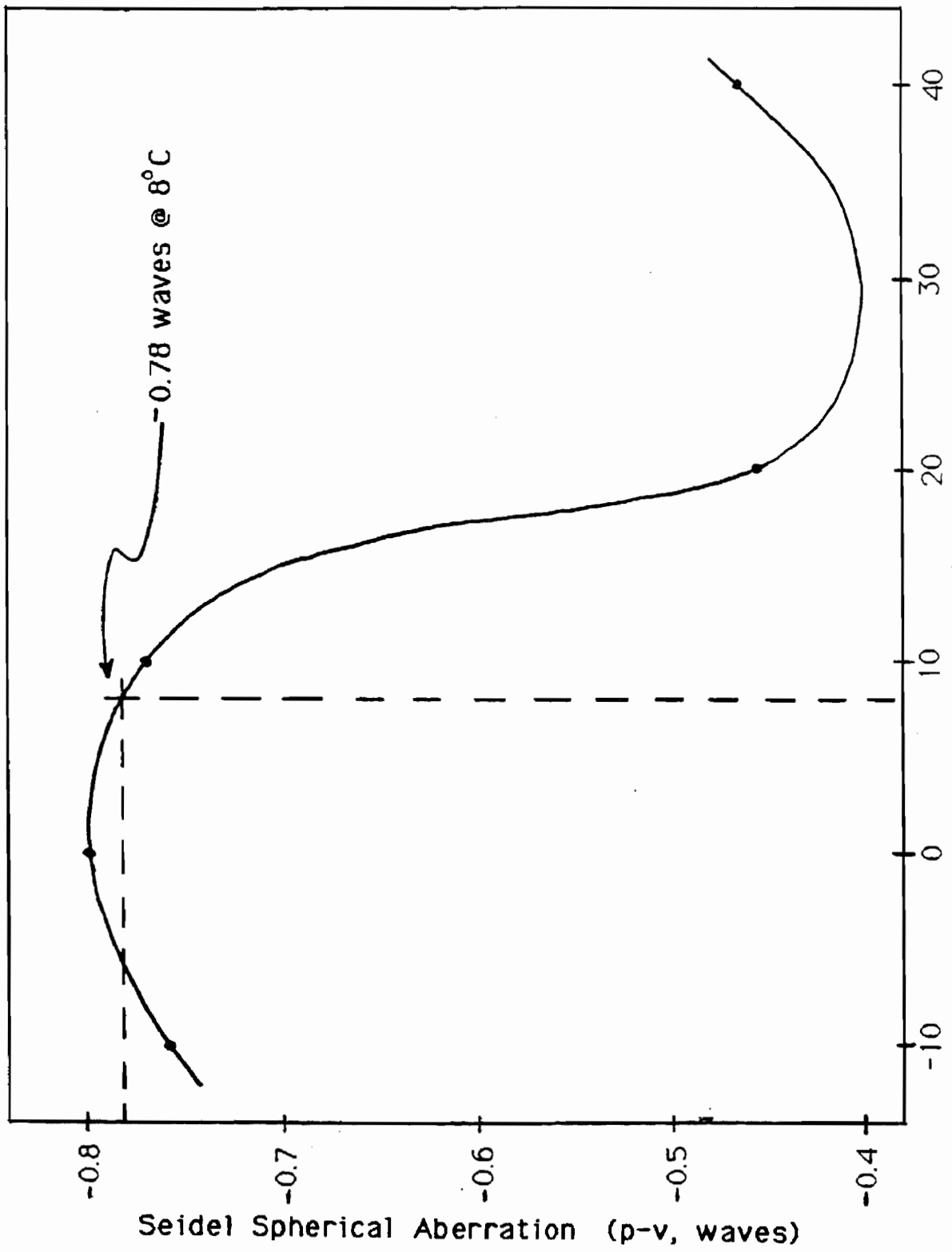

Figure 6

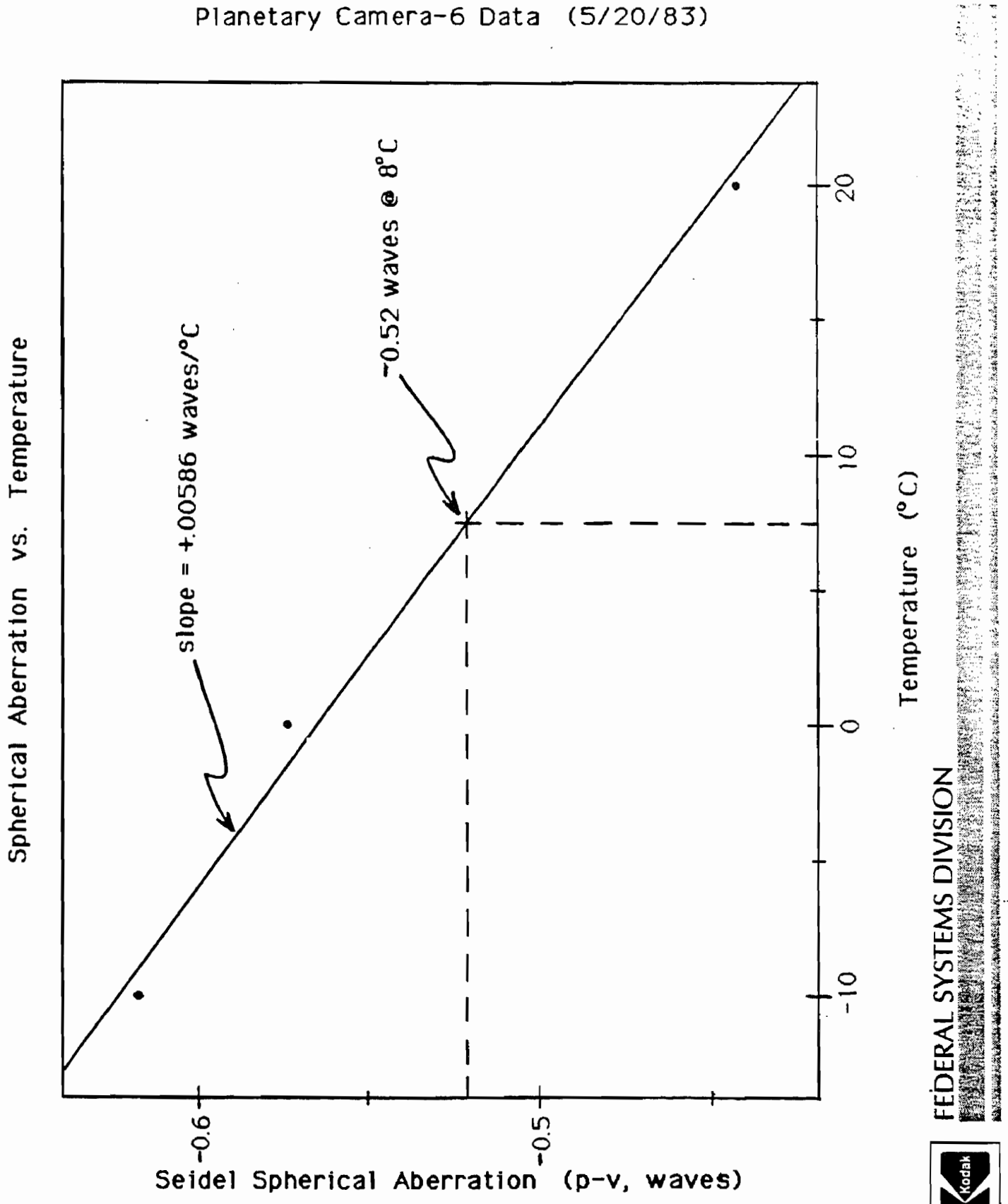
Planetary Camera-6 Data (5/20/83)
Spherical Aberration vs. Temperature
slope = +.00586 waves/°C
-0.52 waves @ 8°C
-0.6
-0.5
Seidel Spherical Aberration (p-v, waves)
20
10
0
-10
Temperature (°C)
FEDERAL SYSTEMS DIVISION
Kodak

Figure 7

Summary Table

Camera Relay	Serial Number	SM Obscuration (%)	Pictures Scanned	Temperature (°C)	Seidel Spherical Aberration (+or- 0.05 waves p-v)	Equivalent Conic Error on ST PM (+or- 0.00008)	Single-Pass Wavefront RMS (+or- 0.01 waves)
WFC-1	05	43.3	3	20	-0.09	-0.00015	0.02
WFC-2	06	43.3	4	20	-0.31	-0.00050	0.03
WFC-3	03	43.3	2	20	-0.42	-0.00070	0.04
			5	8	-0.74	-0.00122	0.04
WFC-4	04	43.3	-	-	-	-	-
PC-5	08	42.1	4	20	?0.55	?0.00090	0.05
PC-6	06	42.1	2	20	-0.53	-0.00086	0.04
			3	8	-0.60	-0.00098	0.04
PC-7	05	42.1	3	20	+0.15	+0.00025	0.03
PC-8	04	42.1	3	20	-0.42	-0.00069	0.03

Figure 8

December 3, 1992

TO: HST Flight Systems and Servicing Project Optics Leads

FROM: HST Optics Lead Engineer/J. Wood/442

SUBJECT: HST Optical Prescription Statistics

This memorandum discusses the data which was used to determine the adopted value for the primary mirror conic constant for the as - built HST. It is a re-issue of the memo of August 28 1991 but with a correction of the Δ K which was adopted by JPL (+ 0.001) which includes PC6 spherical and plate-scale errors, and correction for the proper equation to calculate K from RMS wave front error.

The data is divided into two separate groups: "fossil" data from the measurement program on the reflective null corrector at Danbury and phase retrieval "pr" data derived from images from the cameras aboard HST.

FOSSIL DATA

After all the measurements were completed at Danbury, it was found that the radius of curvature of the upper null corrector mirror was measured short by 59.3μm from the nominal design value. This tended to compensate for the inter-mirror spacing error which was also measured short by 72μm. When all the parameters were available, a new value of the conic constant for the HST primary mirror was calculated by Bill Wetherell of ORA and independently by Laurie Furey of HDOS. Their numbers agreed closely with each other and also came within close agreement with the on-orbit PR data. The following values were presented to the HIORP IX meeting July 2, 1991.

L. Furey: $K = -1.01378 \pm 0.0003$ W. Wetherell: $K = -1.013756 \pm 0.0003$

The error bars are worst case.

After review of the final measurements at Danbury (see HIORP final report by Wetherell):

L. Furey: $K = -1.01377$ W. Wetherell: $K = -1.01376$

PHASE RETRIEVAL

Various teams reported studies of selected FOC and HARP images. I will list here the results from those teams which provided final reports to NASA. Preliminary results from other teams were in general agreement with these data but were not considered finished for lack of a final report to the writer. Residual SA (ΔK) in the PC-6 camera has been measured from interferograms of the relays before launch and from differences between it and WF1 (with no measurable residual SA) on orbit. I am using a Δ conic for the correction for spherical aberration in the PC-6 camera of $\Delta K = +0.001$ based on the best estimate by JPL and the memo by Tom Wolfe (DFMEK #16). The numbers in parenthesis are the number of images used to derive the K value.

Team	Measured value	Corrected for $\Delta K = 0.001$ for PC6*
J. Fienup	PC-6 (few) $= -1.0150 \pm 0.0006$	OTA alone $= -1.0141$
R. Lyon	FOC (7) $= -1.0138 \pm 0.0004$	FOC (7) $= -1.0139$
R. Lyon	PC-6 (19) $= -1.0143 \pm 0.0005$	OTA alone $= -1.0134$
Meinels	PC-6 (96) $= -1.0143 \pm 0.0002$	OTA alone $= -1.0134$
Roddier	PC-6 (30) $= -1.0151 \pm 0.0002$	OTA alone $= -1.0142$
Roddier	FOC (few) $= -1.0131$ N/A	FOC (few) $= -1.0132$
Vaughan	PC-6 (30) $= -1.0147 \pm 0.0003$	OTA alone $= -1.0138$
Vaughan	WF1 (few) $= -1.014472\ ^{+0.0004}_{-0.0002}$	WF1 (few) $= -1.0146$

* all are corrected by -0.0001 for equation: $K = -1.00223 + (Z_{11}/35.3)$. The number 36.03 was used earlier in place of 35.3.

AVERAGES

If one takes the arithmetical mean and computes the population standard deviation (sigma) for all of the right-hand column numbers for phase retrieval alone:

1) $K_{pr} = -1.013825 \pm 0.00044$; $n = 8$

Similarly, the average of the two calculations based on the fossil data gives:

2) $K_f = -1.013765$

If one considers all ten K - values of equal weight and computes the arithmetical mean and population standard deviation:

3) $K_{all} = -1.013813 \pm 0.00040$; n = 10

The straight average of 1) and 2) is:

4) $K_{avg} = -1.013795$

It is probably better to assign lower weight to some of the phase retrieval results. For example, the R. Lyon result from the PC6 data should probably have less weight than his FOC data since the PC secondary obscuration moved around in the pupil in an unpredictable way as a function of the field position of the star image. Only late in the HARP (Hubble Abrerration Recovery Program) program was it discovered that the "optical center" of PC6 is at pixel location 245, 310. Similarly the few FOC images analyzed by the Roddiers should not have equal weight to their 30-image result from PC6 where they were able to find the "optical center" of PC6 and show great detail in the recovered wavefront at the pupil.

We have not included the results from Chris Burrows as no final report has yet been submitted to NASA by him. However, his results as presented to HIORP VII on February 7, 1991 show $K = -1.0137 \pm 0.0008$ (FOC) and $K = -1.0148 \pm 0.0005$ (PC6).

Taking into account the precision of the fossil data and the fact that James Fienup, in his appendix to the HIORP final report, insists on the higher value of $K = -1.0142$ from his phase retrieval analysis using Fresnel diffraction, the HIORP has adopted:

$$\mathbf{K = -1.0139 \pm 0.0003}$$ one sigma

APPENDIX III
ORA FINAL REPORT

prepared for
VITRO CORPORATION
Washington, D.C. 20024

FINAL REPORT TO THE HUBBLE INDEPENDENT OPTICAL REVIEW PANEL ON RNC FOSSIL DATA STUDY

prepared by
Mark Kahan
William B. Wetherell

Final Revision Date:
July 11, 1991

OPTICAL RESEARCH ASSOCIATES
945 Concord Street
Framingham, Massachusetts 01701

TABLE OF CONTENTS

TEXT

TABLES

FIGURES

1.0 INTRODUCTION AND SUMMARY

Optical Research Associates (ORA) has supported the Hubble Independent Optical Review Panel (HIORP) through Vitro Corporation to provide independent verification of analyses performed by Hughes Danbury Optical Systems (HDOS) and other parties to the efforts to quantify the errors in the Hubble Space Telescope (HST) optical telescope assembly (OTA). The ORA efforts were directed mainly at fossil data retrieval to determine the primary mirror conic constant KP of the flight hardware from analysis of the reflecting null corrector (RNC), the refracting null corrector (RvNC), and the inverse null corrector (INC). New computations of KP have been performed based on new measurements of the RNC design parameters as fabricated, and on interferograms taken with the RvNC. We have also analyzed the effects of other components in the OTA on spherical aberration seen on orbit, and changes in the primary mirror conic constant which might arise from gravity release.

1.1 SUMMARY OF RESULTS

Remeasurement of the RNC parameters are now complete, as of July 1, 1991. Based on this data,

$$KP = -1.01376 \pm 0.00031$$

The tolerance represents the range over which KP will vary if all measurement tolerances are simultaneously pegged to the limit either increasing or decreasing KP. The value quoted above agrees very closely with that computed by HDOS, -1.01377. Both values assume the error introduced to be a pure conic. There is in fact a small higher order component to the error, since testing this conic against the most recent RNC model leaves an rms wavefront residual of about 0.005 waves at 632.8 nm.

There has been disagreement between earlier fossil data results and those of the phase retrieval program analyzing images taken by the HST with the wide field/ planetary camera (WF/PC) and the faint object camera (FOC). Adjustments to the fossil data and WF/PC data have brought both into close agreement with FOC phase retrieval data. In the case of the WF/PC, overcorrected spherical aberration in the WF/PC optics added to the OTA error, making the derived KP too large. In the case of the fossil data, three parameters in the RNC (besides the previously discovered field lens position error) were outside cited measurement accuracies, making the derived KP too small. Table 1.1 summarizes the four key parameters and their changes:

TABLE 1.1 Key RNC Parameters Differing from Original Data

RNC Parameter (mm)	Original	New Data	Change
CORI focus to M1 vertex	62.742	62.717	- 0.025
M1 vertex to M2 vertex	469.649	469.577	- 0.072
M2 vertex to field lens	210.751	212.056	+ 1.305
M1 radius	286.727	286.6677	- 0.0593

While waiting for final values for the RNC parameters, much effort was spent in looking into other ways of deriving KP, and in looking for other sources of spherical aberration which might account for the differences seen between early fossil data results and phase retrieval results.

There are four interferograms of the flight primary which were taken with the RvNC. We had hoped these would eliminate doubts about the RNC fossil data. Our analysis suggests that the RvNC is too sensitive to defocus to aid in establishing KP to the level of accuracy we require. Two of the four values of KP we did obtain clustered at - 1.0129, and the other two clustered near - 1.0135.

We also looked for other sources of error in the OTA. Interferograms of the primary and secondary do show small residuals of spherical aberration. That of the primary mirror is undercorrected, based on one set of interferograms. However, there are two sets of interferometric data in circulation, and the primary mirror residual spherical has been removed from one of them. (This is discussed in sections 5.2 and appendix 6.3.) The secondary mirror contributes some overcorrected spherical, but it affects KP by only about - 0.000027. Other possible sources of error are gravity release, errors induced by "hula hooping" of the primary mirror actuators, and deformations introduced when installing the primary mirror in its flight mount. If the deformation-induced wavefront error estimated by HDOS were entirely overcorrected spherical aberration, it would be equivalent to a conic constant change of - 0.0005. However, neither the form nor the sign of the change in shape are definitely known, nor are they expected to produce pure spherical aberration.

1.2 TOPICS DISCUSSED IN THIS REPORT

The bulk of this report was completed prior to receipt of final RNC data, and discusses other topics related to the HST performance analysis. First, our analysis and that of several other parties was performed using Code V®, ORA's commercial lens design package. Several potential error sources within the Code V options which can arise from misinterpretation of program conventions are discussed. Second, potential errors within the RNC which might have affected the results were examined, to assess the likelihood that they occurred. Third, HDOS data reduction of four RvNC interferograms was examined, and the relative sensitivity of the RvNC and RNC to focus errors was analyzed, to assess the credibility of using the RvNC data to determine the true value of KP. Fourth, the OTA model was examined to see what contributions to spherical aberration may be made by surface figure error in the primary and secondary mirrors other than the gross error in the primary mirror conic constant. Fifth, errors which can arise from gravity release effects were considered briefly.

ORA has performed a number of tasks related to HST beyond the direct purview of our HIORP activities. Section 6 discusses two of those tasks, WF/PC tolerancing and analysis of the HDOS SAGE lens, for your information.

2.0 CODE V COMPUTATION TECHNIQUES

Four Code V computation routines have been used in this analysis. AUTO, the automatic design routine, was used to analyze the RNC to determine the values of KP corresponding to various estimates of RNC parameters. WAVE, the rms wavefront error analysis routine was used for RNC, RvNC and OTA performance analysis, the latter modelled with and without interferometric surface figure maps for the primary and secondary mirrors. RSI, which traces individual rays, was used to analyze the amount and form of total spherical aberration by tracing rim rays through the OTA. THO, which tabulates surface contributions to third order Seidel ray aberrations, was also used to analyze the amount and form of third order spherical aberration. Each of these has characteristic restrictions and sign conventions which must be understood to interpret results generated with each.

2.1 AUTO AUTOMATIC DESIGN ROUTINE

AUTO has a number of default values and assumptions which must be understood to correctly interpret results generated with it. The user can choose to base the optimization on ray positions in the focal plane (the default) or optical path along each ray (OPD option). The latter has been used here. A key to the accuracy of the result is the number of rays used to analyze the optical system This is defined by the parameter DEL, which is the distance between rays in a rectangular grid given as a fraction of the normalized pupil radius (see figure 2.1). The default value of DEL is 0.358, which would trace 12 rays in one-half of an unobstructed pupil (since most optical systems show at least bilateral symmetry, it is seldom necessary to trace rays over more than half the pupil area.) The minimum allowable value of DEL is 0.1054, which generates 138 rays in half an unobstructed circular pupil.

Since the rays are set up in a square matrix, each represents a square section of the pupil function, in effect. When a lens system has large amounts of spherical aberration, as does the OTA, a small rectangular grid can misrepresent the amount of spherical aberration present, depending on the number of points in the grid coming close to the pupil boundary. As the grid spacing is reduced by decreasing DEL, the number of rays increases and the positions vary in a way which can affect the outcome of the AUTO optimization. In using AUTO to compute the primary mirror conic constant, we found that the value of KP went through a damped oscillation as DEL varied from 0.358 to 0.1054. Based on an empirical study performed early in the project, we settled on DEL = 0.1108 as a local mean which produced a value consistent to within $\pm$ 0.00002. This was for an unobstructed aperture, however, and DEL = 0.11 may be better for our obstructed aperture.

A final factor, recognized late in the game, is that AUTO ignores any pupil boundaries and obstructions defined by surface parameters within the lens file. In order to model the obstruction, it is necessary to use the AUTO parameter OBS 0.33. This embarrassingly late discovery eliminated a persistent 0.0001 discrepancy between

Figure 2.1: Precision of AUTO depends on ray spacing DEL

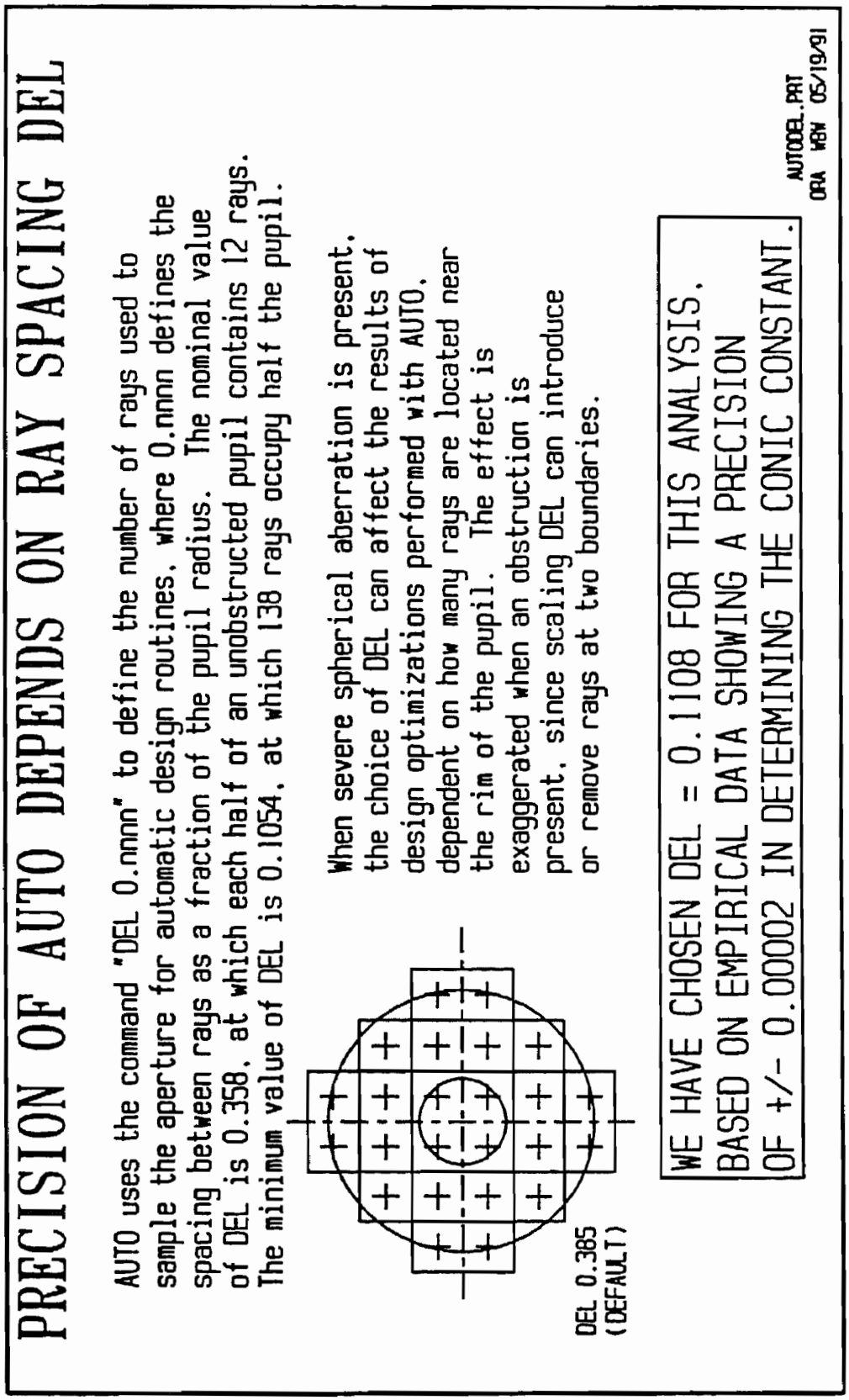

ORA and HDOS values of KP for a given set of RNC parameters. (HDOS uses a proprietary design program capable of analyzing the pupil with rotationally symmetric distributions of rays, which is somewhat more suitable to systems dominated by spherical aberration.)

Before we realized that the OBS command should be used, all AUTO runs were done with the command set AUT;OPD;DEL .1108;GO. More recent AUTO runs have used the command set AUT;OPD;OBS .33;DEL .1108;GO. We have updated all data runs critical to definition of KP to the latter format. We have not rerun some data sets used to compare different error sources, where the resultant +0.0001 error in KP is not critical to interpreting results. The technique used will be identified in each case.

2.2 WAVE RMS WAVEFRONT ERROR ROUTINE

WAVE traces a large square matrix of rays through a lens system to determine its rms wavefront error. In this case, because a diffraction calculation is performed, all defined surface boundaries and obstructions play a part in the calculation, if the ray grid is fine enough to encounter them. We examined the results of varying the number of rays across the pupil, defined by the parameter NRD, on the rms of the OTA. At the nominal value of NRD (20), the computer rms of the OTA can be off by 0.010 (all values of rms are quoted in waves at 632.8 nm, unless otherwise stated.) We settled on NRD 128 for our calculations, since that reduced the rms wavefront error inaccuracy to about 0.001.

WAV can be used in several ways to get at aberration amounts and form. If the parameter NOM is included, it will compute the rms in the exact image surface as defined. It also estimates the distance from the nominal image to the minimum rms wavefront error image, and estimates the rms at both best individual focus and best average focus if more than one image point is specified. The only aberration which displaces the minimum rms image axially from paraxial focus is spherical aberration. Thus if the nominal image surface is placed at paraxial focus, the direction to the minimum rms image surface tells whether the spherical aberration is over- or under-corrected. In overcorrected spherical aberration, the rim ray always strikes the optical axis further along IN THE DIRECTION OF PROPAGATION.

2.3 RSI AND THO

RSI is the command used to trace individual rays. It also computes the OPD of the ray, compared to that along the principal ray, at the nominal image surface. If the image surface is placed at paraxial focus, RSI will unambiguously identify the magnitude and sign of spherical aberration if spherical is the dominant aberration. (More about sign conventions in section 2.4) THO tabulates the third order Seidel contributions of each surface to the ray intercept height at paraxial focus, and can again be unambiguous about sign if properly interpreted. Should any of the powered elements in the system be tilted, however, it may not be an accurate measure of performance even at the "third order" level.

A MACRO named FORDER has been made available to calculate third and fifth order Seidel surface contributions, plus seventh order spherical. Its properties are analogous to those of THO. It is accessed in the same manner as a .SEQ file. Typing IN FORDER 1 0 will tabulate individual and net surface contributions. As with THO, FORDER ignores surface tilts, and does not accurately reflect image quality where tilted power surfaces are present.

2.4 POTENTIAL SIGN AMBIGUITIES

WAVE focus, RSI, THO and FORDER can introduce sign ambiguities if their conventions are not understood. In general, the best place to examine image quality to determine the presence and sign of any spherical aberration is paraxial focus. If the aberration is nearly pure spherical aberration, any of the above four can be used to determine its sign. If there is only a small amount of spherical aberration in a large amount of random wavefront error, WAVE focus direction works best.

Two factors can affect the sign convention, the direction in which light is travelling (+ or - z), and the number of focuses through which the beam has passed.

Focus shift direction defined by WAVE is affected only by the direction in which light is travelling. If light is propagating in the +z direction, a positive focus shift from paraxial to minimum rms focus indicates overcorrected spherical aberration. If light is propagating in the -z direction, then a negative focus shift indicates the presence of overcorrected spherical.

THO, FORDER and the ray height at paraxial focus given by RSI are dependent on whether the image is at an odd- or even-numbered focus. At odd numbered focii, the upper rim ray (RSI 0. 1. 0. 0.) strikes the image surface above the axis for overcorrected spherical, and THO, FORDER and RSI ray height will be positive. At even numbered focii, the upper rim ray strikes below the axis for overcorrected spherical, and the signs are negative. The direction of travel has no effect.

OPD at paraxial focus computed by RSI 0. 1. 0. 0. is unambiguous if third order spherical is the dominant aberration: negative means overcorrected and positive means undercorrected spherical. Only if spherical is a small part of the net rms can the sign on OPD be ambiguous. The presence of an upturned edge or large amounts of higher order spherical may also cause the upper rim ray OPD to give erroneous results on the sign of the net aberration.

3.0 REFLECTING NULL CORRECTOR ANALYSIS

The purpose of the RNC analysis is to compute the value of KP based on new measurements of the RNC design parameters and to evaluate the credibility of results generated from the new measurements. Unfortunately, the long delay in obtaining the final RNC parameters, the radii of the upper and lower mirror, left us with data for the RNC which yielded a value for KP substantially smaller than that derived by phase retrieval, raising credibility issues as to which value should be believed. Much of the analysis described here addresses the credibility issues which existed before the final radii data was obtained. Since differences between the original RNC component spacing measurements and the new measurements are beyond the known measurements mistake in the field lens position, the question of changes in spacings and when they might have occurred was considered to be significant. Although the new radii measurements have resolved the basic difference between fossil and phase retrieval results, this report retains results of analyses performed before radii were proven to be in error.

3.1 RESULTS OF RNC PARAMETERS REMEASUREMENT

New measurements of the RNC component spacings were made directly between the mirror and field lens surfaces, in the test tower. (The RNC has remained undisturbed in the test tower since completion of the primary mirror.) The original measurements were not made directly, but rather were made using metering bars and interferometric techniques to measure differences between centers of curvature of the two mirrors, the vertex of the field lens, and the focus of the CORI interferometer. Figure 3.1 illustrates the two measurement techniques. New measurements have been made of the three metering bars A, B and C, and the component spacings CM, between the CORI focus and the upper mirror M1, MM, between the vertices of M1 and the lower mirror M2, and MF, between M2 and the first vertex of the field lens FL. The error in MF, referred to as the field lens position error FLPE in earlier reports, is the principal source of the conic constant error. However, the error in MM has contributed significantly to the difference between RNC fossil data and phase retrieval data. Values for the six parameters know as of 02/18/91 are given in table 3.1

TABLE 3.1 New Measurements of the Metering Bars and RNC Spacings

Parameter		Value (mm)	Change (mm)
A	(M1 to M2 centers of curvature)	189.912	
B	(M2 center of curvature to FL vertex)	583.560	
C	(M1 center of curvature to CORI focus)	349.458	
CM	(CORI focus to M1 vertex)	62.717	-0.025 ± 0.010
MM	(M1 vertex to M2 vertex)	469.577	-0.072 ± 0.015
MF	(M2 vertex to field lens vertex)	212.056	$+1.305 \pm 0.005$

Figure 3.1: RNC spacing measurement techniques.

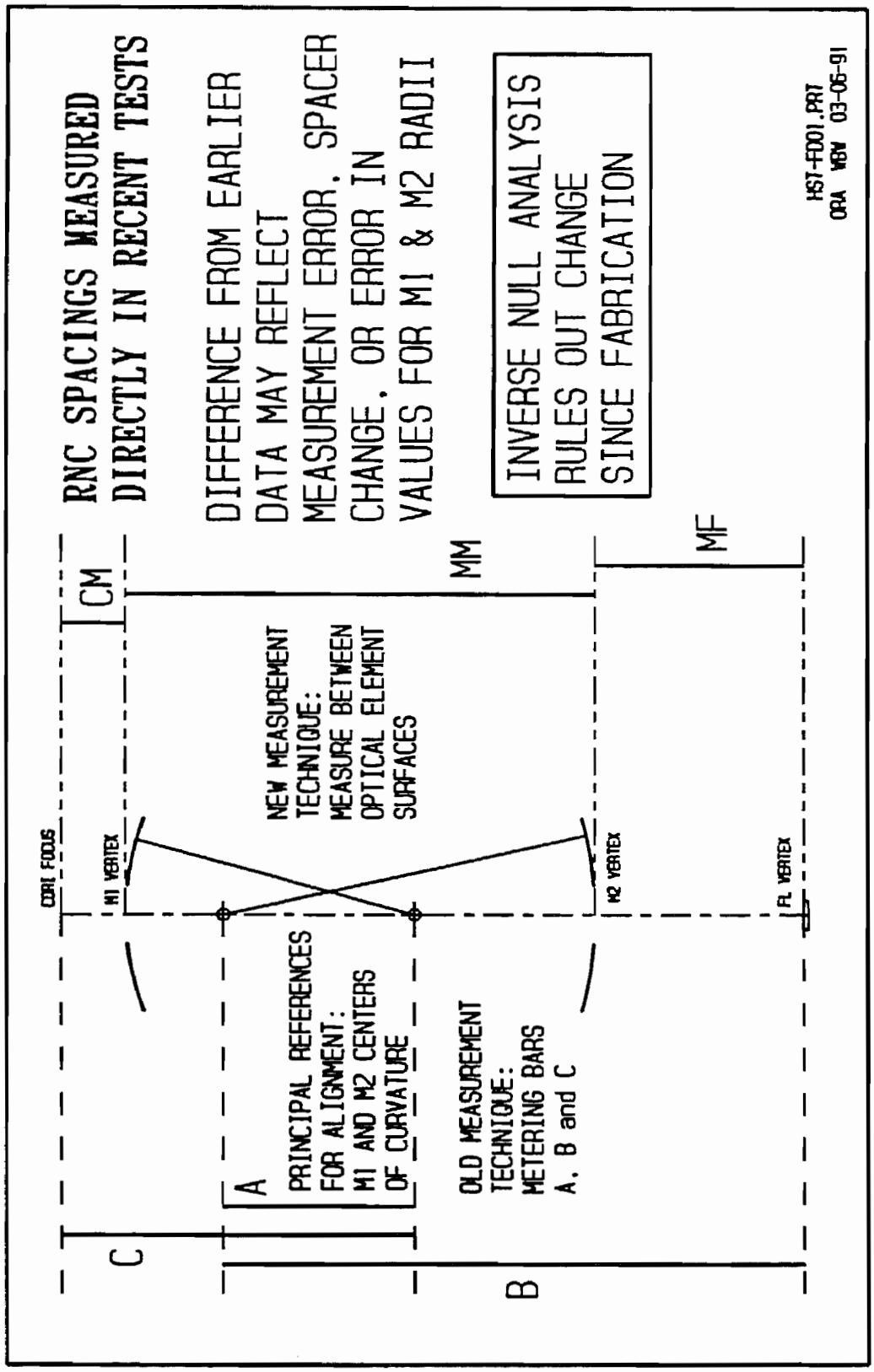

3.2 RNC FOSSIL RESULTS AS OF JULY 1, 1991

If the spacing measurements of table 3.1 were the only errors, then the nominal value of KP would have been - 1.01286 $\pm$0.00039. The values in figure 3.2 have been updated to include the new radii measurement. KP was derived by setting up a lens file containing the RNC data plus a primary mirror having a vertex radius of 11041.7 mm, and using AUTO to correct KP and the distance between the RNC field lens and the primary to minimize the net system rms wavefront error. When only KP and the spacing are corrected, there is a residual wavefront error of 0.005 waves rms, indicating a small residual of higher order spherical aberration. [Earlier in the study, AUTO runs using a combination of conic constant and sixth order aspheric coefficient did reduce the residual to 0.000 ($<$0.0005) waves rms. These have not been repeated for the new RNC parameters, nor with the OBS 0.33 term added to the AUTO run.]

To show the maximum range over which measurement tolerances allow KP to vary, all RNC parameters were pegged at the extreme values indicated by their tolerances as given by HDOS, first at the extreme producing the lowest magnitude for KP, then at the extreme producing the largest magnitude for KP. Figure 3.2 tabulates both the RNC parameters and the resultant values of KP for all three cases. Note that these represent the extreme range of KP, not the range appropriate to a statistical mix of errors.

3.3 INVERSE NULL CORRECTOR MEASUREMENTS

Since the RNC has been sitting idle for about eight years, the possibility that mirror spacings changed over that time has been suggested. There is no way of being completely certain that this has not happened, but there is evidence that changes in MM of the magnitude indicated in table 3.1 did not occur. Interferograms were taken of the RNC coupled with the INC immediately after the primary was completed, and that test has been repeated recently. We have analyzed the results of the change in MM on the RNC/INC combination. While there is little change in the spherical component of the wavefront with change in MM, there is a very large, multiple waves change in defocus which should show up clearly in reducing before and after interferograms. The focus change is much larger than would be caused by expected positioning errors in installing the INC. HDOS has reduced both sets of interferograms, and there is no such focus component evident in their data. We think it unlikely, therefore, that the parameters of the RNC have changed significantly in that interval. New radii measurements eliminate the need to look for such changes.

3.4 RECONCILING OLD AND NEW RNC PARAMETER MEASUREMENTS

Since the new measurement of MM was made between physical points on the mirror surfaces and the old measurement was made between centers of curvature for the two mirrors, adding the radii of the mirrors to determine the vertex spacing, errors in the values of either radius could be responsible for the discrepancy. Investigation of

CONIC CONSTANT CALCULATIONS FROM 02/18/91 + 07/01/91 MEASUREMENTS OF FOSSIL DATA

[FINAL REVISION TO MATCH HDOS DATA COMPLETED 07/09/91]

- THREE CASES RUN:
  - NMKNOM5.SEQ: Nominal as measured values used for all parameters
  - NMKLOW5.SEQ: All parameters pegged to tolerance limits giving lowest KP
  - NMKHIGH5.SEQ: All parameters pegged to tolerance limits giving highest KP
- KP computed using Code V® routine AUT;OPD;DEL 0.1108;OBS .33;GO. (KP Computed to ± 0.00002.)

		NMKLOW5.SEQ	NMKNOM5.SEQ	NMKHIGH5.SEQ
CORI to M1 vertex (mm)	MC	62.707	62.717	62.727
M1 vertex to M2 vertex (mm)	MM	469.562	469.577	469.592
M2 vertex to field lens (mm)	MF	212.051	212.056	212.061
Field Lens thickness (mm)		5.039	5.040	5.041
Field Lens index of refraction		1.515204	1.515205	1.515206
M1 radius (mm)	R1	286.6683	286.6677	286.6671
M2 radius (mm)	R2	372.8294	372.83	372.8306
Field Lens upper radius (mm)		553.893	553.983	554.073
Field Lens lower radius (mm)		184.765	184.755	184.745
DERIVED CONIC CONSTANT KP		**- 1.013453**	**- 1.013757**	**- 1.014063**

PRIMARY MIRROR CONIC CONSTANT = - 1.01376 ± 0.00031

Figure 3.2: RNC fossil data values for primary mirror conic constant.

the effect of varying both radii by HDOS and ORA show KP to be sensitive to changes in the radius R1 of M1. In fact, if the error in the old value of MM were due entirely to a decrease in R1, KP would be close to -1.0140. Based on this analysis, measuring the mirror radii, particularly R1, was given a high priority.

There were reasons to doubt that a change in R1 could be the entire source of the earlier discrepancy between fossil and phase retrieval data. First, test plate data was found which indicated the radius should be as specified. Second, any error in R1 should correlate with errors in other parameters, if we are to reconcile the original spacing data with the new measurements (always excepting the FLPE, whose cause is known.) If the original means of measuring MM and CM are examined, (see figure 3.1), it will be noted that any decrease in MM due to a decrease in R1 should be accompanied by an equal sized INCREASE in CM. As table 3.1 shows, the new measurements indicate both MM and CM are smaller, and by different magnitudes.

Figure 3.3 summarizes the results of a number of analyses of the effects of old and new parameters on the value of the conic constant. (This analysis was completed before the discovery of the need to use OBS 0.33 in the AUTO runs, and may thus have errors on the order of + 0.0001 in KP. The analysis has not been updated.) It will be noted from the last row in the table that it is possible to completely reconcile old and new values of MM and CM by varying R1 and R2, but that the resultant value of KP would be - 1.012453.

There remain two logical reasons for the discrepancies in RNC data, given that the new values are better certified. The first is an error in the original measurements, most likely in the use of metering bar A to locate the two centers of curvature. The second is a change in the spacing of the mirrors in the process of moving the RNC from the laboratory where it was assembled to the test tower.

Completion of the radii measurements and rexamination of the original assembly procedures has clarified the source of the errors. First, the spacing error between mirrors is most likely a result of schedule pressure which resulted in shimming the lower mirror to reduce vignetting after the spacing had been measured. Second, the new radii measurements give R1 = 286.6677 and R2 = 372.830 mm. R2 is within the original measurement specification, But R1 is shorter by 0.0593 mm, well outside specifications, and in the direction to increase KP.

Reasonable explanations have been put forward for the errors in the original spacing measurements. The error in R1 is much harder to understand, since the test plate against which it was figured has been shown to meet its original specification. The new value for R1 does bring fossil and phase retrieval data into agreement, but we would be more comfortable with the results if the error in R1 could be explained.

Figure 3.3: Summary of conic constant calculations comparing old and new measurements of air spaces in RNC.

SUMMARY OF CONIC CONSTANT COMPUTATIONS
COMPARING OLD AND NEW MEASUREMENTS OF AIRSPACES

- KP computed using Code V® routine AUT;OPD;DEL 0.1108;GO. (Computation accurate to ± 0.00002.)

	CM (mm)	MM (mm)	MF (mm)	R1 (mm)	R2 (mm)	KP
NMKOLD1.SEQ Original Data	62.742	469.649	210.751	286.727	372.835	**- 1.002202**
NMKOLD2.SEQ Adj. for new A, B, C	62.731	469.645	210.725	286.727	372.835	**- 1.001939**
NMKNEW1.SEQ MF only altered	62.742	469.649	212.056	286.727	372.835	**- 1.013357**
NMKNEW2.SEQ CM, MM, MF altered	62.716	469.577	212.056	286.727	372.835	**- 1.012787**
NMKNEW3.SEQ CM, MM, MF, R1 altered to reconcile MM	62.716	469.577	212.056	286.655	372.835	**- 1.013879**
NMKNEW4.SEQ CM, MM, MF, R1, R2 altered to reconcile MM plus CM	62.716	469.577	212.056	286.742	372.748	**- 1.012453**

HSTMVG04.DOC

4.0 REFRACTING NULL CORRECTOR ANALYSIS

Four interferograms (or at least four for which we have data) of the primary were taken through the refracting null corrector RvNC. It had been hoped that the RvNC data could be used to determine the exact value of KP, but that now looks unlikely. We have looked at data reduced from these interferograms by HDOS, and have had two of the original interferograms reduced independently by Itek (see page 21.) Our present analysis suggest that the ambiguity of RvNC results is the same order of magnitude as the earlier ambiguity between RNC fossil data and phase retrieval data.

4.1 DETERMINING KP FROM RvNC INTERFEROGRAMS

The RvNC interferograms show a large amount of spherical aberration, as expected. The technique to use in extracting KP data from these interferograms is to set up a computer model in which KP is varied systematically, and the space between the primary and the RvNC is varied to produce a minimum rms value at the focus of the RvNC for each value of KP. It is then possible to generate a transfer curve which plots RvNC rms wavefront error as a function of KP. Such a transfer curve was generated, but when data from the four interferograms was projected against it, the resultant KP values were so far from the expected value that we had to reexamine the process. The problem is that the way we optimized the combination of RvNC and primary mirror does not correspond to how the tests were made. In testing the primary against the RvNC, the spacing was not varied to minimize the rms wavefront error at the RvNC focus. Instead, defocus was allowed, and removed after data reduction by fitting Zernike polynomials to the wavefront and deducting defocus.

To test sensitivity to defocus, we reran the analysis with the RvNC to mirror spacing fixed at 11043.2575 mm, the ideal value for this RvNC for KP = - 1.002367. (This combination of mirror spacing and KP produces the lowest possible residual rms wavefront error.) We reran the series of different KP values and used WAV to estimate the resultant rms wavefront error. This time, however, we did not change either the mirror spacing or the last air space before the output image to get the best focus position, but simply took the WAV estimate of best focus rms as modelling "after data reduction" wavefront fitting.

Figure 4.1 plots the waves rms vs. KP transfer curves for these two cases. As can be seen, errors in RvNC to mirror spacing can result in large errors in the conic constant, in this case approximating the discrepancy between fossil and phase retrieval data which existed before the radii measurements were finished.

In order to back KP data out of the existing interferograms, it is necessary to generate individual transfer curves for each interferograms, based on the amount of defocus indicated in the Zernike coefficient tables. We have done this using a conversion constant developed by Laurie Furey of HDOS relating Zernike defocus to changes in RvNC to mirror spacing. The results are shown in figure 4.2, and the

Figure 4.1: Sensitivity curves, rms wavefront error vs. conic constant for refracting null corrector plus primary mirror

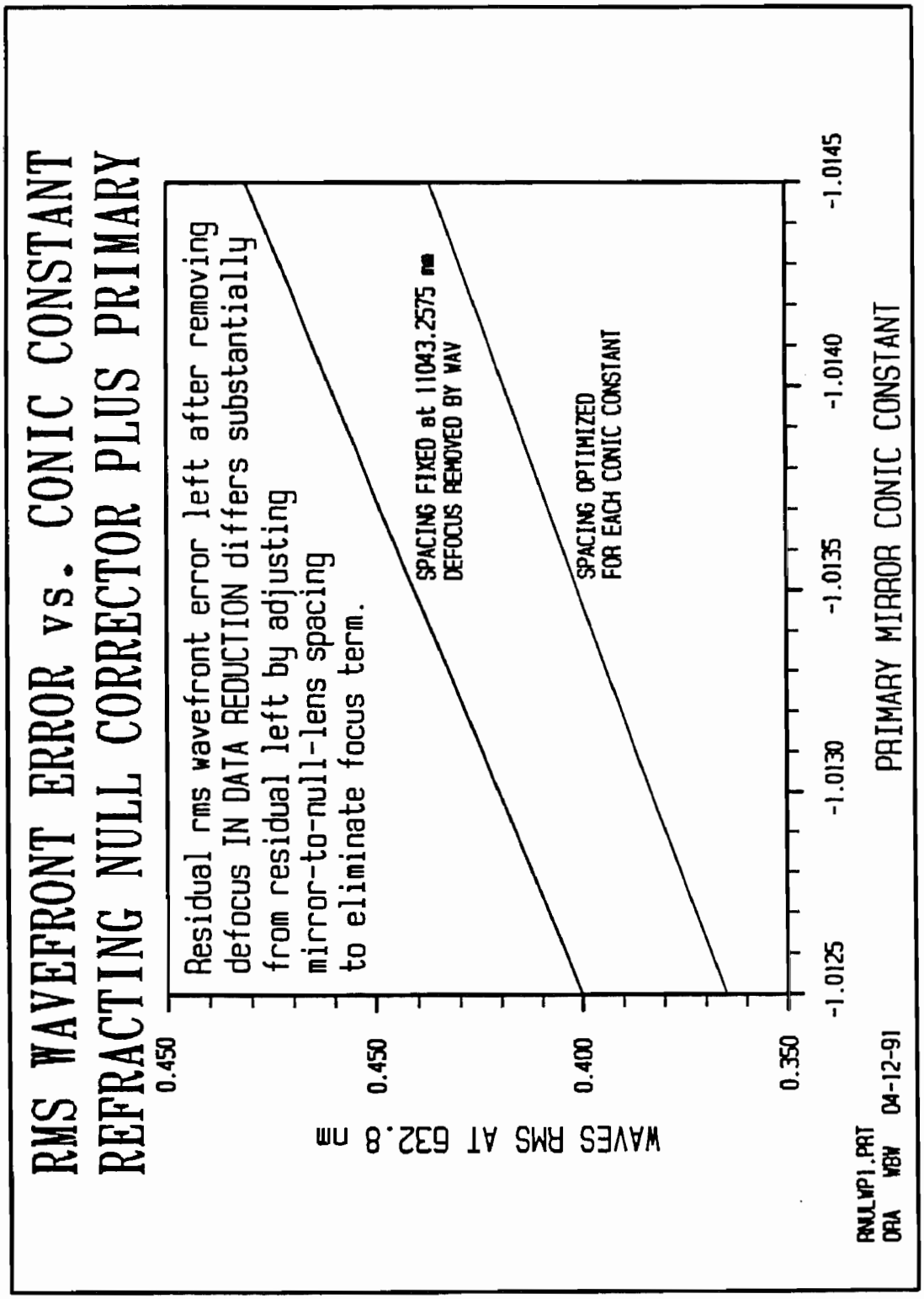

Figure 4.2: Values of KP generated from HDOS reduction of RvNP interferograms.

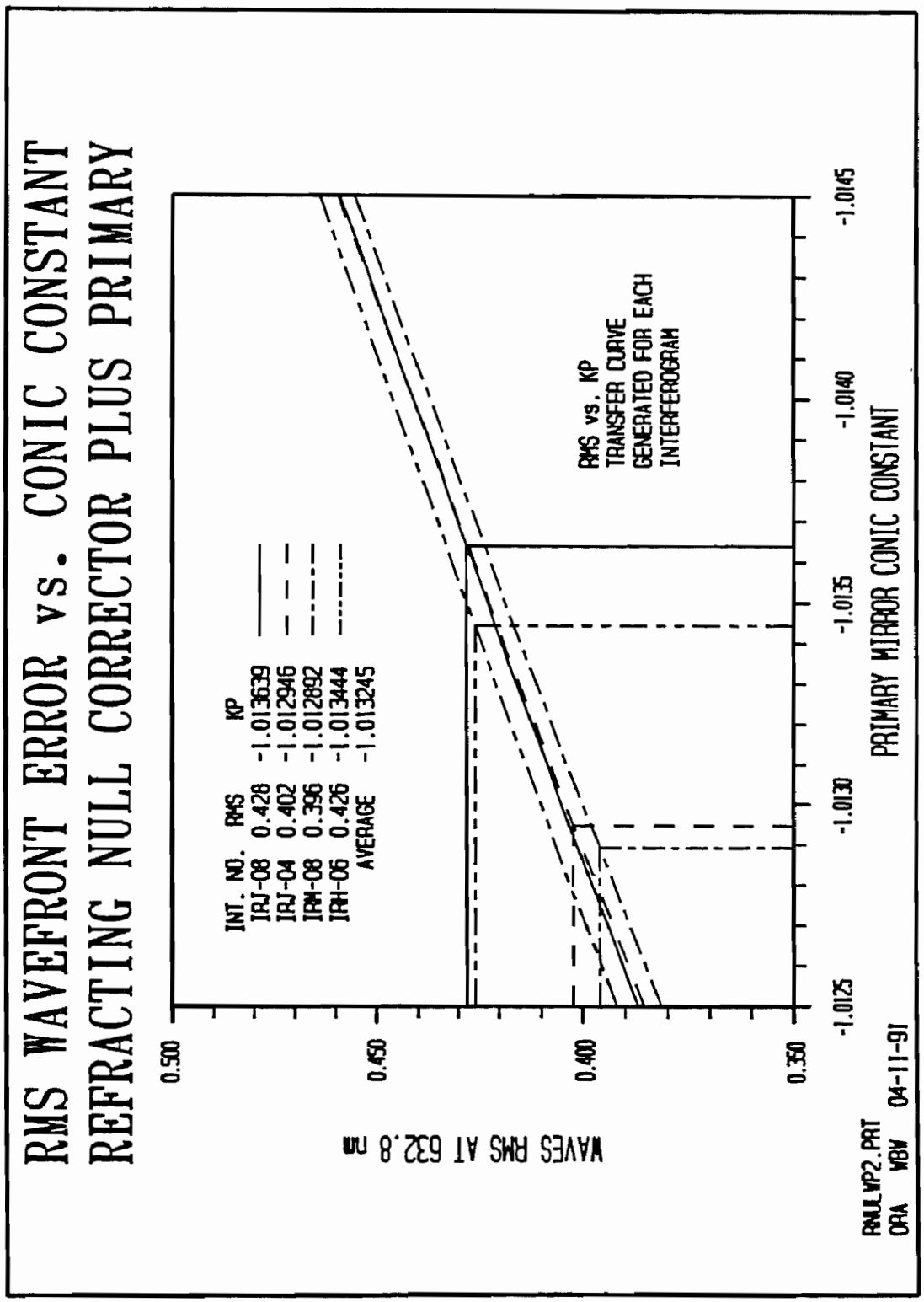

curves have been used to estimate KP from each of the four interferograms. The average of the four values of KP is -1.013245, but this may be misleading. Note that two of the values cluster close to - 1.0129, the earlier fossil data value, while the other two fall reasonably close to - 1.0135, the "baseline" value chosen to get the WF/PC II design underway.

4.2 RELATIVE SENSITIVITY OF RNC AND RvNC TO FOCUS ERROR

We have done a comparative analysis of the sensitivity of the RNC and the RvNC to error in the spacing between each and the primary mirror. We have looked at two cases for each null corrector, one in which the value of KP is the optimum for that null corrector, and the other for which KP departs from optimum by about the same amount. We set up the spacing at its ideal value for each case and determined the residual rms wavefront error. We then varied the spacing in 0.1 mm increments, and used the WAVE focus estimate feature to determine the residual rms to be expected when focus is removed in data reduction. The results are shown in figure 4.3. In the upper set of curves, the values of KP correspond to the ideal for each corrector design. In the lower curves, the ideal RNC and RvNC designs have been used to analyze a common mirror for which KP = - 1.0130. In both cases, the curves for the RNC are nearly flat, showing that it could be used to estimate KP even for mirrors differing substantially from its ideal, even if focus is not exact. NOTE THAT THE RMS VALUES PLOTTED HERE ARE THE RESIDUALS AFTER DEFOCUS HAS BEEN ESTIMATED AND REMOVED BY WAVE. The curve for the RvNC has a minimum at the ideal spacing when it is analyzing its ideal KP mirror. There is no such minimum for the RvNC when KP = - 1.0130, even though the spacing change range is extended. Thus removing defocus error only in data reduction may lead to erroneous estimates of KP if one attempts to derive it from the indicated rms wavefront error. The RvNC is just too sensitive to spacing change.

Perkin-Elmer (nka HDOS) is sometimes faulted for not using the RvNC for the entire mirror figuring job. The more we compare the RNC and RvNC AS DESIGNS, the better the RNC looks. Its only fundamental design fault is that its inherent central obstruction prevents it from being used to determine the vertex curvature of the primary mirror. Even in this respect, the RvNC has faults. In spite of the fact that it was to be used to measure the vertex radius using white light interferometry, THE RvNC DESIGN HAS NOT BEEN ACHROMATIZED. In white light interferometry, one wants to use a large wavelength bandwidth to insure that dark fringes are formed only when the optical path length matches at all detectable wavelengths. The chromatic aberrations of the RvNC are such that this can be done only over a relatively short spread of wavelengths.

It is unfortunate that the RNC fell victim to so many assembly errors, even beyond the catastrophic effect this has had on the primary mirror and the HST program, since the accident has blackened the reputation of a clearly superior design.

Figure 4.3: RMS wavefront error variation with mirror position RNC vs. RvNC

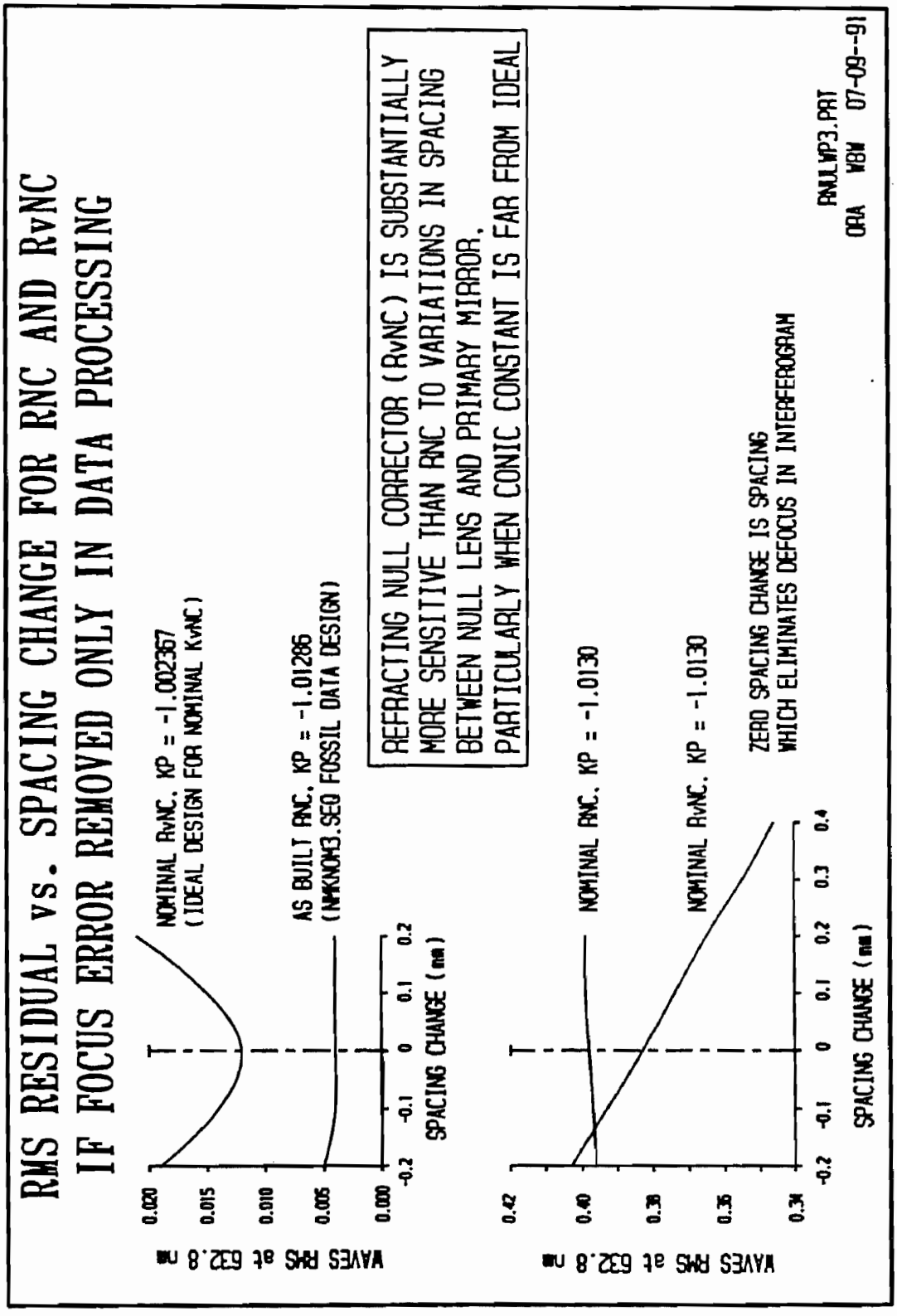

5.0 HST OTA ANALYSIS

Phase retrieval analysis has been carried out on the premise that the error in the system wavefront is due solely to spherical aberration introduced by the error in KP caused by the error in the RNC. While the error in KP induced by the RNC is clearly the major source of the problem, it is not the only source, as demonstrated in recent measurements of the WF/PC optics. Summing up the entire spherical aberration component in terms of an equivalent change in KP, ΔKPEQ, is not unreasonable, but what is really needed is to model the total OTA wavefront error form so that it can be compensated for in WF/PC II and the COSTAR corrector. What needs to be done is to identify all possible sources of spherical aberration in the OTA aside from the error in KP. This includes fabrication residuals in the primary and secondary mirrors represented by interferograms of the flight hardware, despacing of the primary to focus the imagery in the WF/PC or the fine guidance sensors, and gravity release of the primary and secondary mirrors.

5.1 THE NOMINAL PRIMARY CONIC CONSTANT

The ideal value of KP depends on the values used for the primary mirror vertex radius, the secondary mirror parameters, and the primary to secondary mirror spacing needed to place the paraxial focus where it is desired. For the original design, in which the primary radius was 11040 mm and paraxial focus was 1500 mm behind the primary vertex, KP = - 1.0022985. For the as-built primary (rdy = 11041.7 mm) and secondary, with paraxial focus 1500.129 mm behind the primary vertex, this value changes to KP = - 1.002233. For the JPL model having a primary-to-secondary spacing of 4907.01 mm, the ideal KP = - 1.002116, and paraxial focus is 1486.629 mm behind the primary vertex. (The JPL model is adjusted to locate the maximum encircled energy image where desired in KP = - 1.0135.) Thus trying to assign sources of spherical aberration in the actual OTA rather than simply defining an equivalent KP is somewhat moot. However, mirror fabrication residuals are a legitimate additional source.

5.2 PRIMARY AND SECONDARY MIRROR INTERFEROGRAMS

We currently have two sets of reduced data from OTA primary and secondary mirrors, one supplied to us directly from HDOS, and the other coming indirectly through Eastman Kodak and JPL. The former are in two *.INT files, GDIJK.INT (for the primary) and MDNBX.INT (for the secondary), ready for incorporation in Code V models of the OTA. The latter are in PMR1.INT and SMR1.INT, and are identified on surface figure plots as TA No. 913008 (the primary) and TA No. 916002 (the secondary).

We have analyzed these files using Code V, and figures 5.1 and 5.2 reproduced color images of the surface figure maps photographed from a CRT screen. Figure 5.1 pairs the two primary mirror interferograms, and figure 5.2 pairs the two secondary

Figure 5.1 : Primary mirror interferograms.

A. GDIJK.INT

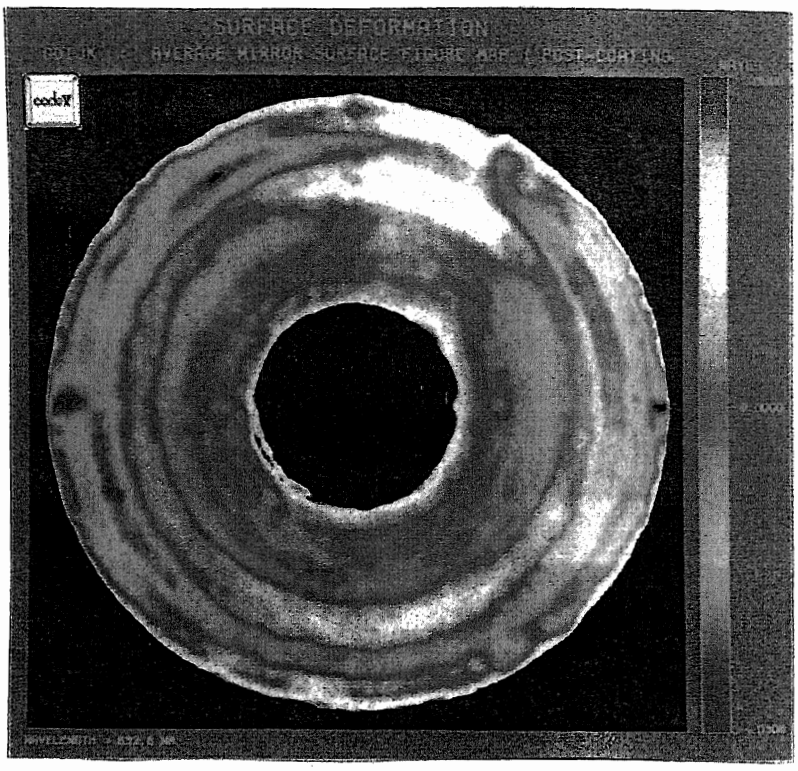

B. PMR1.INT (TA Number = 913008)

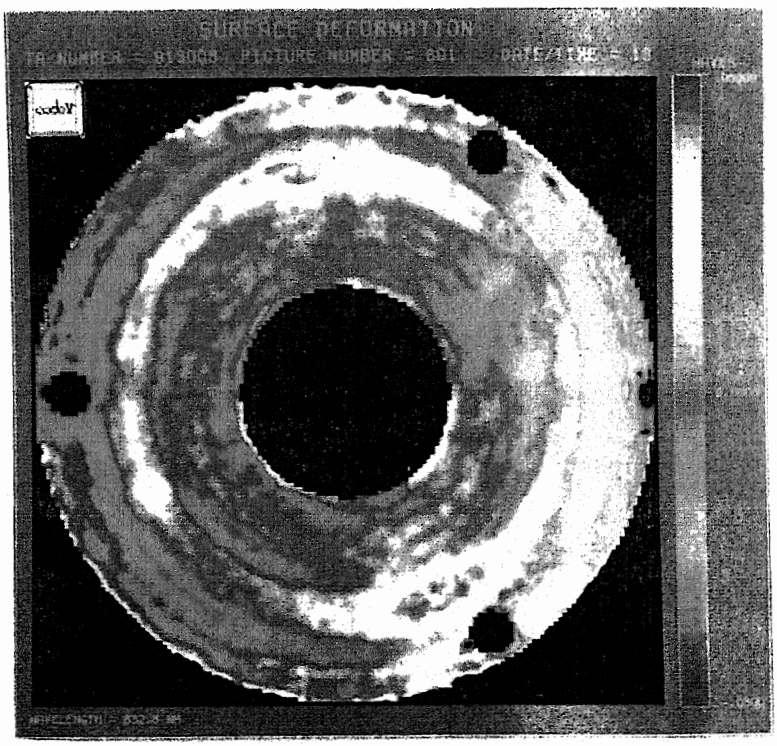

Figure 5.1 : Primary mirror interferograms.

A. GDIJK.INT

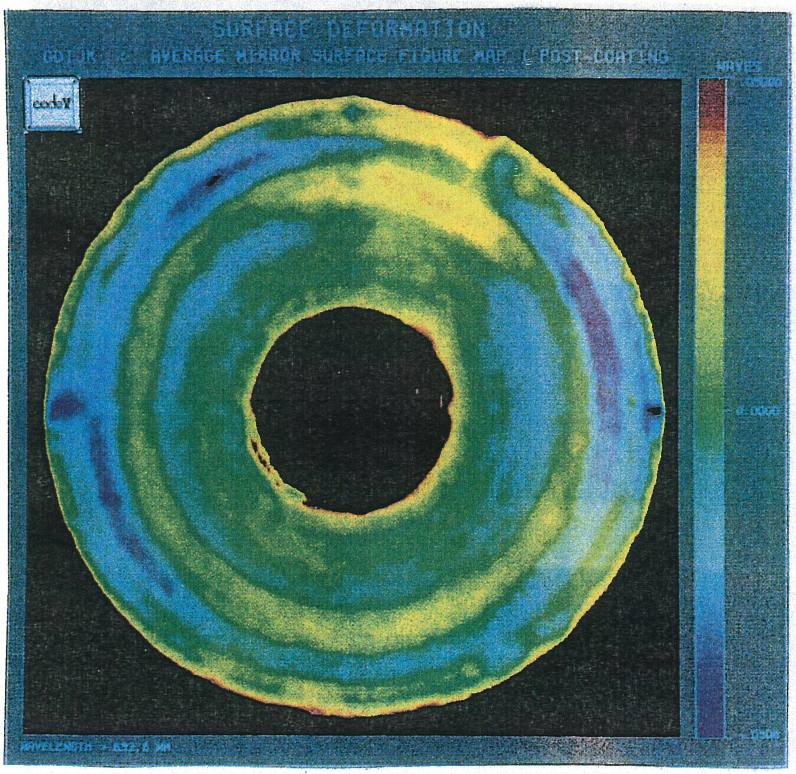

B. PMR1.INT (TA Number = 913008)

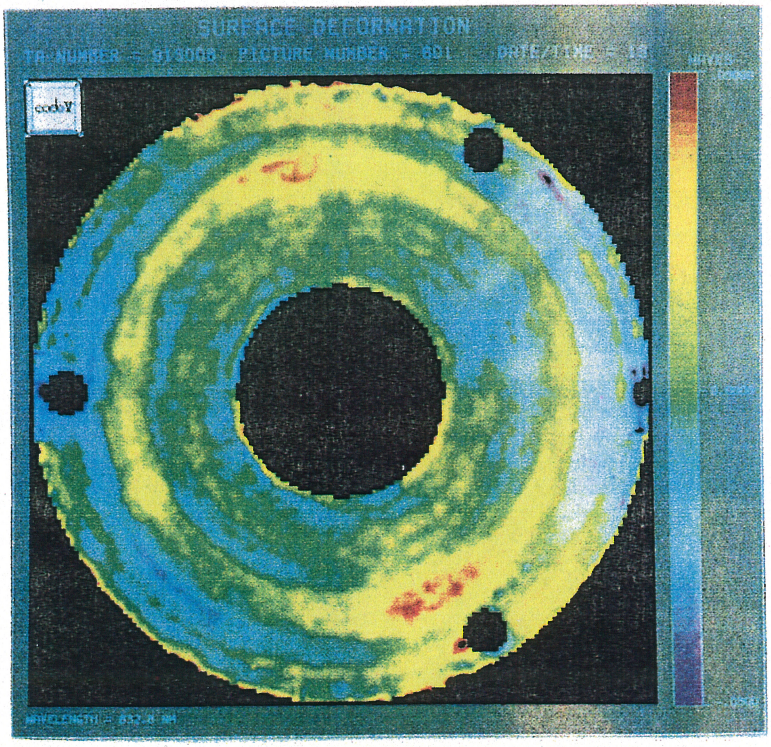

Figure 5.2: Secondary mirror interferograms.

A. MNDBX.INT

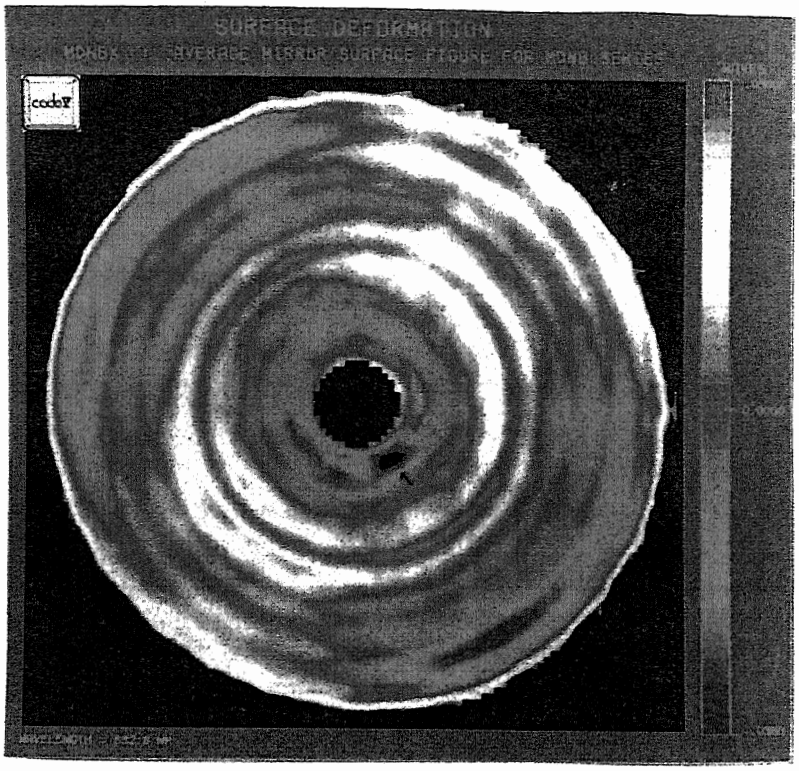

B. SMR1.INT (TA Number = 916002)

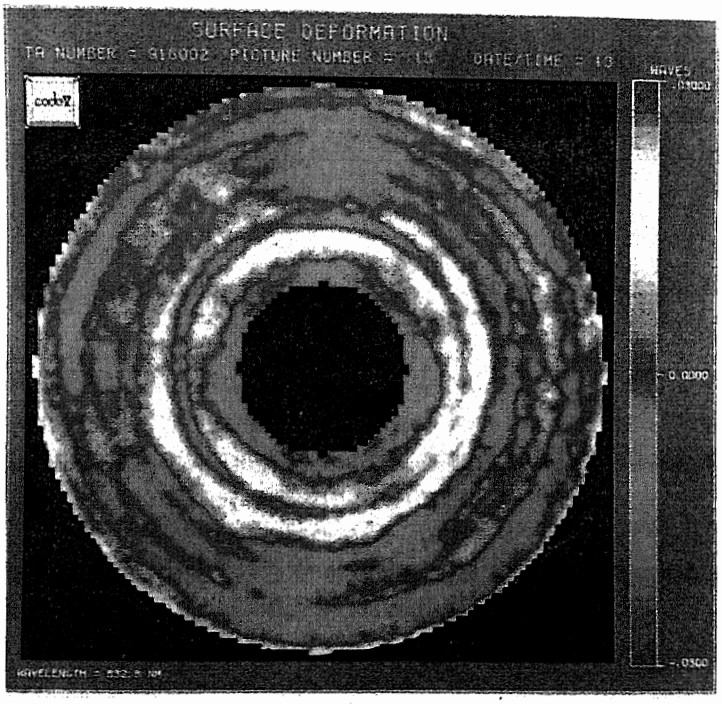

Figure 5.2: Secondary mirror interferograms.

A. MNDBX.INT

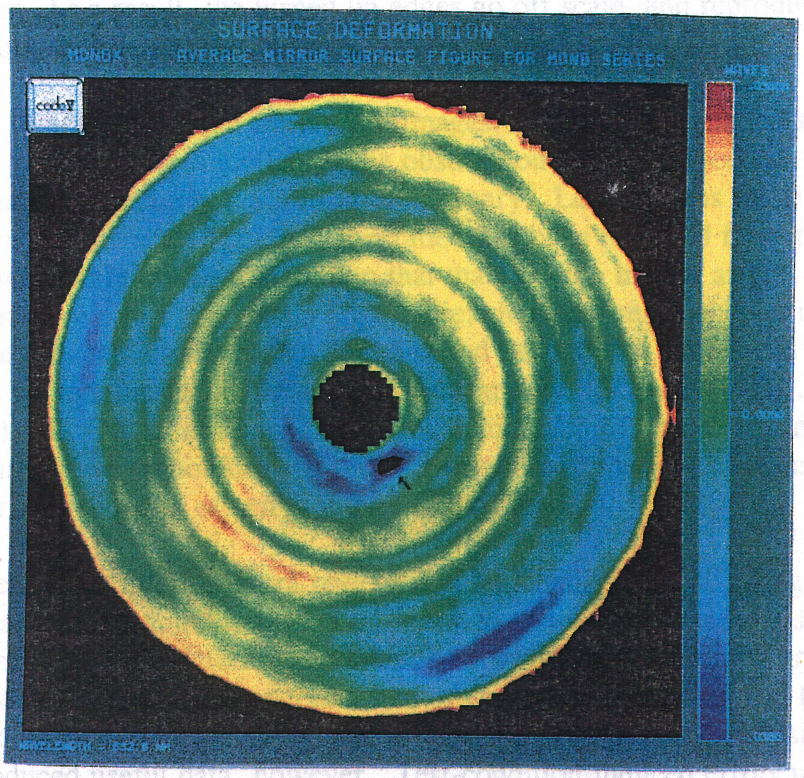

B. SMR1.INT (TA Number = 916002)

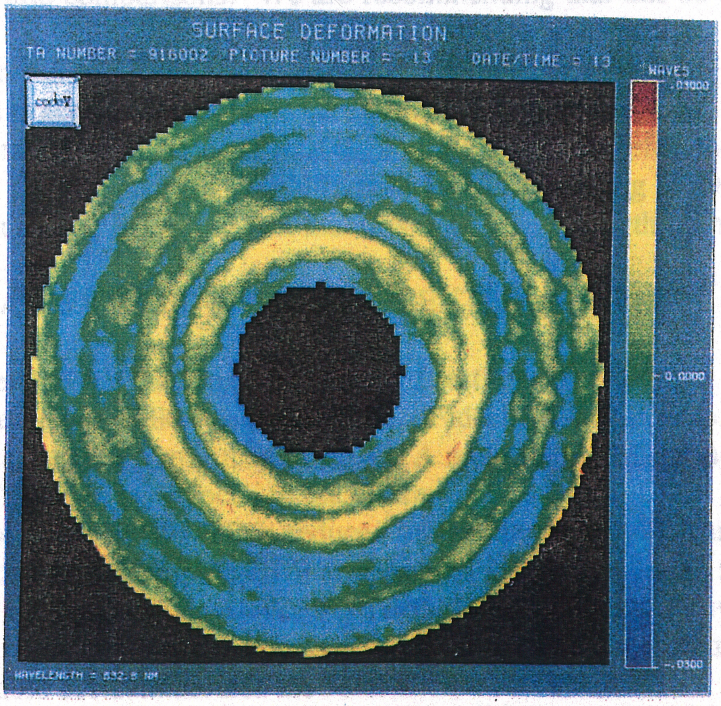

mirror interferograms. In all four cases, the wavefront error scales have been expanded to - 0.0300 to + 0.0300 waves at 632.8 nm to emphasize ripple in the false color images. As a result, the turned up edges go off scale, and reproduce as black, giving the boundaries a ragged appearance.

Several things are evident from these images. Most obviously, the second set, from Kodak, has been massaged to change the obstruction size in the secondary mirror, and to more clearly show the bolt plates in the primary. Less obvious is the fact that a residual of undercorrected spherical aberration has been removed from the latter primary, presumably on the assumption that that is being treated as part of the conic constant error. We feel that this is regrettable, since any residual spherical aberration found in the reduced interferogram is above and beyond that introduced by the RNC FLPE, and we feel that it should be treated separately. (See appendix 6.3 for further comments.) Finally, there seems to be some azimuthal difference in the location of ripple features. We do not know if this is an artifact of the way in which we plotted the data, or an indication of errors in one of the data sets.

An independent interferogram review is being conducted, including analysis of both RNC and RvNC interferograms. Several vendors were sent RFP's to perform interferometric data reduction in accordance with ORA requirements, and Itek offered to process a few of the interferograms free of charge. Three RNC and two RvNC interferograms were selected to be reduced by Itek. Preliminary analysis of the results has not produced useful data, however. Test-condition-induced errors in each RNC interferogram make data from each one hard to compare with data averaged over 32 interferograms. ORA feels that a complete set of 32 interferograms would have to be reduced for valid comparisons. We are recommending that this be done.

Data from the two RvNC interferograms can be compared with HDOS data, in principle. In practice, Itek does not use obstruction weighted Zernike polynomials in reducing interferograms, as does HDOS, and the data is therefore not directly comparable. Further analysis would require RvNC modelling by ORA using the form of Zernikes used by Itek. We feel that this is no longer worth doing.

5.3 FABRICATION RESIDUALS REPRESENTED AS ΔKPEQ

The Code V WAVE option can be used to estimate the ΔKPEQ component in each surface figure map as follows. First set up an ideal OTA with zero wavefront error at paraxial focus. Add a figure map to the OTA and use WAVE to indicate the direction and distance from paraxial focus to the minimum rms focus. Then adjust KP until the focus distance given by WAVE is reduced to near zero (<0.001 mm, in our analysis). The difference between the ideal KP and the new KP will have the same magnitude as ΔKPEQ, but the opposite sign. We have done this for all four individual cases, and then coupled them to show the effects of both primary and secondary mirror fabrication residuals. Table 5.1 summarizes the results.

Table 5.1 ΔKPEQ from mirror surface figure error residuals

*.INT SET	NET RMS	SPHERICAL FORM	ΔKPEQ
MDNBK.INT	0.016	overcorrected	- 0.000027
SMR1.INT	0.015	overcorrected	- 0.000022
GDIJK.INT	0.027	undercorrected	+ 0.000016
PMR1.INT	0.020	overcorrected	- 0.000008
GD + PM	0.030	overcorrected	- 0.000010
PM + SM	0.023	overcorrected	- 0.000031

All values for ΔKPEQ are quite small, and do not significantly alter KP. In the case of GDIJK and MDNBX, the effects tend to cancel, while for PMR1 and SMR1, the effects add. We have no way to verify which models the primary more closely, but feel that removal of residual spherical from the interferograms is poor practice.

5.4 MODELLING THE OTA INCLUDING FABRICATION ERROR

We have generated a model for the OTA using first order parameters from the JPL model, for which KP = - 1.0135 and the mirror separation is 4907.01 mm, which also incorporates GDIJK.INT and MDNBK.INT. This is available from ORA in DOS floppy disk form as a Code V sequence file HSTOTAKJ.SEQ, coupled with the two *.INT files, which must be included. [NOTE: the K in the *.SEQ file name implies we have used a pure conic model for the RNC-induced error. The J implies use of the JPL-generated first order parameters, including KP = -1.0135.]

Correctly incorporating the figure error maps and setting up the resultant OTA model to couple with various SIs requires a knowledge of the coordinate systems involved. Figure 5.3 shows the relationship between OTA and Code V coordinate systems, and is based on data from the OTA Handbook, version 1, dated May, 1990. Figure 5.4 shows a map of the pupil obstruction pattern in Code V coordinates which is incorporated in HSTOTAKJ.SEQ. Each mirror's interferograms have a separate set of coordinates, defined by fiducial marks and viewing the mirror face on. Figures 5.5 and 5.6 show these, and include indications of how the coordinate axes are translated into Code V and OTA coordinates.

Analysis of the HSTOTAKJ.SEQ indicates a net rms wavefront error of 0.398 at minimum rms focus. This is actually lower than the wavefront error for the system without the figure error maps, and is indicative of the turned up inner and outer edges of the primary mirror surface.

Figure 5.3: OTA vs. Code V coordinate systems.

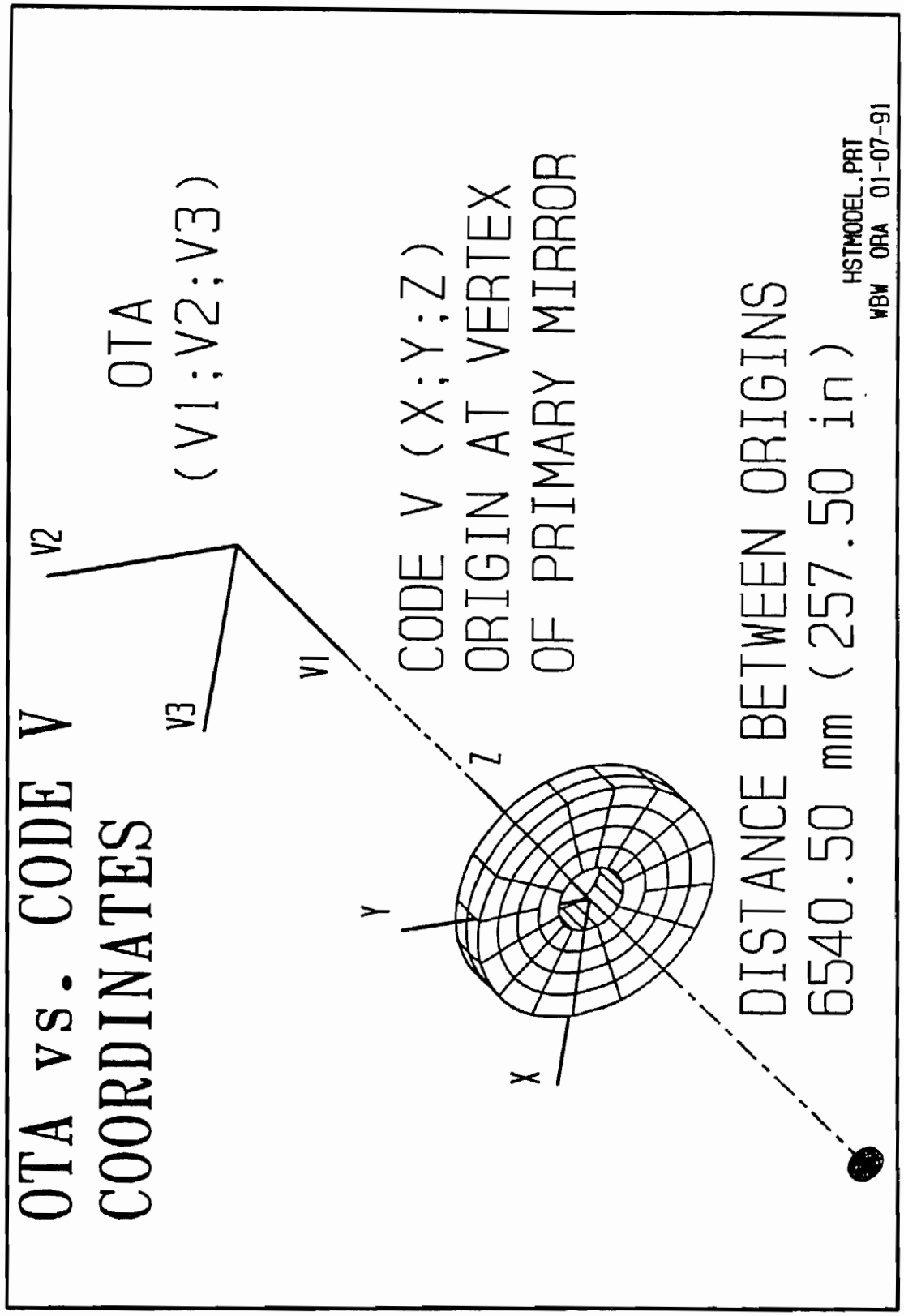

Figure 5.4: HST aperture showing obstructions and spiders in Code V coordinates.

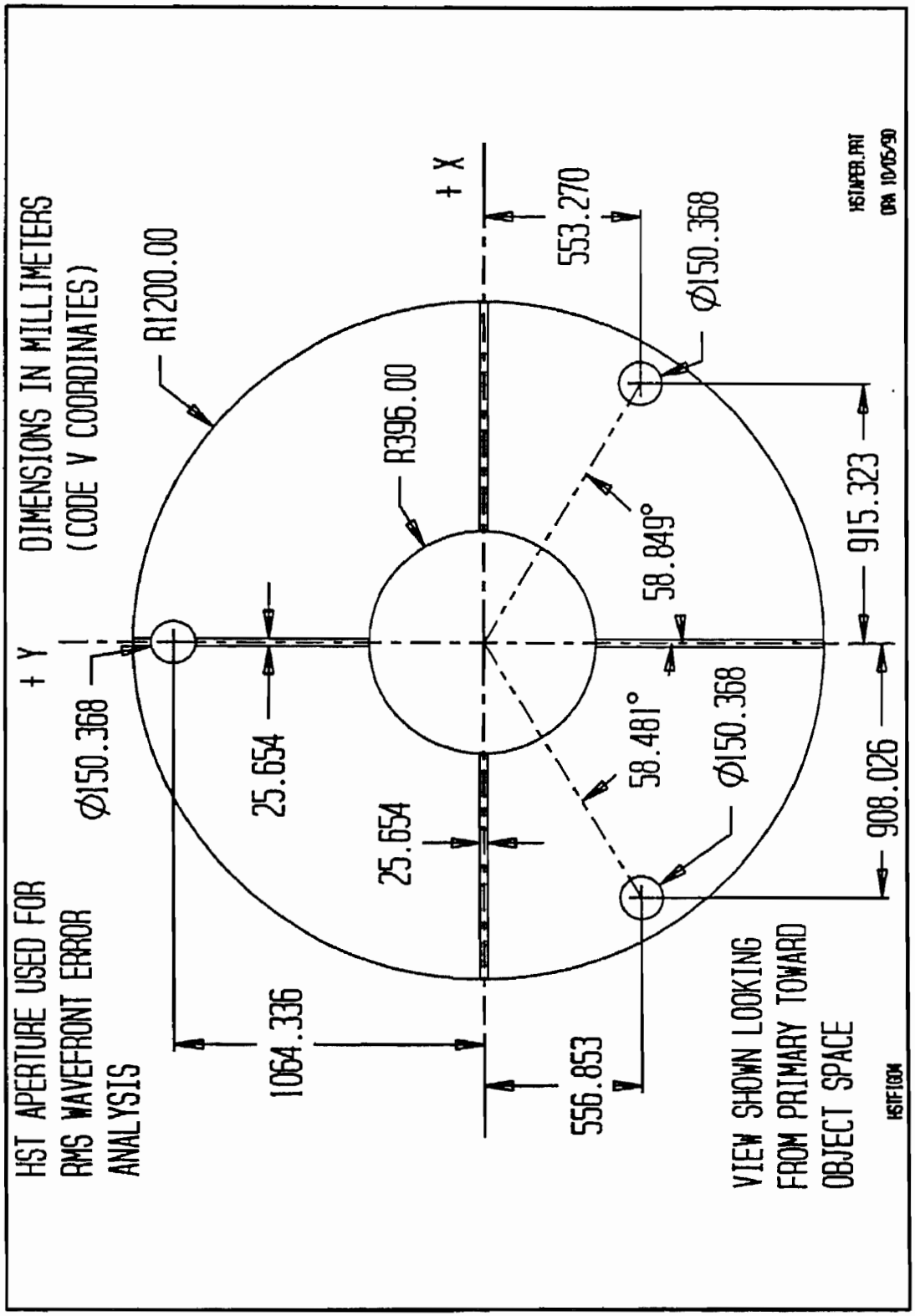

Figure 5.5: Primary mirror fiducials.

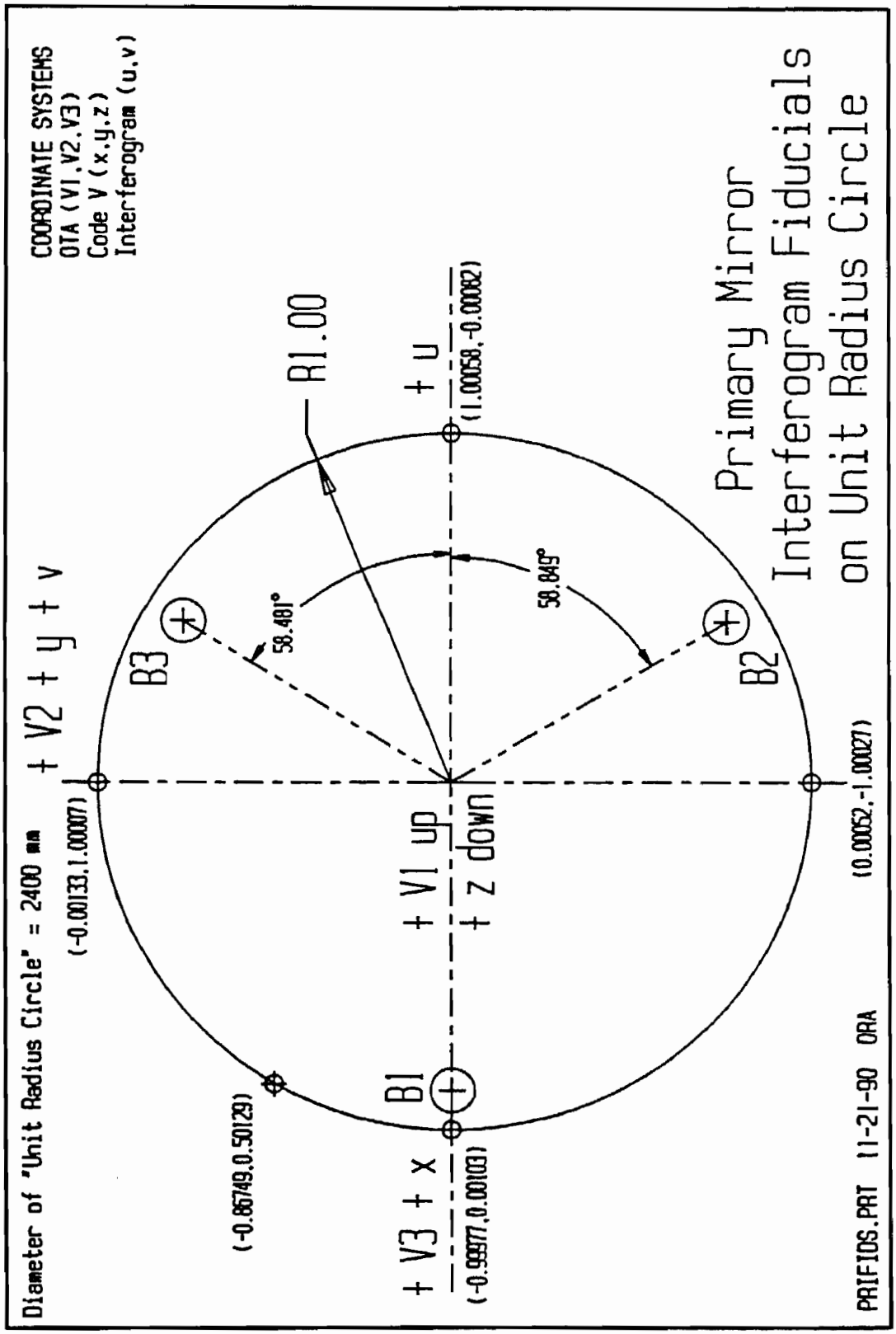

Figure 5.6: Secondary mirror fiducials.

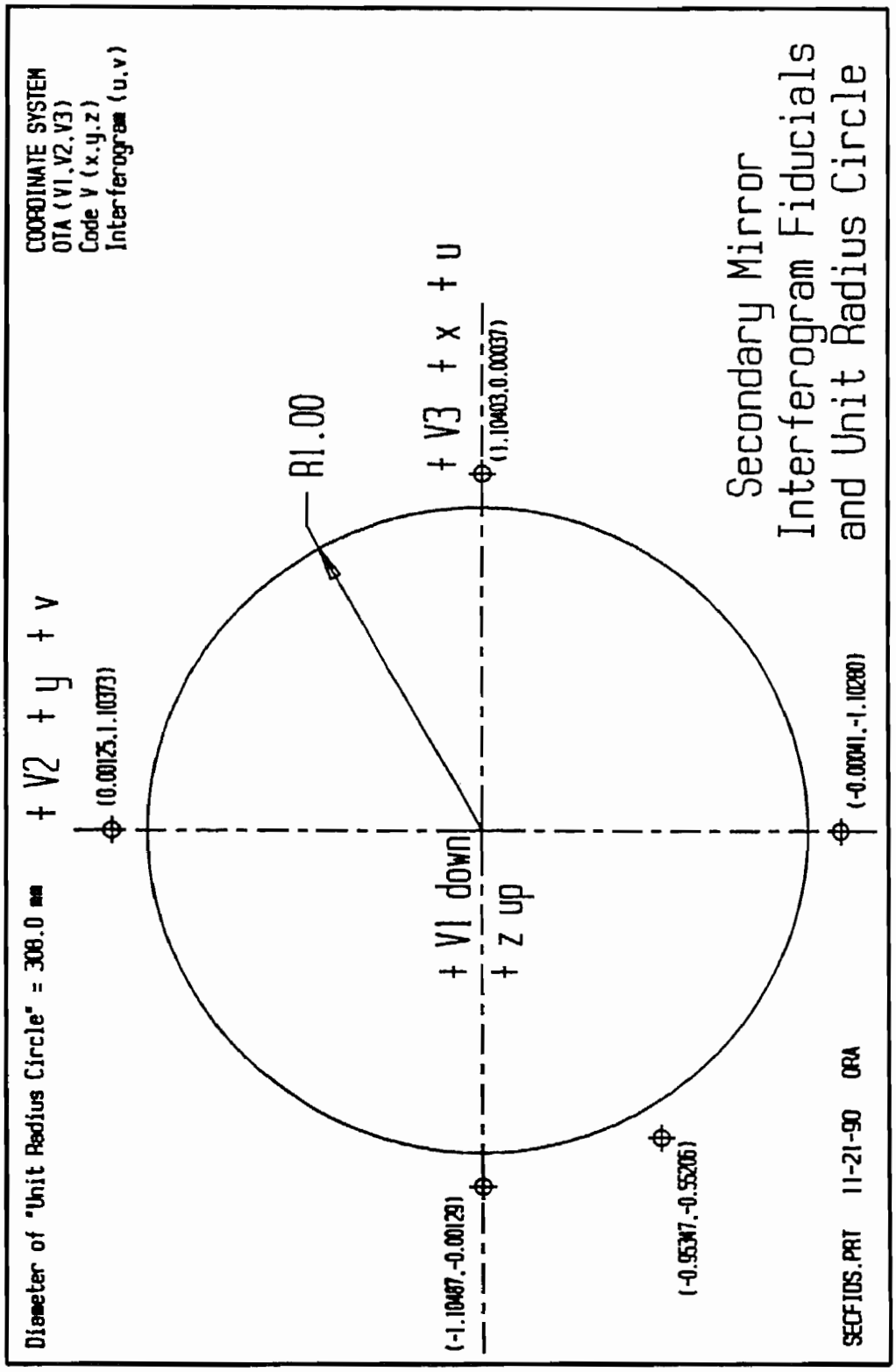

5.5 RAYTRACE ANALYSIS AT THE OTA FOCUS

One study requested by the HIORP was to show the position of paraxial focus, minimum rms focus, and maximum encircled energy focus as a function of KP. This was started, but the locations of maximum encircled energy focii remain to be determined. None of this data has been updated for the new radii measurements.

Figure 5.7 plots focus shift for the outer rim ray, inner rim ray and minimum rms focus, relative to paraxial focus, as a function of KP for two values of the primary-to-secondary separation S. Although B, the distance from paraxial focus to the primary vertex, differs by nearly 14 mm in these cases, the additional distance to the other focii does not change by much. Figure 5.8 plots the mirror spacing S vs. KP required to place the indicated focus 1500.128 mm behind the primary vertex. This may be a more useful measure of OTA parameter manipulations required to match KP to the SI imaging requirements. A pure conic OTA model devoid of surface error maps was used in figures 5.7 an 5.8. Figure 5.9 plots ray paths between paraxial focus and outer rim ray focus to compare performance for the pure conic model (on the left) to that for a model including fabrication errors. In the latter case, upturned inner and outer edges on the primary (at 0.33 and 1.0 normalized pupil height) cause a substantial shift in the points at which the inner and outer rim rays cross the optical axis.

5.6 GRAVITY RELEASE EFFECTS

The HST primary was fabricated and tested in a one G gravity field, but is being used in a zero G field. Gravity release can change the shape of the mirror surface from that measured interferometrically. HDOS estimates that the fabrication-to-orbit changes for the primary and secondary will total 0.0152 waves RMS. (Data taken from Figure 3-2 of Rev D of the July 1985 OTA Wavefront Error Budget Report Number PR-182D). This estimate was increased to 0.0184 waves, given the higher than desired primary mirror strain free mirror mount test results (see the 14 December 1983 Report Number AV-04/TE 679-4422, Section 4, page 9). If all of this appears as spherical aberration, it would imply a ΔKPEQ of 0.00051. There are two problems with applying this directly to KP at present: 1) we are not certain that all of the effect produces spherical aberration instead of power change; and 2) even if it is all spherical aberration, we cannot be certain of the sign. We would need data on the metrology mounts used during testing to determine the form of the change in mirror shape due to gravity release. This, plus primary mirror distortions induced by mirror mount actuators remain for further consideration.

5.7 INTERACTION OF OTA AND SI ABERRATIONS

A question which keeps surfacing is how aberrations from the OTA interact with the SI optics, whether the latter are aberrated or not. The OTA output couples to the SIs as a coherent wavefront, and the combined wavefront distortions should be directly additive. The only way to be certain of the combined wavefront error would be to

Figure 5.7: Focus shift vs. KP

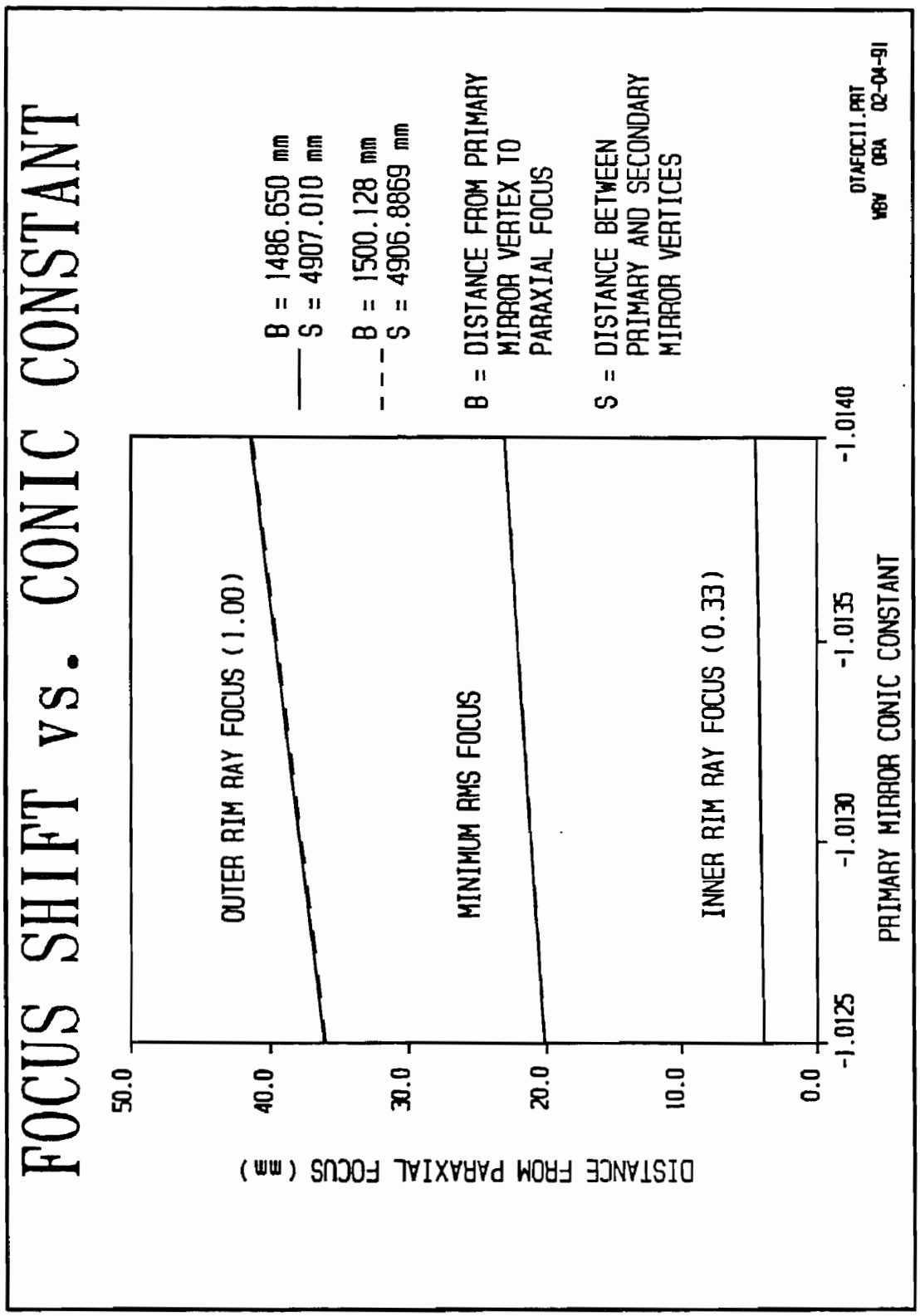

Figure 5.8: Mirror spacing vs. KP to place focus 1500.128 mm behind primary.

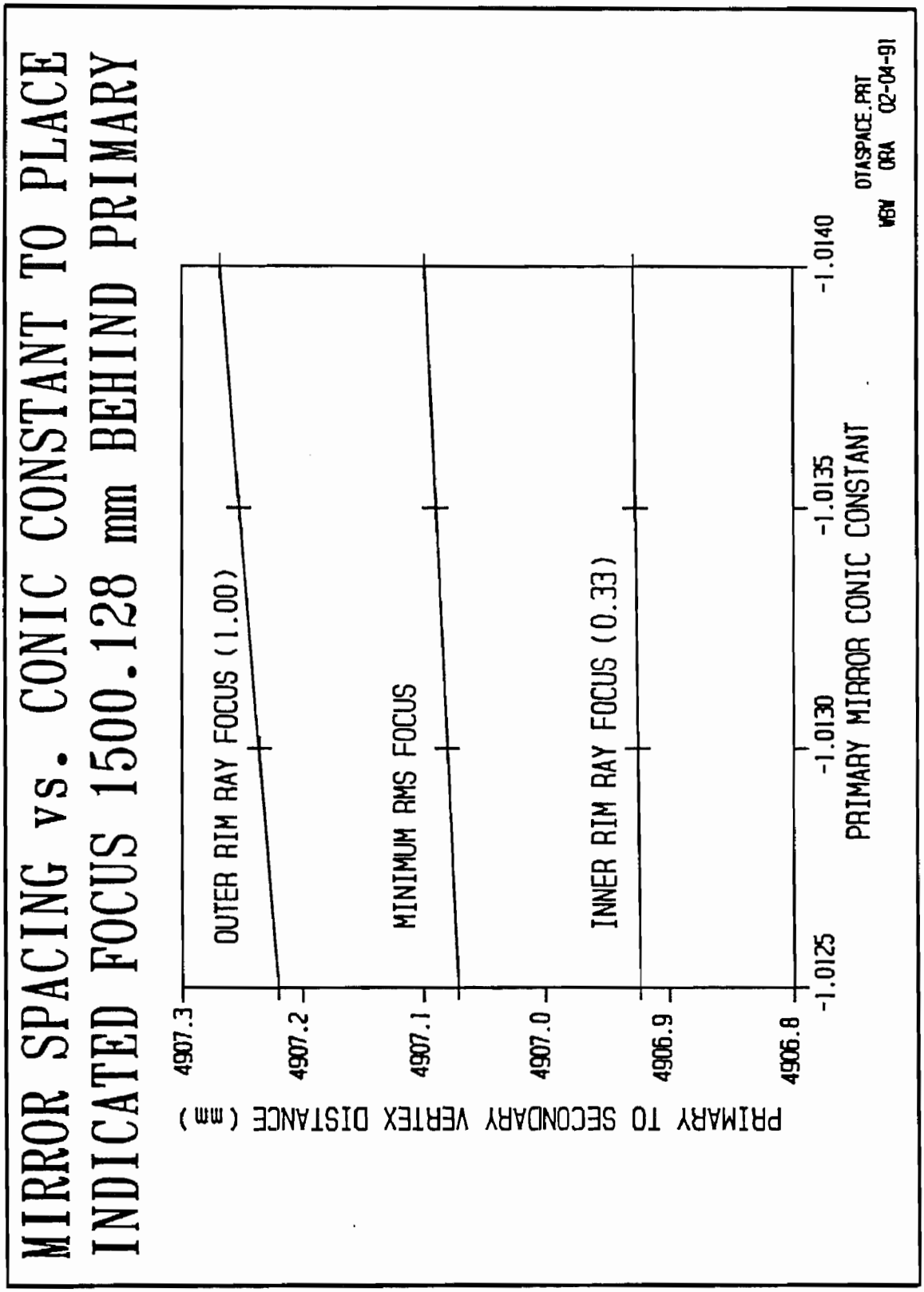

Figure 5.9: Ray fans at OTA focus.

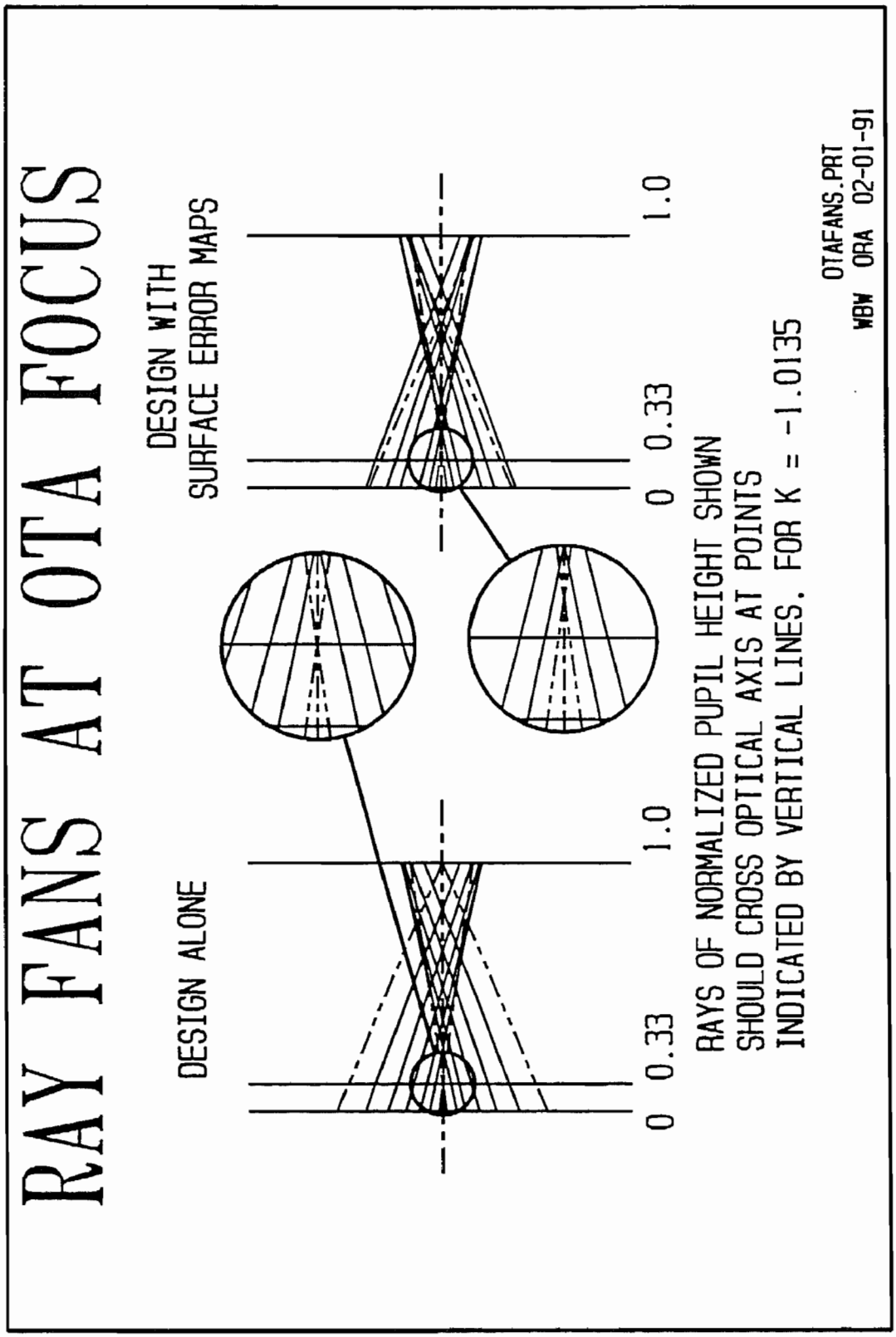

raytrace an accurate model of the complete optical system. This, unfortunately, is not possible at present. Several comments of a general nature are worth making here on the subject.

a) If the SI has no measurable wavefront error over its entire pupil area for each field point, nor over areas outside its nominal pupil through which misplaced rays from the OTA can pass unvignetted, then the distorted OTA wavefront should pass unaltered through the SI to the image sensor.

b) If the SI has a systematic form of aberration, such as spherical aberration, and all unvignetted ray paths through it are well behaved, then the main OTA and SI aberration components should be linearly additive, ray by ray. That is, both wavefront error maps, referenced to a common pupil, should be additive point-by-point, with due care about sign. One caveat should be made on this statement concerning finer scale fabrication errors. If these exist in both OTA and SI, then simplistic modelling may not predict how they interact. For this higher spatial frequency residual, statistical analysis (such as rss addition) may be valid.

c) If the rays exiting the OTA depart drastically from their nominal paths and are not vignetted in the SI, and if the SI is not well behaved outside its design pupil, then the combined wavefront error will be harder to predict. The stop in the SI optics is actually an image of the stop in the OTA, which is an aperture just in front of the primary mirror. If OTA aberrations and OTA/SI misalignments change the size and location of the pupil image in the SI optics, then individual rays will follow erroneous paths through the SI which can affect combined performance in ways not easily predictable except by ray trace analysis.

Our inclination is to believe that b) is the correct model for the OTA WF/PC combination.

5.8 PRELIMINARY ESTIMATES OF COMBINED OTA-WF/PC PERFORMANCE

We were at last able to transition from fossil data review to work on the OTA models as coupled with the SI's, specifically the WF/PC. The intent here is to insure that the Code V models are correct, that the tolerances being assigned to hardware are meaningful, and that performance will be as advertised. We have not yet seen a document which summarizes performance requirements, but have been told by JPL engineers that the redesign is to provide 70% encircled energy/EE in a 0.2 arc-sec diameter circle based upon the OTA alone, with an additional allowance for up to another 10% loss, i.e. 60%, when WF/PC errors are accounted for. Furthermore, that a design goal has been established which if achieved would result in 65% EE at the WF/PC. Tolerancing is being performed against a 1/14 wave RMS WFE criterion at 632.8nm. JPL work on cross-correlating this measure with both EE and Strehl Ratio (the ratio of the light intensity at the peak of the diffraction pattern of an aberrated image to that at the peak of an aberration free image) is being encouraged, but it may

prove necessary for ORA to do some independent analysis on both this as well as allowable pupil shear/magnification changes if JPL results are not available by mid-July. We haven't heard anyone discuss issues of distortion or plate scale relative to setting tolerances, and this has us concerned. It is an area we are discussing with JPL. NASA Headquarters would also like us to expend some effort on the alignment of the OTA and the SI's (we are attempting to get sufficient mechanical definition to determine relevant rotation points, etc.), closing on schedule/costs as need be with Vitro. We will incorporate these concerns in our follow-on work with Vitro (i.e. the "bridge" effort). At any rate, to complete these tasks the work noted is currently underway or has been completed, and we have also begun a review of the OCA/Tinsley null lens work (e.g. 16 April 1991 memo of K. Thompson/ORA to D. Bajuk/Tinsley), as well as the Ground Stimulus' opto-mechanical and thermo-optical sensitivity (JPL D-8416 dated April 1991 and discussions with R. Chave).

A back-of-the-envelope evaluation of expected WF/PC performance was completed. The ideal value of KP for the as-built radius is - 1.002233 (vs - 1.0022985, the nominal design value.) If the fossil conic is taken to be - 1.01376, and spherical aberration in the WF/PC contributes about - 0.001 of equivalent KP error (estimated from PC6 data presented to the HIORP), which plate scale errors increase to - 0.0013, then we estimate the magnitude of the conic error to be about 0.0128. This would give about 11% encircled energy (EE) in a 0.1 arc-sec radius, compared to the goal of 65% for WF/PC. If the effects of residual spherical in the OTA due to sources other than the RNC errors, gravity release, and mirror mount induced errors are added in, the conic error might be changed by as much as 0.0005, increasing 0.0128 to as much as 0.0133. But the magnitude and sign of this added change are hard to estimate, so it has been omitted.

If WF/PC II is designed to balance the OTA conic error to a tolerance of 0.0006, and if its equivalent conic error still has a magnitude of 0.0013, the "fixed" WF/PC would still induce about an 8.8% loss in EE, based on the above estimate. Another way of saying this is that when all is said and done, the HST EE might climb from 11% to 61%, accounting for other tolerances. This analysis is pretty elementary, and the effects of pupil shear and pupil magnification errors need careful review, but it does say that meeting the design goals will not be easy. Our hope is that the non-linear nature of the loss mechanisms will result in 4-5% better performance than predicted here, allowing performance levels close to 65% EE to be achieved.

Further computer modelling in this area is underway to refine this estimate of expected performance.

6.0 APPENDICES

ORA has performed several other tasks concerning the HST which are not under the direct purview of the HIORP. We include comments here on two of those tasks in sections 6.1 and 6.2. Section 6.3 adds some comments on interferogram reduction procedures, as a result of questions asked by readers of the draft report.

6.1 WF/PC TOLERANCING

A fairly detailed review of the tolerancing of the WF/PC II has been completed and the results communicated directly to the project (cf. WF/PC DFM # 1589/OSA DFM #91-46, 14 March 1991, J. McGuire/JPL). The early/draft documentation by J. McGuire has been very helpful in facilitating our review and input. Items noted included correction of pupil shear values in Figure 1 to Peak rather than RMS wavefront error, the need to treat the cosine of the angle in fold tolerancing (freeing up a bit of error to use on other sources), the need to limit power tolerances on folds (where refocussing isn't effective as power viewed oblique gives rise to astigmatism rather than defocussing), the need to consider thermal expansion inhomogeneities and anisotropies as well as temperature gradients, and errors introduced via mounting and coating, effects of material creep, etc. (we have requested a copy of JPL IOM 3541/DB/430/90 by D. Brent to better assess the error sources which have been considered), the need for an opto-mechanical error budget to control relay primary-to-secondary spacings, mathematical updates/Code V results which show the need for an added factor of 2X in peak-to-RMS ratios (fortunately these factors were unused in driving the draft error budget computations), and providing added insight into error budget statistics (cf. Smith, Modern Optical Engineering, 1966, pg. 425). These comments will be incorporated into J. McGuire's next release (Rev B). The items he notes as needed in this memo are, we agree, important, and we will also be looking to review each as they are available (alignment plan, means to achieve orthogonal tip/tilt adjustments without introducing cross-coupling, etc.). We hope to concentrate heavily next on the issue of independently verifying the expected pupil shear as one component of the error budget, accounting for real-world issues/material properties, etc. (under 55μ is apparently expected by JPL where 105μ is ok and 50μ may be heartache, dependent upon the design form).

6.2 COMMENTS ON ANALYSIS OF THE HDOS SAGE LENS

References:
1. Telecon with John Wood/GSFC, John Moody/Swales, Mac MacFarlane/HDOS, Mark Kahan/ORAE, Bill Wetherell/ORAE,and Kevin Thompson/ORAW on 05/16/91.
2. Fax from John Wood/GSFC, "CODE V Sign of SA".
3. Fax: Fed. Ex. from John Moody/Swales, "CODE V Analysis of HDOS Sage Lens", Received 05/16/91:05/17/91.

ORA has reviewed the data sent in References 2 and 3 relative to the issues raised in the Reference 1 telecon. From the Reference 1 conversation it was recognized that there were at least two issues that ORA should address and these are discussed below. We are awaiting further input from GSFC before we address any direct comparison of CODE V and SYNOPSIS results. The main issues considered by ORA were:

1) whether the aspheric equation for the HDOS Sage Lens is correctly specified in HDOS drawing 911-6832-001, particularly with respect to the sign of the terms, and
2) why does the Swales analysis reported on May 12 predict a spherical aberration term of magnitude 1.2197 waves versus a prediction of 1.1245 waves for the Space Telescope with a conic of -1.0135 (ignoring the sign of the coefficient which is addressed in 1) above and concentrating on magnitude.

ISSUE 1

This is the most important issue. Swales, using CODE V, has postulated that the Sage lens is generating the incorrect sign of the spherical aberration. As a first step, we took an independently developed OTA model and verified that we predict the same magnitude and sign for the Zernike spherical aberration for the OTA with a primary mirror conic of -1.0135. We also verified that the signs of the exit pupil radii match during the fit and that the result is independent of whether the calculation is made after an odd or an even number of reflections. As a second step we took the Swales CODE V listing of the Sage lens and verified their analysis of the "concave" configuration, which Swales believes to be the HDOS design. We then looked at the same configuration with a "convex" lens and found we did not duplicate their result. Swales is in the process of providing a prescription for the "convex" lens, but we have not yet received it. We therefore tried changing the sign of the fourth order aspheric coefficient to see what would happen. When we did this, we changed the sign of both terms, and this matched their analysis labeled "convex". We believe that the issue actually is not so much whether the lens is concave or convex, but rather whether the edge is an up or a down-edge. The radius (set based on assuming a base parabola and computing a radius to match the aperture squared term) should be simply the best fit radius for fabrication and not directly relevant to the issue of spherical aberration generation. Thus, we have concentrated on the up- or down-edge issue.

First, we expect the lens to have an up-edge, i.e. more negative lens power at the edge to cause the marginal rays to focus long. The primary mirror is "flatter" than intended and therefore the marginal rays are focusing long. The Sage lens is intended to simulate the OTA aberration (not to correct it). To illustrate these two cases, we plotted the aspheric departures. The data was generated using the FAB;SAG option in CODE V. Reviewing this data, we believe we have identified the problem. It is traceable to the interpretation of the HDOS print for the Sage lens.

In their analysis, Swales assumed the sign of the coefficients shown in the drawing were the signs to be input into CODE V. We believe this is not the case (the HDOS

Print 911-6832-001 was included as page 4 of the Reference 2 fax). The print is dangerously ambiguous regarding the specification of the correct sign of the coefficients to enter into a computer model of the lens. However, we believe that the interpretation that is intended is to assume there is a coordinate system implicit to the print that defines positive sag to be to the right. Then, noting also that the asphere is placed on the R1 surface, to the left on the drawing, the "ASPHERE EQUATION" describes a surface which starts with a positive sag departure, i.e. convex surface, which is then overtaken by the negative term at higher aperture to provide an up-edge. This is the situation shown in our plots and is also equivalent to the "convex" design described by Swales. This means that it is likely that HDOS has manufactured the correct lens. We can see how one could be easily misled by the print.

To complete closure on this postulate, we have recommended that Swales obtain the null lens geometry being used to verify the lens figure. This information should unambiguously demonstrate whether an up- or a down-edge has been manufactured.

ISSUE 2

Relative to the second issue on the matching of the spherical aberration magnitudes; we can duplicate NGSFC's results for the Sage lens (FRINGE No. 9: 0.94 waves), using no defined optical apertures on the surfaces, however, this is not a good practice when doing Zernike fits. The Swales analysis sent in Reference 3 predicts a terms of 1.02 waves for the Sage lens (B&W Zernike Term 13: 1.02 waves); this is obtained by adding a CIR aperture on the Sage lens that sets the f/number precisely to f/24 using real rays. Therefore we believe the discrepancy between the NGSFC analysis and that done by Swales is the exact aperture over which the fit is made. The Swales listing provided to ORA in Reference 3 is not the one which Swales used for analysis so we cannot confirm this, but it seems plausible at this stage. We cannot reproduce the value provide to NGSFC in the Swales letter of May 12 that was sent to us in the Reference 2 fax. The value shown there (SA = 1.22 waves) does not agree with the value predicted in Swales analysis dated 05/16/91 (SA = 1.02 waves) that was delivered to ORA.

Relative to Issue 2 then, we recommend that Swales/HDOS/NGSFC agree on the exact fitting radius before comparisons are made. Also, HDOS, in the Reference 1 telecon, mentioned that this lens was designed very early on and may not have been designed for a primary mirror conic of -1.0135. This issue should be pursued directly with HDOS. The choice of fit aperture and the control of the used area on the Sage lens is critical to the successful use of this lens.

We are awaiting the SYNOPSIS output from GSFC and intend to review it upon receipt.

6.3 COMMENTS ON DATA REDUCTION IN INTERFEROMETRY

When an interferogram is reduced, the raw optical path difference data contains some OPD due to the mirror, and some OPD due to the test setup. A customary procedure used in reducing interferometric data is to rotate the piece under test relative to the test equipment to isolate which errors are in the piece under test and which are in the test equipment. (In the case of the HST interferograms in question, several sets of interferograms were taken with various combinations of (A) fringes rotated into various azimuthal orientations, and (B) test equipment rotated into various azimuthal orientations relative to the primary mirror.) As a part of the data reduction one then fits the data with a Zernike polynomial of relatively low order. This helps define all the asymmetric low order terms likely to be due to the test setup. After this Zernike has been defined, it is subtracted from the raw OPD map to help separate the low order test and mirror surface errors (low spatial frequency components defined by the Zernike) from the higher spatial frequency ripple on the mirror surface.

The Zernike map for each interferogram is processed to remove certain low order terms attributed to the test setup. This modified Zernike map is then recombined with the higher order residual to represent the mirror surface, and averaged with all the other interferograms. There is a question as to which terms in the Zernike map should be removed. Tilt, piston and defocus terms are nearly always removed. Coma terms are almost always removed as well, since the most likely source of coma is in lateral misalignments of the mirror under test and its null corrector. All of these terms have been removed in processing all of the interferograms provided to us for our use in evaluating HST performance.

Interferograms for the primary show a small residual of undercorrected spherical aberration, due in part to edge roll-up at the inner and outer edges of the annular mirror. NOTE THAT THIS RESIDUAL HAS NOTHING TO DO WITH THE CONIC CONSTANT ERROR. It is a residual left over when compared to the conic which best matches the as-built RNC. As such, we feel that it should be accounted for separately, by leaving it in the interferogram data for the primary, not by removing it. However, it has been removed from the PMR1.INT data set; in fact, it has been replaced by a very small overcorrected residual. Presumably this was inadvertent. This can be seen by comparing the ΔKPEQ columns for GDIJK.INT and PMR1.INT in table 5.1, on page 22.

The numbers are quite small. They may in fact be comparable to the error introduced by treating the conic error as a pure third order conic term and ignoring higher order terms in the aspheric equation, and are probably smaller than the effects of g-release. It still seems unwise to us to remove any component from the interferometric data that is not definitely a result of the test setup.

APPENDIX IV
IMAGE METROLOGY
FINAL REPORT

OSAS DFM # 91-68
19 April 1991

Subject: HIORP FINAL REPORT: IMAGE METROLOGY

From: A. B.. Meinel and M. P. Meinel, JPL

SUMMARY

This section of Image Metrology reports the work by A. H. Vaughan, JPL, and A. B. Meinel and M. P. Meinel, JPL. The task was to make measurements on the actual PC images obtained at different D-spaces* and thereby derive a value for the apparent conic constant .

The principle behind this work is that it is possible to identify features of the out-of-focus image, measure them and compare the results with ray traces of what the image should show at these D-spaces.

Measurement by the Meinels used three features: 1) the three pads, 2) the outer rim, and 3) the inner hole (when it could be seen). Measurements by Vaughan are of the positions of the three pads only.

The best values for the apparent conic constant obtained by this method as determined from PC-6 images are:

Vaughan:	**k = - 1.014472**	**- 0.00025 + 0.0004** for WF1
	k = - 1.01469	**± 0.00025** for PC 6
Meinel:	**k = - 1.01429**	**± 0.0002** for PC 6

These values are before correction for the camera contribution to the spherical aberration.

1. Measurement criteria

Three features are available for measurement: 1) the three pads, 2) the outer rim, and 3) the inner hole (when it could be seen). Measurements by Vaughan are of the positions of the three pads, while the Meinels measured all three observables. The entrance pupil geometry of the rim, pads and central obscuration are shown in Fig. 1.

2. Measurements by the Meinels

Measurement of discrete features in the images presents some challenges. The pad position is the best defined of the three features used. It is a diffraction feature appearing in the center of the shadow of the pad. Its is most conspicuous at 0.487 μm, less visible at 0.631 μm and weakly visible or invisible at 0.889 and 0.230 μm. Inasmuch as the center of the image is ill-defined the pad measurement was between sets of pads. The effective radius was then calculated from this set of three measurements.

*OTA focus position

Fig. 2 shows a typical image with the measured positions of features indicated by the dots. All measurement was done on precision prints of images from PC-6, with a few from PC-5, provided by the JPL WF/PC Office.

It is difficult to the locate the "rim" since the intensity at this edge falls smoothly into the background. The intensity level on the prints had been cut at a brightness level that appeared to reject the wing of the image, giving a reasonable depiction of the image diameter. The Meinel measurements located at least two positions for the rim of the image, as illustrated for a typical image in Fig. 2. These points were selected in regions away from the diffraction spikes that result from the support vanes. The consistency of measurements indicates that this was a reliable procedure in spite of the subtleties of the intensity gradient at the rim of the image. With the natural scatter of measurements we could see no significant difference between these two cameras.

Fig. 3 shows each of the measured points at the D-space values indicated by the vertical lines. The lateral spread of points at each D-space is to enable each point to be plotted where the density of points would otherwise prevent accurate assessment of the density of points. There is considerable scatter, especially for the outer rim, as would be expected from the observed fall-off of brightness of a typical image.

The lines in Fig. 3 show the best fit of lines to the scatter of points. Note that at large – D-spaces the aperture rim crosses the optical axis, creating a hole in the image. We have reflected the measured points below the optical axis so that they can be considered when drawing the best fit line. The abscissa of Fig. 3 is in units of HST D-space.

Jitter affects pad location, rim, and center hole positions differently. Jitter still preserves the center of the pad spot. Jitter, however, tends to soften the rim and central hole. This would contribute to the larger scatter of measurements of the rim, shown in Fig. 3.

Fig. 4 is the ray trace trajectories for the outer rim, pad location, and central obscuration based on ray traces provided by D. Schulte. These lines were based on a conic constant of -1.01350 for the HST primary mirror. They ignore the contribution of the PC-6 camera. It was thus recognized that the best fit of the measured point would not fall directly on the lines of Fig. 4 if the apparent conic constant were different from -1.01350. The difference between the Schulte lines and the measured pints, however, enables calculation of a Δk term to be added to -1.01350.

The abscissa of Fig. 4 is in units of Design D-space. The outer rim of the image should be at 5.75 asec diameter at the paraxial focus. This is based on exact ray traces of the OTA plus PC optical train for the above value of k. Note that this differs from the OTA primary image size that would be measured at prime focus and with the same k. This difference is significant in calculating the revised conic constant based on the image measurements.

In earlier reports of our measurements we used only the images from the Small Sweep (+50 to -50 μm D-space) and calculated a revised conic constant from the

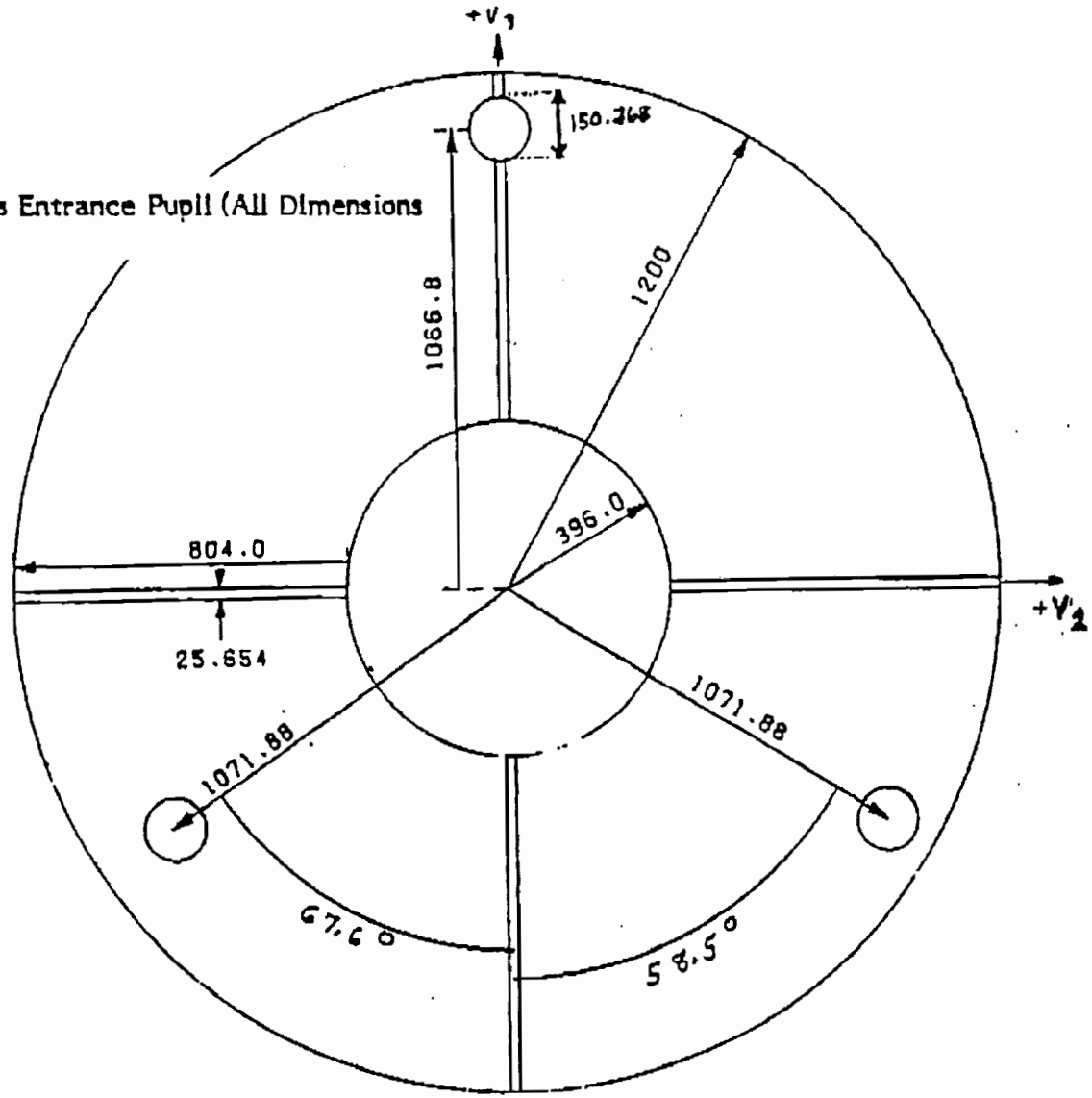

Fig. 1. Measurements of the relevant features used in direct image measurements.

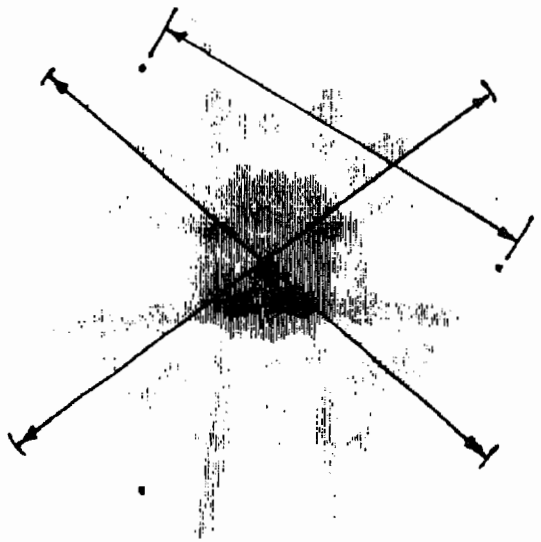

Fig. 2. A typical PC-6 image showing the points defining the center of the diffraction spot and the periphery of the image.

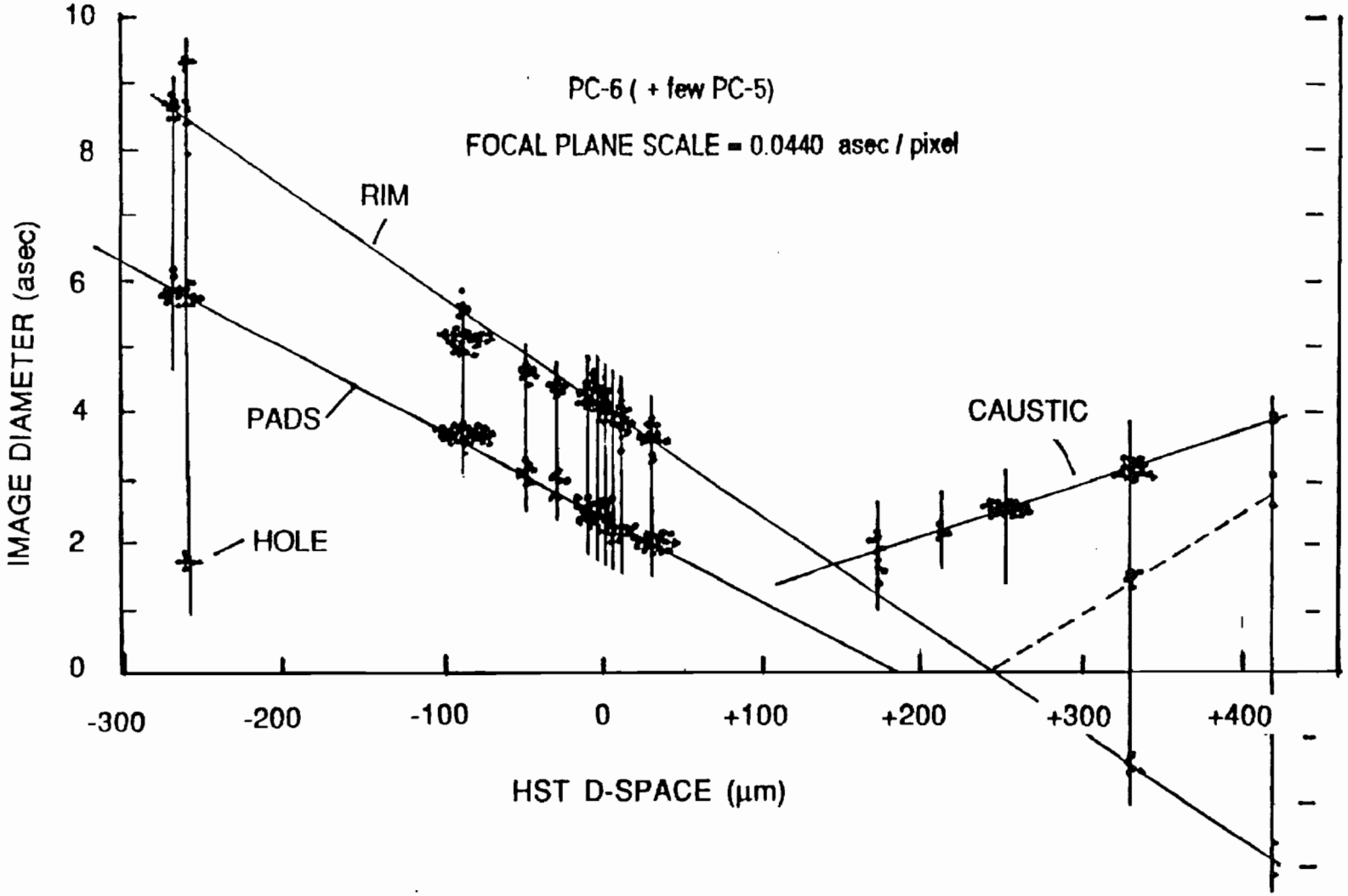

Fig. 3. Measured points for outer rim, pads and inner hole positions from prints of images from PC-6 with a few from PC-5.

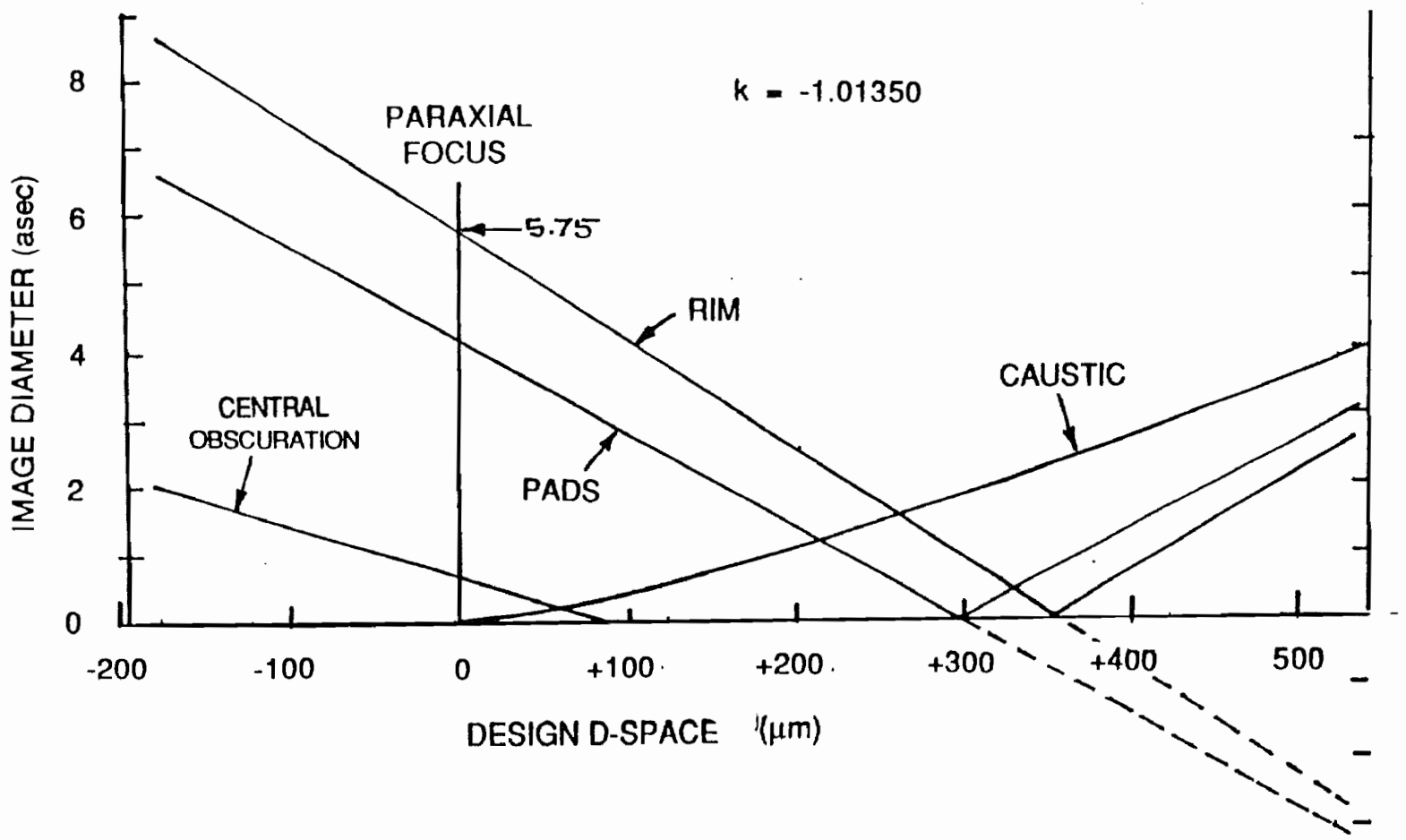

Fig. 4. Ray trace lines for the outer rim, pads, inner hole and caustic for OTA primary k = -1.01350 by Schulte. Cross-overs of rays are shown by dashed lines.

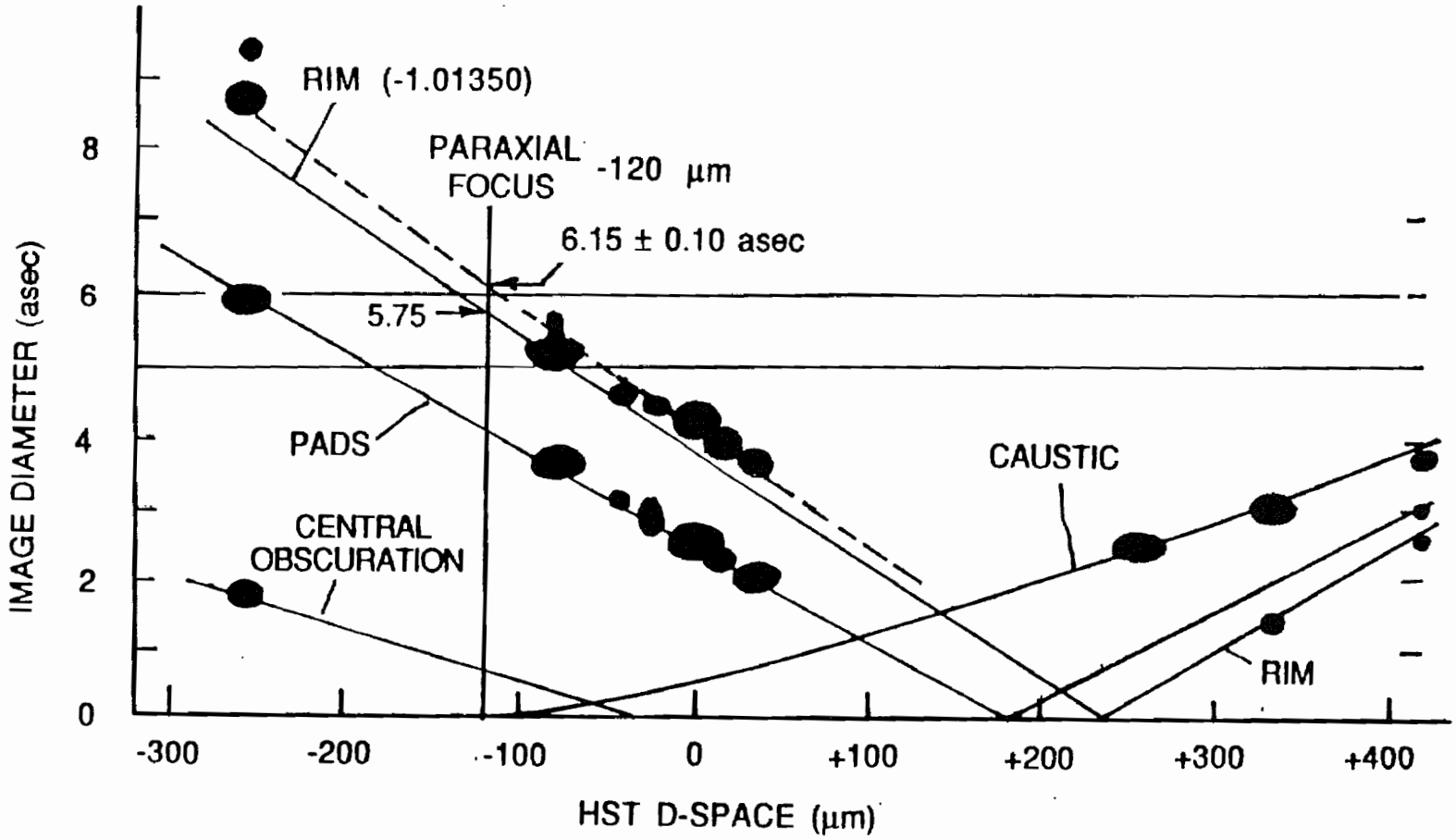

Fig. 5 . Best fit of measured points to Schulte lines defines the paraxial focus as being at -120 µm and the rim image diameter as being 6.15 ± 0.1 asec, which leads to a conic constant of -1.01429 ± 0.0002.

straight line through the outer rim measurements, extrapolated to position of the "paraxial focus." From GSFC data this position was given to us as being -107 μm D-space, along with the plate scale of 0.0430.

We subsequently discovered that the actual PC effective focal length at the center of each CCD was 0.0440. This resulted in an increase in the revised K value.

When we were supplied with a full set of PC imagery from all of the Sweeps we were able to determine the paraxial focus strictly from image measurements. The procedure was to take the measured points (Fig. 3) and shift them along the abscissa until the points ahead of best focus and following best focus were best-fitted to the ray trace lines from Schulte. This "best fit" is shown in Fig. 5. For simplicity the measured points are indicated by elliptical spots.

To determine paraxial focus the key feature we used was optimum placement of the spots for the pads (left side) and caustic (right side). This placement determined paraxial focus to be at -120 μm HST D-space scale.

It can then be seen in Fig. 5 that the rim points lie distinctly above the line for k = -1.01350. The intercept with the vertical line at paraxial focus is at 6.15 asec. This additional amount results in a best value for the *apparent* conic constant for the OTA of

$$\mathbf{k = -1.01429 \pm 0.0002}$$

The uncertainty is set by the range of intercepts with the paraxial focus of a line drawn through the scatter of points. We estimate this intercept uncertainty to be ± 0.10 asec.

Inasmuch as fossil data for PC-6 show that it has contributed to the apparent spherical aberration of the OTA by about 0.0003, the best value we have obtained for the OTA alone is

$$\mathbf{k = -1.0140 \pm 0.0002.}$$

2. Vaughan measurements of pad positions

Inasmuch as differing values for k determined from image measurements of the mounting pad positions have been reported at HIORP meetings during the months of the study it is important to look at the reasons why these values differ and why the final values supersede the earlier ones. This history of determinations of k from pad measurements is given below. The notation is the WF/PC Design File Memorandum number.

DFM 1484, 14 November 1990. A value of **k = -1.013609 ± 0.0005** was reported, based on an estimated HST mirror intervertex spacing reported in DFM 1492 of the same date. Only two images were measured. The uncertainty was estimated as resulting from uncertainties in the intervertex spacing value thus derived.

DFM 1506, 11 December 1990. A value of **k = -1.01352 ± 0.00036** was derived from measurement of 30 images. This result used the same intervertex spacing as above. This result takes into account OTA shrinkage using a value of 0.12 (μm/day derived from analysis of images recorded over a span of 165 days). The stated uncertainty is the standard deviation (S.D.) of an individual measurement computed from internal scatter of the measurements. There is, in addition, an estimated systematic error of ± **0.0005** due to focus uncertainty.

DFM 1542, 30 January 1991. A value of **k = -1.014844 ± 0.0003** (S.D.) was reported from PC 6 images. This result takes into account a re-calibration of the OTA intervertex spacing provided by M. Wilson (communicated by telephone). Vaughan regards this result as systematically uncertain by ≈ ± 0.0005 because of uncertainty in the actual intervertex spacing in the OTA.

DFM 1551, 12 Feb 1991. A value of **k = -1.01509 ± 0.00025** (S.D.) was reported, the correction of -0.000256 being based on calculation of the effect of zones on the OTA primary located in the vicinity of the pads. The estimated systematic uncertainty remained at ± 0.0005, reflecting the uncertainty in the intervertex spacing.

Final value. Values of **k = -1.01469 ± 0.00025 (S.D.)** for PC 6 and **- 1.014472 -0.00025 + 0.0004** for WF1, resulted from a further revision in the intervertex spacing communicated by M. Wilson to H. J. Wood of 20 January 1991. The revised value places the OTA primary and secondary 8 μm closer together than the value assumed in DFM 1542. The difference between the results for PC 6 and WF1 appears to be caused by residual spherical aberration in PC 6.

Vaughan states that an overall systematic uncertainty persists in knowledge of the intervertex spacing of the OTA mirrors. He estimates this uncertainty as ≈ ±0.0005. The internal precision of pad measurements, however, is sufficient to distinguish differences between cameras of the order of ± 0.0002 that arise from differences in residual spherical aberration of the cameras.

3. Discussion of Vaughan and Meinel measurements

The basic difference between the Meinel and Vaughan measurements is that the Vaughan measurements depend upon a value for the intervertex spacing provided by M. Wilson, whereas the Meinel measurements are self-calibrated because measurements were made of the entire caustic, thus enabling a best fit for determining the effective paraxial focus. The agreement of **-1.01429** for the Meinels and the mean value of **-1.01458** for Vaughan is as close as the uncertainties in measurement permit.

4. 4/3 Slope Method

During the course of the HIORP investigation we tried another means for establishing where the rim of the image was located. This method relied on the fact that for pure 3rd order spherical aberration the encircled radial intensity distribution in the near paraxial region is described by a 4/3 power relationship. Measurements of this

quantity did indeed show a 4/3 slope when plotted on log scales. A distinct break from this slope was at first thought to be an indication of the geometrical edge of the image. Diffraction modeling by R. Lyon, however, showed that while such a break was obtained, it was not at the rim of the image. Just why is still not clear. We suspected that it was because of the missing aperture caused by the three pads. When we took this assumption into account and used the radius value of the pad position in calculating a revised conic constant the value was very close to the above value. The uncertainties of this approach, however, are such that we discount its importance in arriving at a best value for the OTA and thus do not present its value.

Captions:

Fig. 1. Measurements of the relevant features used in direct image measurements.

Fig. 2. A typical PC-6 image showing the points defining the center of the diffraction spot and the periphery of the image.

Fig. 3. Measured points for outer rim, pads, and inner hole positions from prints of images from PC-6 with a few from PC-5.

Fig. 4. Ray trace lines for the outer rim, pads, inner hole, and caustic for OTA primary k = -1.01350 by Schulte. Cross-overs of rays are shown by dashed lines.

Fig. 5 . Best fit of measured points to Schulte lines defines the paraxial focus as being at -120 μm and rim image diameter as being 6.15 ± 0.1 asec, which leads to a conic constant of -1.01429 ± 0.0002.

APPENDIX V
PHASE RETRIEVAL
FINAL REPORT

ERIM

Report to the HST Independent Optical Review Panel on Phase Retrieval

J.R. Fienup
Optical & IR Science Laboratory
Environmental Research Institute of Michigan
P.O. Box 134001, Ann Arbor, MI 48113

August 1991

Summary

An adjusted estimate of the spherical aberration of the OTA+PC6 by the accumulated results of several phase-retrieval groups is about −0.295 microns rms of wavefront error, or a conic constant of −1.0152. After subtracting the spherical aberration of PC6, the net estimate of the conic constant of the OTA is approximately −1.0142. The current level of accuracy in a_{11}* is probably beginning to approach the ±0.01 microns rms (conic constant at ±0.00044) level for each of the two mirrors of the OTA, but it cannot be said with confidence that this goal has been achieved. In order to have high confidence in a_{11} at the ±0.01 microns rms level, further sophistication will have to be added to the algorithms, accurate system models will have to be used, further Monte Carlo experiments will have to be performed, and possibly additional data will have to be collected.

1 INTRODUCTION

The term phase retrieval, as applied to the Hubble Space Telescope (HST) problem, comprises several methods of determining the aberrations of the HST from images of stars measured on orbit. Besides the images of stars, which represent estimates of the point-spread function (PSF) of the HST, phase retrieval makes use of knowledge of the optical design parameters of the system, most importantly the shape of the system's aperture

*The Zernike coefficient for 3rd order spherical aberration.

function (pupil) and the plate scale (arcseconds per pixel) at the CCD array detector (where images of the stars are formed). The goal of phase retrieval is to find an aberrated optical wavefront in the aperture plane, which, when digitally propagated to the detector plane, produces a PSF consistent with the measured PSF. Then the phase of that wavefront corresponds to the aberrations of the system that we wish to discover. Knowing those aberrations allows one to design the optics in the replacement instruments, such as the Wide Field/Planetary Camera-2 (WF/PC-2), that will compensate for the aberrations of the HST's Optical Telescope Assembly (OTA) and produce imagery as fine as would have been produced had the telescope been built to specification. In addition, knowledge of the aberrations of the telescope will make possible the accurate alignment of the secondary mirror of the OTA, since certain misalignments cause astigmatism or coma. Furthermore, detailed knowledge of the aberrations will allow one to analytically compute the PSF for all spectral filters, focus settings, cameras, and positions in the field of view. These analytically computed PSF's will enable one to do the best possible job of deblurring the images that are being collected with the present telescope.

2 ALGORITHM TYPES

Although phase retrieval is an immature science with regard to practical experience with real-world applications (except for the field of x-ray crystallography), it is very rich and diverse: dozens of different algorithms have been investigated over the years. In this report there is only space to briefly comment upon two major classes of algorithms that were found to be particularly useful for this application: polynomial fitting and iterative transform algorithms.

For both classes of algorithms, the problem is cast in terms of optimizing a merit function, for example, minimizing the mean squared difference between the measured PSF and a PSF computed from a model of the aberrated system. Several other merit functions, including the difference between the magnitudes (square root of intensity) of the PSF's, maximum likelihood, maximum entropy, and various weighted error metrics can be used as well.

In the polynomial fitting algorithms, the phase errors are expressed in terms of a polynomial expansion, and the coefficients of the polynomials are the parameters that are

optimized to make the computed PSF's match the measured ones. Any of the standard nonlinear optimization routines can be employed to find the polynomial coefficients that minimize the error metric. Examples include Newton-Raphson, Levenberg-Marquardt, conjugate gradient, Davidon Fletcher-Powell, and linear programming, to name a few. Use of an analytic expression for the gradient of an error metric, as opposed to computation by finite differences, speeds the gradient search algorithms several-fold.

The polynomials taken to be the standard, in order to make comparison of results easier, are the Zernike polynomials orthonormal over a 0.330-obscured annular aperture, as listed in the OTA Handbook. The 11th polynomial, $Z_{11}(r)$, is the third-order spherical aberration term (which includes an r^4* term) that was introduced by the incorrect spacing of the null lens during the manufacture of the OTA primary mirror. This is the dominant term, along with the $Z_4(r)$ (focus) term. The coefficient, a_{11}, of the Z_{11} polynomial, when stated in microns, gives the number of microns rms of wavefront error due to spherical aberration (had the wavefront been present over the entire 0.330 obscured annular aperture). This can be related to other system parameters, such as the as-built conic constant of the primary mirror, which is given by $\kappa = -1.0023 + 0.043841\ a_{11}$. Typically up to 11 terms or 22 terms (through fifth-order spherical aberration including an r^6 term) are employed.

In the iterative transform algorithm, one parameterizes the phase error not by polynomial coefficients, but by a point-by-point phase map within the aperture. The aperture might be described by, say, a 256 by 256 array of numbers, allowing for tens of thousands of phase values. Then one digitally, iteratively, propagates a wavefront from the aperture plane to the PSF plane (at the CCD) and back again, imposing the measured data and known constraints in each plane until a wavefront is found that agrees with all the data and constraints in all planes. These algorithms are variations on the Gerchberg-Saxton/Misell/Fienup algorithms. This class of algorithms has the ability of determining the fine structure in the phase that cannot be described by a reasonable number of Zernike polynomials. It was found that for this application it was necessary to first perform a Zernike polynomial fit to the phase, then use that smooth phase, which is near to the true phase, as an initial estimate to the iterative transform algorithm in order to avoid problems with nonphysical local minima.

*The r^4 term describes the SA3 wavefront (W_{040}). The expression for Z11 is (r^4 - 1.108900 r^2 + 0.241243), thus Z11 includes a focus term (r^2) as well as a piston term. The magnitude of the SA3 term is obtained by multiplying the Z11 term value by the normalization factor 16.895979.

For phase retrieval problems in general, there are typically local minima of the merit functions in which the algorithms can become trapped, representing false solutions. There is also the possibility of non-unique solutions, that is, two substantially different sets of aberrations that agree equally well with the data, giving two different global minima. This non-uniqueness is considered to be unlikely, especially if the aberrations are made to fit more than one PSF. Computer simulation studies by R. Lyon (HDOS) have shown that in a sizable area in parameter space about the true global minimum there were no seriously troubling local minima for the cases investigated. Since the approximate location of the global minimum is already thought to be known, problems with local minima are not expected to be severe. Multiple starting points are generally used, and confidence is placed in a solution only if it yields the smallest minima found and if it is arrived at from multiple different starting points.

3 RESULTS TO DATE AND PROBLEMS TO BE OVERCOME

The results to date, across several different research teams using several different phase retrieval algorithms, have been fairly consistent in the prediction of a_{11}. The average solutions for each of the teams has been in the range of about –0.26 to –0.30 microns rms (of wavefront error). This corresponds to conic constants of –1.0137 to –1.01545. This range of solutions extends beyond the desired accuracy of about ±0.01 microns rms. Furthermore, it is possible that all the phase retrieval results could be suffering from the same systematic error that biases the solution (as discussed below). It will be argued later that, by accounting for systematic errors in many of the results, one arrives at a spherical aberration with magnitude near the larger end of the range above.

There is much less agreement about the other Zernike coefficients, which are much smaller (mostly all well below 0.08 microns rms). These other coefficients are also important, however, since they infer the state of alignment of the telescope and can be used to properly align the secondary mirror of the OTA, which is thought to be far out of alignment for long periods of time.

For many months the phase retrieval algorithms were in a constant state of flux, with additional features being added frequently in order to more fully model the physics of the HST and allow for a better fit between the computed PSF's and the measured PSF's. A

list of the features that could be included in the system model are (1) multiple planes of diffraction, (2) reconstructed (as opposed to designed) pupil functions, (3) telescope jitter during the integration time of a specific PSF, (4) the optimization over imperfectly known system parameters, such as plate scale, or at least the use of the latest (field-position-dependent) estimates of these parameters, (5) finite optical bandwidth, (6) geometrical effects not modelled by Fresnel propagation (but that could be modelled by ray tracing), (7) the effects of undersampling by the CCD pixels and integration by CCD pixels over finite areas, (8) statistical model of the noise and bias properties of the detected PSF's, (9) higher-order phase terms beyond 22 Zernike polynomials, (10) knowledge of locations of glitches in the measured data, (11) measured flat fields, (12) accounting for the possibility of aberrations in both the OTA primary and the OTA secondary, (13) knowledge of the ray-trace design aberrations as a function of field position, and (14) accounting for the possibility of non-pointlike stars. Also being included to improve the solution are incorporation of (15) multiple different PSF's simultaneously and (16) the phase maps reduced from the interferograms of the finished OTA primary and secondary mirrors. Also necessary is the subtraction of the spherical aberration estimated to be present in the camera in order to arrive at the spherical aberration of the OTA. With increasing sophistication, the algorithms can require prodigious amounts of computation (hundreds of giga-floating-point operations per reconstruction).

Some teams incorporated certain of the elements mentioned above, but not others. It does not appear that any team has incorporated the entire list; this is a result of both technical problems with combining certain approaches and of time and budgetary constraints. Nevertheless, as long as each element is investigated by at least one team, so that the magnitude of its effect is understood, then each effect can be considered to be understood and taken into account at some level. This author is not aware that a full accounting of all the pertinent elements has been performed.

Photon noise and CCD readout noise can be a limiting factor. However, for the far out-of-focus images it has been shown experimentally and through information-theoretic analysis (Cramer-Rao lower bounds on mean-squared error of the estimate) that photon noise will not cause uncertainties beyond ±0.01 microns rms for the WF/PC. Photon noise is a limiting factor for images taken near the diffraction focus, and for the count-rate-limited faint-object camera (FOC). The far out-of-focus images yield much better results because

underestimated if too small a value of plate scale is used. Therefore it may be that many of the older phase retrieval results using the lower values of plate scale may be underestimating the spherical aberration. This could also explain the fact that phase retrieval results from HARP1B data tended to have greater spherical aberration than results from HARP1A data. Since more of the HARP1B data was taken away from the center of the CCD chip, where the plate scale is smaller, there was probably less underestimation of the plate scale and of the spherical aberration for the HARP1B data than for the HARP1A data.

Considerable work was performed to estimate the probable errors in the phase retrieval estimates. Unfortunately the largest source of error was probably not noise, which could be studied statistically. The largest sources of errors were systematic errors due to imperfectly modelled system parameters and jitter. Lyon showed in simulations that jitter could cause errors as large as ±0.02 microns rms, depending on the focus setting used. As mentioned above, many of the results were obtained with a plate scale now known to be underestimated. M. Shao's group at JPL set the goal of including in their algorithm the optimization over unknown parameters and including the jitter, in which case those sources of uncertainty may have been removed; however, a report of these details was not available at the time of this writing. The error bars are probably beginning to approach the originally desired level of ±0.01 microns rms (conic constant ±0.0044); but this evaluation is based on an engineering guesstimate rather than solid analysis, so we do not have high confidence that the desired level of accuracy has been achieved.

For the most accurate results, ray tracing is required to convert phase retrieval descriptions of Zernike coefficients or phase maps to system parameters that can be used in the redesign of WF/PC II. This is also necessary to account for the field and focus dependence expected in the aberrations. This is referred to as prescription retrieval. It has been under development, but a reliable implementation has not been reviewed by the phase retrieval community by the time of this writing.

At one point it was suggested that the r^4 term in the 22nd Zernike polynomial, $Z_{22}(r)$, (describing fifth-order spherical aberration)* be included in the prescription. It was concluded that this should not be done unless the entire $Z_{22}(r)$ term is corrected.

*The r^6 term describes the SA5 wavefront (W_{060}). The expression for Z22 is (r^6 - 1.66335 r^4 + 0.803136 r^2 - 0.104406), thus Z22 includes a term (r^4) a focus term (r^2) as well as a piston term (constant). Multiplying Z22 by its normalization factor 74.782446 yields SA5.

the dynamic range of the data is much lower, and many times more total photons can be collected without saturating the detectors.

Another limiting factor has been telescope jitter which imparts to the PSF's additional blurring beyond the blurring due to the telescope aberrations. Some progress was made toward deconvolving the jitter prior to phase retrieval and toward including jitter effects in the phase retrieval algorithm.

In order to get high-confidence results, more and better data from the telescope may be required. The properties of the needed data are that there be multiple data sets with a variety of field positions, focus settings, and possibly wavelengths, and that each data set be narrow-band, of wavelength longer than 0.500 microns for the PC, far out of focus, jitter-free, flat-fielded, and well exposed (nearly full well in the CCD). High signal-to-noise-ratio data sets from the FOC may also be necessary to be able to distinguish between aberrations in the primary mirror vs. the secondary mirror of the OTA.

Of the parameters that are uncertain, the pupil function has been of particular concern. Both by the iterative transform algorithm and by measured asymmetries in the PSF's across the field, it has been discovered that the WF/PC does not appear to be accurately aligned with the OTA, resulting in the central obscurations from the two sets of optics not precisely overlapping for PSF's at the center of the CCD chips (although they were designed to be). Since the pupil functions are the primary *a priori* information used to help retrieve the phase, errors in the assumed pupil functions will translate to errors in the phase estimate. For example, C. Burrows (STScI), by assuming different WF/PC central obscuration sizes from 7.4 mm to 8.4 mm, got a_{11} of –0.274 to –0.312 microns, proving the sensitivity of a_{11} estimation to pupil obscuration assumptions. Furthermore, if not accounted for, the pupil-shift error would cause the WF/PC II correction optics to be laterally displaced, resulting in large amounts of residual coma.

Another major parameter of concern is plate scale. Early phase retrieval results assumed a plate scale of 0.043 arcsec per pixel for the PC. Later it was reported to be 0.0436 arcsec per pixel, and later still (after almost all the phase retrieval work was completed), 0.0442 arcsec per pixel for the center of the chip and decreasing to as small as 0.0425 at a corner of the PC chip. It was also observed that spherical aberration was

Only when all the major features of the measured PSF's are explained by the models will there be high confidence that the results are accurate to the ±0.01 microns rms level.

In order to increase confidence in the estimate of the spherical aberration, a model of the aberrated system should be constructed that predicts results that are consistent with the results from all the approaches that use the imagery, including the Hartmann-like tests by A. Vaughan (JPL) and image-extent tests by A. Meinel (JPL) and R. Lyon, as well as the phase retrieval approached described here.

4 SUMMARY OF PHASE RETRIEVAL RESULTS

To make the best use of the results to date from several different groups, one should carefully consider which of the possible features of a complete and accurate system model was used for each individual result and consider the quality of the PSF data used and the quality of the fit of the computed PSF with the measured PSF. Then, if possible, an appropriate adjusting of the answers should be made to compensate for now-known system parameter inaccuracies and model insufficiencies. An appropriate weighting of each result should be made when averaging the results. Unfortunately such an exercise would entail considerable effort. A more practical weighting scheme, considering the current funding situation, is to average together only the results from the phase retrieval algorithms employing the most complete system models and using the results only from a few of the very best PSF's, while still trying to adjust for systematic errors. With only some of those details in hand, a guess as to such a result for the OTA+PC6 would be in the neighborhood of −0.295 microns rms of wavefront error, or a conic constant of −1.0152. This estimate is arrived at by starting with the averaged figure of −0.290 microns rms, compiled from the results of several groups by R. Korechoff (JPL), and then making an adjustment of −0.005 microns rms to approximately account for underestimation of plate scale and the use of only single-plane (as opposed to multiple-plane) diffraction for most of the results. [The results of this author indicate a greater spherical aberration of −0.299 microns rms, or a conic constant of −1.0154.] Subtracting the estimated spherical aberration of PC6, equivalent to a conic constant of about −0.0010, from the weighted average of −1.0152 yields the net estimated conic constant of the OTA primary mirror of −1.0142. In contrast, an averaging of all phase retrieval results would yield a smaller spherical aberration, which would probably underestimate the true spherical aberration.

In summary, there has been much progress, and considerable sophistication has been added to many of the phase retrieval algorithms. An adjusted estimate of the spherical aberration of the OTA+PC6 by the accumulated results of several phase-retrieval groups is about −0.295 microns rms of wavefront error, or a conic constant of −1.0152. After subtracting the spherical aberration of PC6, the net conic constant of the OTA is approximately −1.0142. The current level of accuracy in a_{11} is probably beginning to approach the ±0.01 microns rms (conic constant at ±0.00044) level for each of the two mirrors of the OTA, but it cannot be said with confidence that this goal has been achieved. In order to have high confidence in a_{11} at the ±0.01 microns rms level, further sophistication will have to be added to the algorithms, accurate system models will have to be used, further Monte Carlo experiments will have to be performed, and possibly additional data will have to be collected.

APPENDIX VI
TUTORIAL ON SPHERICAL ABERRATION

Appendix 2: Spherical Aberration

The principle aberration affecting the Hubble Space Telescope (HST) is spherical aberration. In this appendix some of the characteristics of spherical aberration are reviewed.

The capability of an optical system to form a good image of a point object is determined by the shape of the wavefront as it converges to the image point. The wavefront is a surface of uniform optical phase. A spherical wavefront (of which a plane wavefront is a special case) is the ideal condition for achieving the best imaging. This is true whether one considers geometrical or diffraction theory. The principle task of the designer and builder of telescopes is to achieve an ideal spherical wavefront converging to the image surface.

Optical aberrations are the departure of the actual wavefront from the ideal spherical shape. Aberrations may be due to manufacturing error in the optical components or intrinsic limitations of the design itself. For wavefronts which are converging or diverging at a modest rate -- which is true of the HST -- the ideal spherical wavefront and the actual wavefront may be described by $W_{ref}(x,y)$ and $W(x,y)$ and the wavefront aberration by $\Delta W(x,y)$ such that

$$\Delta W(x,y) = W(x,y) - W_{ref}(x,y)$$

where x and y are the transverse coordinates of the converging wavefront. We may display the aberration function, $\Delta W(x,y)$, without consideration of the base sphere upon which it lies. Very often the wavefront aberrations are displayed using normalized transverse coordinates. The magnitude and form of wavefront aberrations is essentially unchanged as a wavefront propagates through an optical system. In contrast, ray aberrations based on the normals to the wavefronts, change scale depending on the divergence or convergence. This makes wavefront aberration especially useful for characterizing a system. One may, to a reasonable approximation, sum the wavefront aberrations of constituent components. For large aberrations, the nature of the aberration is affected by propagation of the light and a simple summation of the constituent wavefront errors will not be strictly accurate.

The term spherical aberration is applied to any aberration which is axially symmetric in the pupil, i.e., of the form,

$$\Delta W(x,y) = W(r^2)$$

where $r^2 = x^2 + y^2$ is the radius of the transverse radius. The term spherical aberration was given in the early days of optical systems because it arose when more easily manufactured spherical surfaces were used in

optical systems instead of surfaces which were the correct mathematical shape. Spherical aberration may be described in a number of forms. The oldest and simplest form is derived from Seidel aberration theory and may be described by the polynomials:

$W_{020} = r^2$	defocus
$W_{040} = r^4$	4th order spherical
$W_{060} = r^6$	6th order spherical
.	
.	
$W_{0N0} = r^N$	Nth order spherical

The defocus term W_{020} is generally not considered a true spherical aberration term because it may be removed by shifting the center of the reference sphere. The higher order spherical aberrations can be mitigated by changing the center of the reference sphere -- refocusing the image plane -- but not completely removed. The nomenclature for Seidel aberrations is of the form W_{KLM} where L describes the radial variation and K and M determine the field and azimuthal dependencies. The advantage of the W_{KLM} description is that it is obvious what order of aberration is described. In the HST, the spherical aberration due to the design of the elements is primarily 4th order spherical. The computer controlled polishing of the primary and secondary mirrors produced some very high order spherical aberration in the form of turned edges and annular rings of phase -- often called zonal aberration. In general these zonal aberrations have not been found to depart significantly from the tolerances allowed for them and will not be the focus of attention here.

2.0. Sign of spherical aberration

The spherical aberration of a single positive lens is considered to be undercorrected. Taking the form given above for the wavefront minus the reference surface, we find that undercorrected spherical aberration should have a positive sign for W_{040}. The spherical aberration of the HST is overcorrected spherical aberration and has minus sign.

2.1. Spherical aberration specification

Aberration may be specified in several forms. The wavefront error may be specified in terms of physical dimensions such a microns or in fractions of a wavelength of some specific spectral components. The HST has a very broad range of wavelengths so specification of aberration by fractional wavelength can cause

confusion. The reason a fractional wavelength form is so often used is that it is magnitude of the aberration in wavelengths of the light which determines the effect of the aberration on the image formed at that wavelength. The form of spherical aberration is the same (apart from scale factors) for a given number of wavelengths of aberration independent of the actual value of the wavelength. The trained observer can identify the nature and magnitude of aberration in terms of fractions of the observational wavelength from inspecting the image distribution. Indeed, astronomers assessing the images of the HST arrived at very accurate values for the magnitude of the spherical aberration, by simple observation of the images.

The manufacturer of optical components may also use spherical aberration terms. In this application, the aberration terms are most often used to specify the surface deformation -- one half the magnitude of the wavefront aberration which is produced. The manufacturer's attention is concentrated on the correction of the surface and, therefore, surface deformation is a much more appropriate form of description. The manufacturer may use a mechanical measurement of the surface, called profilometry in which surface deformation is directly observed. The component may also be tested optically by interferometers -- most commonly using a helium-neon laser operating at .6328 microns. At the time when HST components were tested in the early 1980's most interferometry was done by photographing the wavefront produced by the interferometer and using computer data reduction to determine the surface deformations. Some interferometric configurations are single pass because the test beam of the interferogram hits the surface once; others are double pass because they hit the surface twice. A given surface defect produces twice the error in the wavefront of the interferogram in a double pass configuration than in a single pass configuration. In the data reduction process should resolve the single or double pass issues and take into account the test wavelength to calculate the surface deformations. Using the photographic methods, some care must be exercised to be certain that appropriate correction factors have been made. An additional difficulty of photographic methods is that the interferogram gives the sign but not the magnitude of the aberration. During measurement, the technician determines the sign of the aberrations by perturbing the interferometer and marks the photograph. The sign may also be determined if there is a known characteristic defect in the mirror such as a rolled down edge.

2.3 Conic Constant

Historically, the mirrors generated by axial rotation of conic sections -- parabola, hyperbola, ellipse, or sphere -- played an important role in reflective telescope design. The classical Cassegrain design consisted of a parabolic primary and hyperbolic secondary. The parabolic mirror produced a virtual image free of

spherical aberration and the hyperbolic secondary reimaged the virtual image to form a real image beyond the primary -- also free of spherical aberration. This configuration could be shown mathematically to be free of spherical aberration of all orders. The parabola provides a perfect point image for an infinite object at its focus point and the hyperbola provides a perfect image at one focal point if the object is placed at the other focal point. The classical cassegrain also had the advantage that both the parabolic primary and hyperbolic secondary could be null tested. The primary could be tested in autocollimation with a flat mirror and the hyperbolic secondary could be tested at the proper conjugates with a Hindle sphere test. These null tests could be done without construction of special test optics called null lenses and could be done with a simple test such as a Focault test rather interferometry which has only recently become widely available.

The classical Cassegrain, while free of all orders of spherical, suffers from coma, an off-axis aberration that produces a comet like tail. Asymmetrical aberrations are particularly objectionable in a telescope. A modified Cassegrain called the Ritchey-Chretien (RC), allows correction of fourth order spherical aberration and coma. This is achieved by making the formerly parabolic primary slightly hyperbolic and readjusting the hyperbolic shape of the secondary slightly. For relatively shallow mirrors like those of the HST the higher order spherical is not significant. Higher order spherical aberration terms could be added to the mirrors were the higher order spherical terms important. An exact null test of the primary in autocollimation is no longer possible, but for a large primary mirror such as the 2.4 m HST a flat of sufficient size for autocollimation is not readily available and measurement at the center-of-curvature of the parabola is preferred. The center-of-curvature measurement requires a null test. Null optics can readily be designed to compensate for the aberration of either the exact parabolic shape of the classical parabola or the hyperbolic shape of the RC telescope primary, so there are no significant regrets in testing associated with the use of the RC design. Numerous programs have evaluated different designs for a large variety of applications. The RC design has been by far the most successful.

The conic sections were originally defined mathematically by the eccentricity, ε. The conic constant, $\kappa = -\varepsilon^2$ is much more widely used in optical design and in optical design computer programs. The surface deformation from a sphere takes the form,

$$\Delta S = \frac{cr^2}{1 + (1 - (1+\kappa)c^2r^2)^{1/2}} + a_4r^4 + a_6r^6 + \ldots$$

Table 2.1 Conic constants for different conic surfaces.

parabola	$\kappa = -1$
hyperbola	$\kappa < -1$
ellipse (prolate spheroid)	$-1 < \kappa < 0$
sphere	$\kappa = 0$
oblate spheroid	$0 < \kappa$

Optical design programs augment the conic term with specific higher order coefficients a_4, a_6, etc. The a_4 term is highly correlated with the conic term and description of the surface using both terms is usually ill-advised.

The conic term is not exactly the same as the Seidel term W_{040}. The conic term may be expanded in a power series in the form,

$$\Delta s = \frac{cr^2}{2}\left(1-\left(\frac{(1+\kappa)c^2r^2}{4}\right)+\left(\frac{(1+\kappa)c^2r^2}{4}\right)^2\right)\cdots$$

The series expansion gives the parabolic, fourth, sixth, and higher order terms. With $\kappa = -1$we have only the parabolic term. The ratio of the sixth to the fourth order term is

$$\text{ratio of sixth to fourth order spherical} = \left(\frac{(1+\kappa)c^2r^2}{4}\right) = 6.8\times10^{-6}$$

where the HST primary values of $r = 120$cm, $c = .0009058\text{cm}^{-1}$, and $\kappa = -1.0023$, were used. For the HST specification, the conic constant bears a 1:1 relationship to fourth order spherical aberration to an accuracy well within the tolerances of the system. The above equation gives the relationship between the error in the conic constant and fourth order spherical aberration.

$$W_{040} = \frac{c^3r^4}{8}\Delta\kappa = 192.6\,\Delta\kappa \text{ (microns of surface deformation)}$$

$$= 385.3\,\Delta\kappa \text{ (microns of wavefront aberration)}$$

2.3. Wavefront Variance

The Seidel form of spherical aberration gives a clear description of the magnitude of the aberration. It does not, however, give good information about the effect of the aberration on the image. The wavefront variance σ^2 is defined to be,

$$\sigma^2 = \frac{\iint W(x,y)^2 I(x,y)dxdy}{\iint I(x,y)dxdy} - \left(\frac{\iint W(x,y)I(x,y)dxdy}{\iint I(x,y)dxdy} \right)^2$$

where $I(x,y)$ is the intensity distribution in the pupil.

For small amounts of aberration there is an approximate relationship to the Strehl ratio,

$$\text{Strehl ratio} = e^{-k^2\sigma^2}$$

For small aberration, the wavefront variance gives useful information about the reduction in performance and to a considerable degree the degradation is the same for any type of aberration having the same wavefront variance independent of the form of the aberration. For large aberration, such as with the HST, the Strehl ratio is not a good measure of performance. Perhaps more importantly the value of the wavefront variance for a given amount of spherical aberration depends upon the exact pupil function including the obscuration of the Hubble secondary and struts and the obscuration and struts of a camera used to evaluate the image such as the wide-field camera. To compound the problem the exact pupil irradiance function varies with field position so that the wavefront variance will vary somewhat even though the wavefront aberration is held exactly fixed.

The reason wavefront variance is so widely used in discussing the HST may be that interferogram reduction software use Zernike polynomials to characterize the aberration. Zernike polynomials are orthogonal over a unit circle and are theoretically complete if all terms are used. Unfortunately various forms of the Zernike polynomials are in use. The classical form is normalized to unit wavefront value at the edge of the pupil. More recently polynomial sets using wavefront variance normalization have been in common use. In addition there are differences in the ordering of the terms. For example, clover aberration with a cubic dependency on the azimuthal angle, may or may not be included. The Zernike terms are generally referred to by their number in the particular sequence used, so it is necessary to have a listing of the exact polynomials to understand what a given coefficient means. Fourth and sixth order spherical are commonly defined as Z11 and Z22. The classical Zernike polynomials are not orthogonal over the HST pupil because of the central

obscuration and struts so this advantage is lost for the HST application. The form of polynomials used to evaluate the HST primary are

$$\sigma = 16.895979\, Z_{11}\,(r^4 - 1.108900r^2 + .241243)$$

$$\sigma = 74.782446\, Z_{22}(r^6 - 1.663350r^4 + 0.803136r^2 - 0.104406)$$

as given by the OTA Handbook Version 1.0. These polynomials have been normalized for a .33 obscuration. The obscuration of the pupil of the telescope cameras is different for each camera and the effect of the struts must be included.

Because of the complications of associating the exit pupil obscurations with the wavefront variance value, it is much more convenient to have the telescope error described either as W_{040} or the conic constant, with higher order spherical terms as required.

2.4. Sampling required to resolve the spherical aberrations

Computer modeling of the images and phase retrieval methods require an accurate modeling of the spherical aberration. Fourth order aberrations is relatively slowly varying in the pupil, but the complex amplitude for such a large amount of aberration is rapidly varying.

$$\text{complex amplitude } a(x,y) = e^{j\frac{2\pi}{\lambda}W(x,y)}$$

The sampling rules apply to the complex amplitude which is much more rapidly varying for large magnitude of aberration than the aberration polynomial.

The sampling requirement for the spherical aberration may be determined from the local spatial frequency of the wavefront,

$$\text{local phase in cycles} = \theta = \frac{1}{\lambda}W_{040}\frac{r^4}{r_n^4}$$

where r_n is the normalizing radius. The local spatial frequency is

$$\text{local spatial frequency} = f = \frac{d\theta}{dr} = \frac{4}{\lambda}W_{040}\frac{r^3}{r_n^4}$$

The maximum spatial frequency is

$$\text{maximum spatial frequency} = \frac{4}{\lambda} W_{040} \frac{1}{r_n} \approx 5\text{cm}^{-1}$$

Nyquist sampling requires a minimum of two sample points per cycle leading to a sample point at least every 2.5 centimeters of aperture. A minimum of 100 sample points across the aperture are required. In general, it is best to sample two to three times the Nyquist rate, leading to 200 to 300 sample points across the aperture. An array size of 256 × 256 will barely meet the Nyquist requirement. A better choice is 512 × 512. Shorter wavelengths lead to higher aberration in terms of wavefront error and require higher sampling densities. The 512 × 512 should be used at the shorter wavelengths -- above about 0.5 microns.

The choice of observation plane can add or subtract defocus from the image and increase or decrease the sampling requirements. The approximate rules given above apply to the paraxial focal point. Working at the plane giving minimum wavefront variance will reduce the spatial frequency by a factor of 2. Observations with the HST have been made over approximately 1 mm of secondary mirror translation leading to a large range of defocus values.

Figures 2.1 and 2.2 show the far-field pattern for 6.5 waves of spherical aberration, in an F/24 beam. A 512 × 512 array was used with sample points every 2 cm. The very generous guardband allows good resolution of detail in the far-field. Figure 2.3 illustrates schematically the calculation of through-focus intensity scans of the image. Figure 2.4 shows a section 3.2 cm long and .048 cm wide of transverse scans at different focus positions. One can see the high degree of structure in the image.

Geometrical theory identifies several properties of the spherically aberrated image. Fourth order aberration forms a very characteristic structure called the caustic. Figure 5 illustrates some of the properties of the caustic. Taking the paraxial focus as a reference, Table 2.2 gives the position of several geometrical properties of the caustic

Table 2.2. Geometrical properties of the spherical aberration caustic. Distance from paraxial focus in terms of W_{040} and the f-number, based on F/24, $\lambda = .5 \times 10^{-4}$ cm, $W_{040} = 6.5\lambda$.

End of outer caustic	$48 W_{040} F_n^2$,	≈ 9cm
Marginal ray axial intercept	$16 W_{040} F_n^2$,	≈ 3cm
Minimum blur circle	$12 W_{040} F_n^2$,	≈ 2.25cm
Minimum rms ray error	$\frac{32}{3} W_{040} F_n^2$,	≈ 2.0cm
Minimum wavefront variance	$8 W_{040} F_n^2$,	≈ 1.5cm

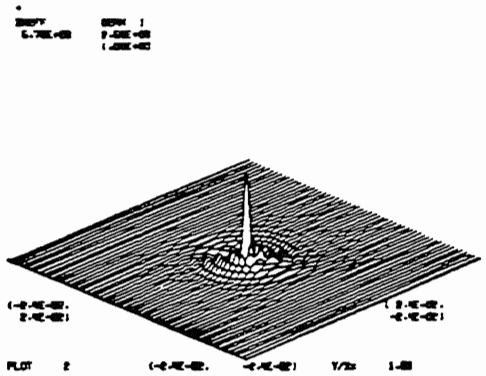

Fig. 2.1. Isometric of intensity at paraxial image.

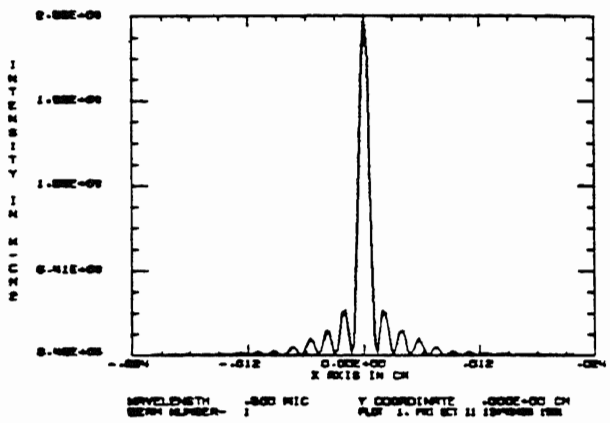

Fig. 2.2. Single slice through paraxial image.

For a near-diffraction limited wavefront, the plane of minimum wavefront variance might be a logical choice. For approximately 6.5 waves of spherical aberration, there may be a considerable divergence of opinion about the optimum focus position.

2.5. Comparison of spherical aberration with other aberrations

Fourth order spherical aberration is not the only aberration present in the HST. The images show small amounts of coma and astigmatism and, particularly at short wavelengths, the effects of high order zonal spherical. Coma and astigmatism may be either field-dependent or field-independent. The usual Seidel form of coma and astigmatism is field-dependent. Field-dependent astigmatism is a basic property of the RC

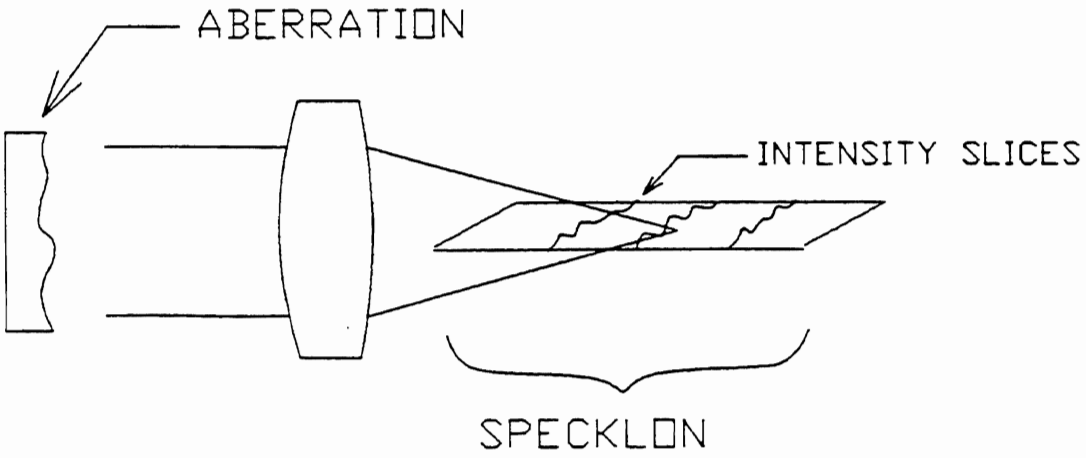

Fig. 2.3. Configuration for examining a series of transverse scans of the image.

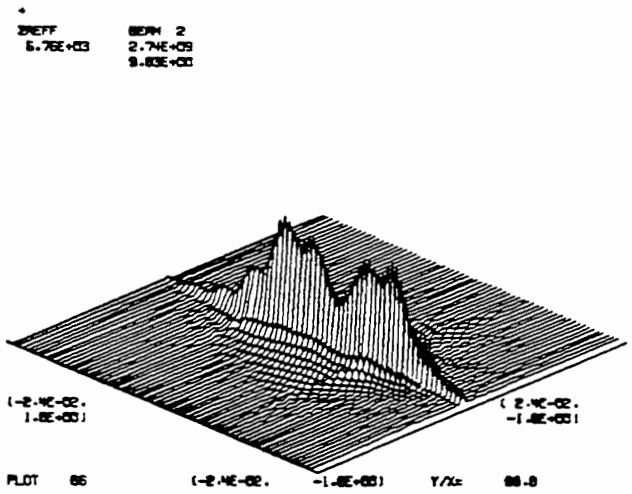

Fig. 2.4. Through focus scans of the image with 6.5 waves of overcorrected aberration and a .41 central obscuration of the pupil.

telescope design. In principle, there should be no field-dependent coma if the RC is properly corrected. If the spherical aberration were not on the primary, as indicated by the problems identified with the null lens used in primary mirror testing, but instead on the secondary mirror, some field-dependent coma would be produced. The relatively small field-of-view of the cameras on the HST make observation of the field-dependent coma somewhat difficult. The fine guidance sensors (FGS's) were expected to provide the most

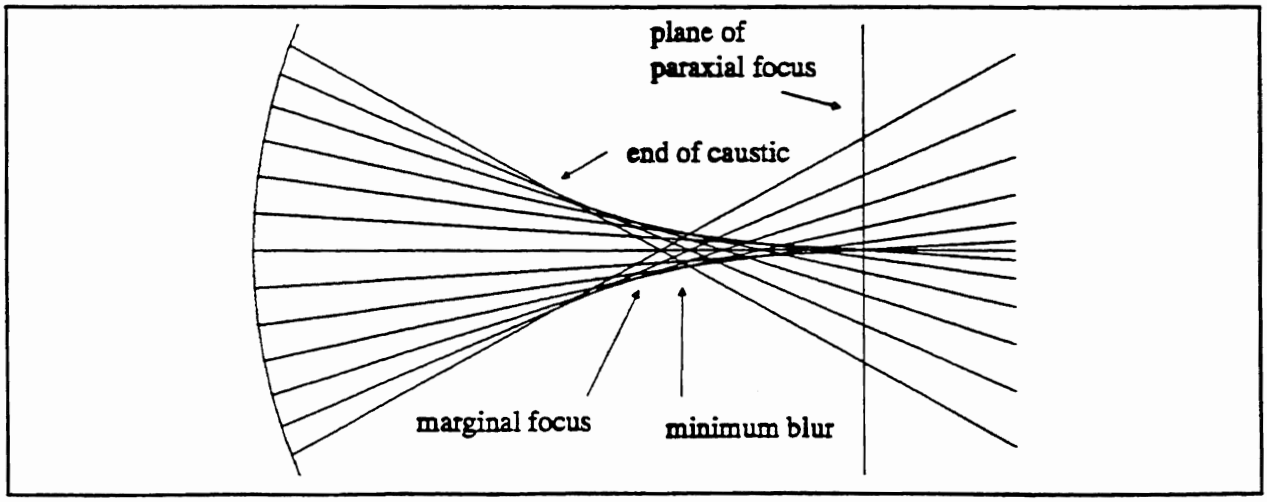

Fig. 2.5. Caustic based on geometrical optics showing critical points. The diffraction calculation shown in Fig. 2.4 indicated a much greater level of detail than exists in the geometrical picture.

accurate measurement of field-dependent coma. No clear evidence of field-dependent coma has been observed by either the cameras or FGS's to date.

The primary source of field-independent coma and astigmatism is misalignment of the secondary mirror. By tilting and decentering the secondary using the positioning actuators provided for this purpose, the field-independent aberrations may be removed. Consequently these aberrations are not considered defects of the HST.

Effects which are generally negligible may become important in the presence of such a large amount of spherical aberration. Normally there is no appreciable aberration if the pupil of a camera is slightly sheared (shifted transverse to the axis). In the presence of approximately 6.5 waves of spherical aberration, a relative pupil shear will transform some of the spherical into coma. This may cause the various instruments to have different amounts of field-independent coma.

2.7 Considerations of the secondary mirror

As mentioned above, the spherical aberration determined from on-orbit observations, could be due to the HST primary or secondary. The historical evidence provides compelling evidence in favor of the spherical aberration being on the primary mirror and no conflicting evidence of field-dependent coma has been observed. Even if one assumed, in spite of the evidence, that all the spherical aberration were on the secondary instead of the primary, the limited field-of-view of the HST cameras would not be especially sensitive to the field-dependent coma.

The secondary mirror is known to have a fine zonal spherical aberration. This magnitude of this aberration appears to be consistent with the tolerances on wavefront variance. However, these fine zones do contribute a ring-like structure to the very short wavelength images. Since the fine zones are of high spatial frequency, the ring structure in the image is well outside the central core of the image and is, therefore, readily visible. For small surface deformations, the energy diffracted is inversely related to the square of the wavelength. A visual judgment of the short wavelength images may lead to the conclusion that the zonal structure is of greater consequence than is actually the case.

It should be noted that the movement of the secondary mirror to correct partially compensate for the spherical aberration introduces a slight amount of spherical aberration because of the shift in conjugates of the secondary mirror.

APPENDIX VII

FINAL TEST REPORT ON

BACKUP SECONDARY MIRROR

Grant No. NAG8-863

Final Technical Report

Hubble Space Telescope Secondary Mirror Vertex Radius/Conic Constant Test

Robert Parks
Optical Sciences Center
University of Arizona
Tucson, Arizona 85721

Prepared for:

George C. Marshall Space Flight Center
Marshall Space Flight Center, AL 35812

March 15, 1991

Hubble Space Telescope Secondary Mirror Vertex Radius/Conic Constant Test
(Backup Secondary S/N 003)

Executive Summary

The Hubble Space Telescope (HST) backup secondary mirror was tested at the University of Arizona Optical Sciences Center (OSC) Large Optical Shop on December 28-29, 1990 to determine the vertex radius and conic constant. The tests were performed according to procedures submitted to and approved by MSFC and other interested NASA centers. Three completely independent tests (to the same procedure) were performed. Similar measurements in the three tests were highly consistent. The values obtained for the vertex radius and conic constant were the nominal design values within the error bars associated with the tests. Visual examination of the interferometric data did not show any measurable zonal figure error in the secondary mirror.

Introduction and Background

Although all evidence to date indicates that the imaging error in the HST is due to the incorrect conic constant on the primary mirror, it seemed prudent to perform a test on the backup HST secondary mirror to see if it was figured to the correct radius and conic constant. Because the backup secondary mirror was polished and tested concurrently with the flight secondary by the same personnel, there is good reason to believe the global characteristics (vertex radius and conic constant) of the backup mirror are within fabrication tolerances of being the same. On the other hand, because every optic is an individual work of a highly skilled craftsman, there is no reason to believe that the fine scale surface structure on the two mirrors is the same.

As a result of these considerations, it was proposed to test the backup secondary to see if the vertex radius and conic constant were the nominal design values. The test most easily performed was the traditional Hindle test using a large, fast sphere to autoreflect the test beam back to an interferometer. Although this test was easy to perform using existing test equipment at OSC, it had 2 regrets; only 85% of the on-axis aperture of the secondary could be viewed, and the long optical path required for this test meant that the interferometric data would be "noisy" due to atmospheric turbulence and vibration. These regrets are minor within the objectives of the test to determine the radius and conic constant.

The test actually performed by Perkin Elmer (now Hughes-Danbury Optical Systems) at the time of the manufacture of the secondaries was a better test than the one now being reported on in the sense that the full clear aperture of the mirror could be seen, and the unequal optical path was very short so there was little noise due to turbulence and vibration. The test performed at Optical Sciences had the advantage, however, that it was done with different test equipment and in a fundamentally different manner than the original test and thus provided a completely independent check on the original test.

In the following sections of this report, we will go over the details of the tests and the test data. We begin by describing where the test was performed and by whom it was witnessed. This is followed by a description of the principles of the test. Then the raw data from the 3 individual tests is given. An analysis is made of the systematic and statistical errors in the data and then the values are given for the vertex radius and conic constant. This is followed by an analysis of the interferometric figure error data for third order spherical aberration.

Details of the HST Secondary Mirror Tests

Comments on the test environment

The tests were conducted in the Large Optics Shop at the Optical Sciences Center, University of Arizona in Tucson. The room is about 10 × 40 meters with an 8-meter ceiling height. The room is below ground and has a laminar air flow system. These circumstances makes the room exceptionally free of vibration and the temperature is generally constant to half a degree fahrenheit over days at a time.

Overall test layout

All the test hardware was assembled on a 4 × 20 foot Newport table with the exception of the 60-in. Hindle sphere and the 6-in. fold flat (a list of test equipment used appears in Appendix A). The Newport table, Hindle sphere and fold flat stand were all grounded (not floating) to the shop floor so there would be no relative movement between parts of the test set up. A schematic layout of the test set up is shown in Fig. 1.

Temporal sequence of the tests and calibrations

The actual test was run 3 times "for real," plus once prior to this to be sure of alignment of all components and to find out if there were any hidden surprises. Then a partial test at the end was run, with the secondary rotated 90° in its cell, to see if there were any errors attributable to mounting distortion of the secondary. In the first and the subsequent "for real" tests, every piece of test equipment was

moved from its position in the previous test and repositioned following the written procedures. The measuring rods used to set up the test conjugate positions were calibrated both before the tests were run and again after doing the 3 tests. The interferometer/diverger pairs and the Hindle sphere were each calibrated just once following the tests of the secondary. The calibration data in these tests was consistent with similar data taken for other previous tests in the shop.

Witnesses to the testing

The following individuals witnessed some or all of the testing reported on here. All witnessed at least one of the "for real" tests. Only Amanda Harris, Richard Sumner, and Lian Zhen Shao witnessed the interferometric test data taking in order to minimize the disturbance to the test environment.

Tom Dubos	HDOS	Henry Garrett	JPL
Howard Hall	HDOS	Lian-Zhen Shao	TORC
Amanda Harris	MSFC	Richard Sumner	OSC
Danny Johnston	MSFC	George Lawrence	OSC
Edward Motts	JPL	Robert Parks	OSC

Explanation of the principles of the test

The vertex radius and conic constant of a perfect hyperbolic secondary mirror can be calculated from the object and image conjugates as shown in Fig. 2. A perfect hyperboloid will perfectly image an on-axis object at the short conjugate into the focal plane of the long conjugate. Knowing the long and short conjugate distances from the secondary vertex allows one to calculate the vertex radius and conic constant exactly, assuming a perfect hyperbolic figure.

In general, the figure will not be perfect so we adopted the following strategy. A distance equal to the design value of the sum of the long and short conjugates was established. The secondary mirror was inserted between the two conjugates near its nominally correct position. The secondary was then adjusted along the axis defined by the conjugates until it autoreflected to the previously set long conjugate.

At this point the vertex radius and a provisional conic constant were calculated as shown below. Error bars associated with the measurements of the conjugates were also applied to the values of the radius and conic constant. Any residual third order spherical aberration found in the interferometric test data could then be added to (or subtracted from) the provisional conic constant to give the apparent conic constant. The actual test procedure followed in the tests is given in Appendix B.

Conjugate test data

Because a distance equal to the sum of the long and short conjugates was established prior to inserting the secondary mirror, this number (6687.847 mm) is constant for all three tests and has an associated error (0.628 mm) as derived in the error analysis in Appendix C. Once the secondary mirror was inserted in the test and moved axially to obtain the best visual focus at the long conjugate, a value of the short conjugate distance was obtained for each of the 3 tests. These values were:

	Short conjugate distance
Test #1	611.059 mm
Test #2	611.033 mm
Test #3	611.059 mm
Average Value	611.050 mm $\pm$ 0.015 mm

with the scatter in measured data much less than the systematic error estimated in the error analysis in Appendix C.

Using the derivation for vertex radius and conic constant given in Appendix C along with the estimated errors of the conjugate measurements, we find:

	Measured	Design
Vertex radius	1358.726 $\pm$ 0.257 mm	1358.0 mm
Conic constant	-1.49718 $\pm$ 0.00012	-1.49686

Interferometric data analysis

In this section we discuss the analysis of the interferometric data taken of the secondary mirror. This data was taken with two purposes in mind. First, if there was residual spherical aberration in the figure of the secondary, this could be scaled and added to the conic constant derived from the conjugate data. Second, if there was a significant amount of astigmatism in the test results, it might indicate that the secondary mirror was being distorted in its cell and thus the measurements of the conjugates might be affected by the distortion. We will treat each of these cases separately.

Test error sources

In trying to determine if there was any residual spherical aberration in the secondary mirror to the level of 0.01λ rms, it was necessary to be sure there was no residual spherical in any of the test optics. This made it necessary to calibrate the interferometer with each of the divergers used during the tests as well as calibrating the Hindle sphere. These wavefront errors then had to be subtracted out of the Hindle test data before making a determination of residual spherical in the secondary.

Because the errors we were looking for were quite small and the interferometric data somewhat noisy because of the long optical path of the test, we only did the analysis on the third order spherical aberration (or the 8th Zernike coefficient). For the mounting error part of the analysis, we used just the 2 Zernike astigmatism coefficients, c_4 and c_5. In all cases referred to here, we are using the full aperture Zernike coefficients (ones that do not take into account the central obscuration) because the raw data was reduced by drawing fringes right through the central obstruction.

Method of calibration — interferometer/diverger

The method of calibrating the interferometer and diverger is outlined at the beginning of the Procedure and data sheet contained in Appendix D. This calibration must be done for each of the 2 divergers used in the tests. The actual Hindle test was done with an f/15 diverger because the f/number of the long conjugate is very slow, about f/25. The Hindle sphere however is reasonably fast and was tested using an f/2.5 diverger.

Once the calibration is complete, average values for the residual astigmatism and spherical aberration Zernike coefficients of the interferometer/diverger are obtained. These errors are units of waves of surface error expressed as Zernike coefficients. Since about 25 interferograms are made during the calibration, the average values of the coefficients have associated variances that indicate the noise in the measurement.

Method of calibrating the Hindle sphere

The Hindle sphere is calibrated by making a series of interferograms of the surface error in the sphere. The residual errors in the fast interferometer/diverger are then subtracted, leaving just the errors in the Hindle sphere. Again, averaging of the interferograms gives variances for an indication of noise in the test.

Correcting the Hindle test data

A series of about 10 interferograms were taken during each of the 3 Hindle tests. The surface error Zernike coefficients of these groups of interferograms were averaged and saved in 3 separate files. First the errors in the slow interferometer/diverger and then the errors (astigmatism and spherical aberration) in the Hindle sphere were subtracted from each set of data separately to yield the error just in the Hindle test alone, that is, in the secondary. These values were then divided by 2, because the secondary surface errors affect the wavefront twice. The final value gives the secondary mirror surface error expressed in terms of Zernike coefficients.

Outline of data treatment

The procedure described above was applied to the data for each of the 3 tests as shown on the data sheets in Appendix E. To give a feel for the operation in a more concise form, we provide a line by line outline similar to a tax form.

1. Hindle sphere surface error data
2. Fast interferometer/diverger data expressed as surface error
3. Line 1) minus line 2) - Pure Hindle sphere surface error
4. Hindle test data expressed as surface error (WF divided by 2). Slow interferometer/diverger data expressed as surface error
6. Line 4) minus line 5) - Pure Hindle test surface error
7. Line 6) minus line 3) - Pure secondary mirror wavefront error
8. Line 7) divided by 2 - Secondary mirror surface error

Results of the tests

The data from the three Hindle tests were averaged to find the magnitude of the astigmatism and spherical aberration in the secondary mirror. The third-order spherical aberration amounted to 0.028λ peak-to-valley $\pm 0.026\lambda$ or 0.009λ rms at $\lambda = 0.633\ \mu m$. This can also be expressed as a change in the conic constant of $\Delta K = -0.008 \pm 0.008$. This would make the measured value of the conic constant using the conjugate plus interferometric data to be $K = -1.505 \pm 0.008$.

We feel the spherical aberration results are realistic because of the consistency with the astigmatism results. If the values of the astigmatism coefficients for the 3 tests are averaged, we find $c_4 = 0.018 \pm 0.079$ and $c_5 = 0.042 \pm 0.084$ or there was astigmatism with a magnitude of $0.092 \pm$

0.230λ peak-to-valley with an orientation of 23.2° above the x-axis. This is the residual astigmatism in the secondary mirror after subtracting about 4 times this much astigmatism due to the Hindle sphere.

As a check on the procedure, the secondary was rotated 90° clockwise in its cell (when viewed from the mirrored surface side) and another set of interferograms were taken. When this data was reduced, the residual astigmatism in the secondary was 0.092 ± 0.252λ peak-to-valley oriented at 57.3° above the x-axis. The magnitudes of the error agree identically (as they should if the Hindle sphere astigmatism error was being subtracted correctly and the cell was not influencing the secondary mirror shape). The angle also agrees within 10° of what it should when the left-to-right image flip is taken into account when the mirror is rotated the 90°. Given the noisy nature of the data, the consistency is remarkable and gives one confidence in the data-reduction method.

Alternative method of treating the interferometric data

If one is more interested in analyzing the results of the interferometric testing in a manner that matches the drawing specification for the secondary mirror, then we can approach the data in the following way. Since the errors in the secondary mirror and the test optics are considered in an rms or lump-sum sense, we will add (or subtract) the errors quadratically and in all cases, add the variances quadratically.

The actual data are dealt with in Appendix F. Our approach was to add quadratically the interferometer calibration errors to those of the Hindle sphere and Hindle test data. We then subtracted (quadratically) the Hindle sphere from the Hindle test data for each of the 3 tests. When these data were averaged and divided by 2 to account for the double-pass nature of the Hindle test, we find our original figures for R_v and K, i.e., 1358.714 mm and -1.49716 with a residual rms surface error on the secondary of 0.043 ± 0.14λ at 633 nm.

This value of rms surface error is consistent with the astigmatism and spherical aberration values found above and is typical of the magnitude of error obtained when testing large optics over air paths of 10s of meters. This is not to say the error could not be reduced by more care and more data. Recall, hoever, that the test originally done by Perkin-Elmer was the test designed to give the least error due to the environment. Also, we do not know the definite pedigree of the back up mirror to the flight version.

Conclusion

The backup secondary mirror was tested using the traditional Hindle test and found to match the nominal design within the errors of the test. The mean value of the test data showed overcorrection by a ΔK of -0.008 ± 0.008.

The test did not turn up any surprises and leads on to conclude that the original test was correctly performed within the originally established error budget. Although this retest gave a mean value of K indicating a small overcorrection, the error bars associated with this test and the lack of a good pedigree with the flight mirror indicate that fossil data for the flight mirror should be the primary source of data used in any attempt to correct the errors in the HST.

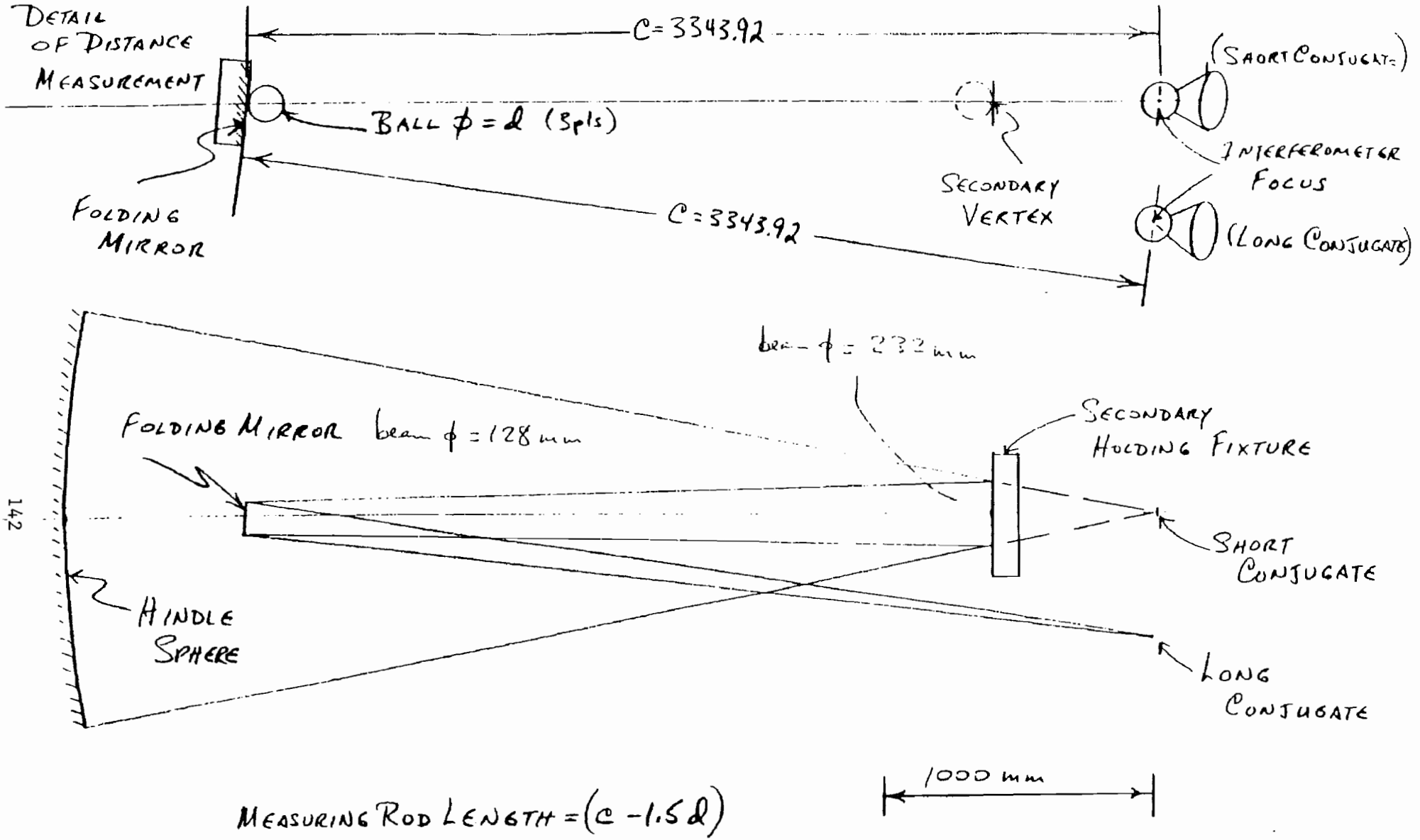

Fig. 1. Schematic layout of Hindle secondary mirror test.

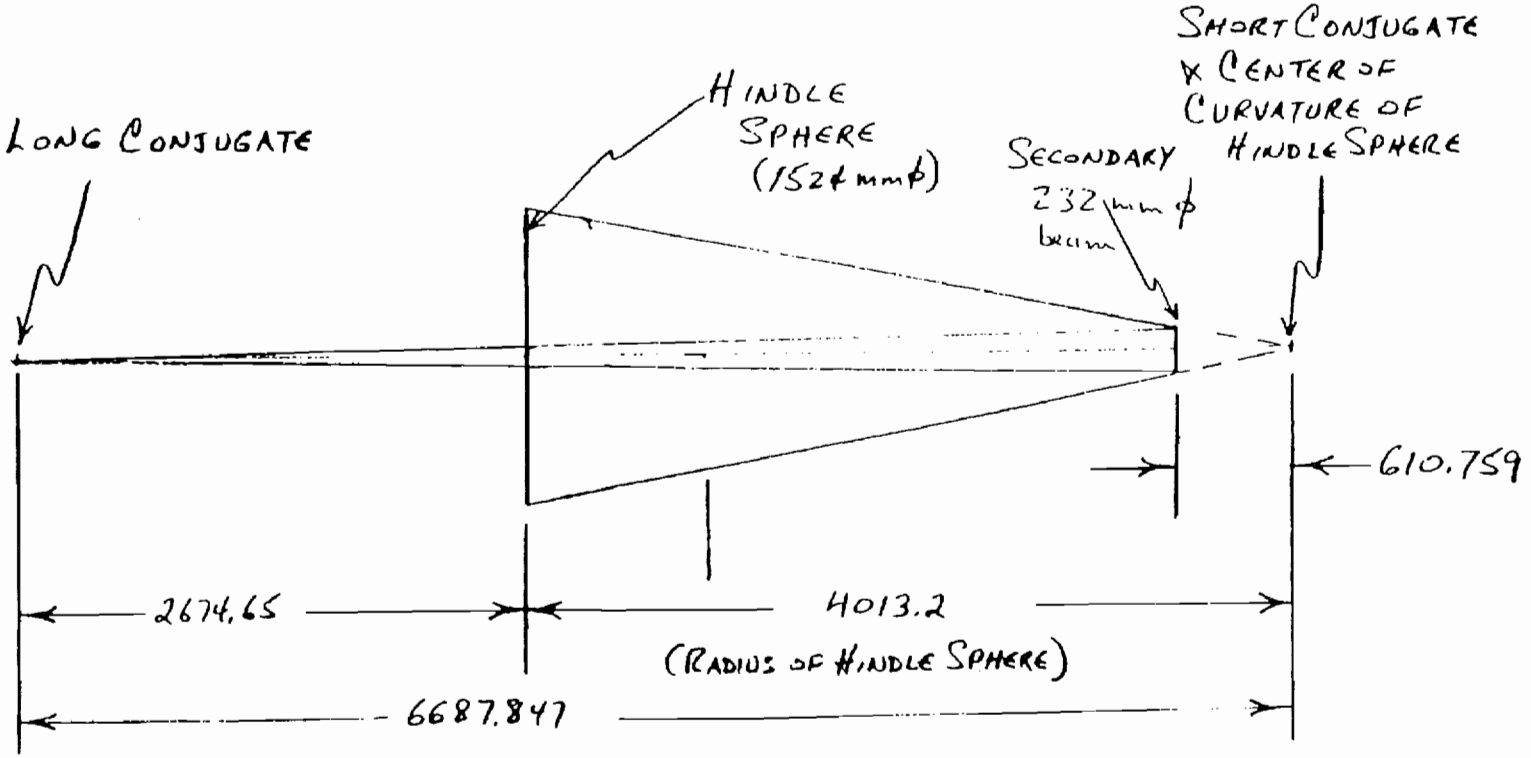

SHORT CONJUGATE, $s = 610.759$

LONG CONJUGATE, $s' = 6077.088$

$s + s' = 6687.847$

$$R_s = 2\frac{ss'}{s-s'}$$

$$K = -\left(\frac{s+s'}{s-s'}\right)^2$$

Fig. 2. Parameters of HST secondary mirror Hindle test.

Appendix A

Equipment List

Steel balls, 0.5" diameter, class 25

Dummy secondary mirror made of aluminum

Point source microscope and light source (made up of Ealing and EG&G components)

Phase measuring interferometer and objectives (built at Optical Sciences)

2 - x-y-z positioning stages, not used for measuring

2 - x-y positioning stages, not used for measuring

1 - x motion stage only, not used for measuring

Mirror mount, 6" diameter with tilt adjustments

Set of measuring rods, custom made and calibrated

Pair of 72" vernier calipers, calibrated 12/90

Inside micrometer, Starrett with 26" capacity

Plano mirror, coated and certified to $\lambda/10$

2 - Stands to support measuring rods

Stand to hold 6" mirror and mount

Large mirror mount to hold secondary mirror and cell (3 translation and 2 tilt adjustments)

Cell and cover for secondary mirror

Large Newport optical table to support interferometer and secondary mirror

Hindle sphere and mount, 60" diameter $\times$ 158" radius

Appendix B

Procedure for Measuring the Vertex Radius and Conic Constant of the Backup HST Secondary Mirror

Note: Refer to the Figure for details of the test setup.

Procedure:

1. Place a point source microscope at the center of curvature of the Hindle sphere. Adjust microscope for best focus.

2. Without touching the microscope, move a 0.50" diameter steel ball in front of the microscope such that the center of the ball is coincident with the focus of the microscope.

3. Position the folding mirror longitudinally. The folding mirror is a 6" diameter flat certified to $\lambda/10$ and has a 0.50" diameter steel ball cemented to its center. Using the calibrated measuring rod of length 3324.86 mm (130.900"), move the folding mirror up to the measuring rod. This will place the surface of the mirror at 3343.92 mm from center of curvature of the Hindle sphere. (In performing this step, first bring one end of the rod up to the ball at the center of curvature of the Hindle sphere. Use a piece of thin shim stock to determine position of rod relative to the ball. Then bring the ball on the fold mirror up to other end of the rod, again using shim stock.)

4. Locate another 0.50" diameter steel ball at roughly the same height as the ball at the center of curvature of the Hindle sphere and about 400 mm to the side of it. Use the 3324.86 mm measuring rod to determine the longitudinal spacing of this ball. Use the same method as in step 3) to position this ball.

5. Adjust an interferometer with a nominally 300 mm focal length diverger that has already been calibrated per the appropriate procedure so that the focus of the diverger is coincident with the center of the ball located in step 4). The axis of the interferometer should be pointing at the center of the fold mirror. (The interferometer will now be focused at the long conjugate of the Hindle test.)

6. Offset the steel ball at the interferometer focus so the interferometer diverging beam illuminates the fold mirror.

7. Insert the secondary mirror/cell assembly into the large mirror holder that is located about 600 mm from the short test conjugate (the conjugate at the center of curvature of the Hindle sphere). Handle the mirror using the overhead crane to move the assembly from its special storage box to the mirror holder. When the mirror is in place and before removing the lifting strap, secure the mirror assembly with 2 bolts.

7a. Remove the Lexan protective cover from the secondary mirror.

8. Adjust the tilt of the secondary until the autoreflected light beam is centered on the interferometer diverger and there is an indication of fringes.

9. Continue to adjust the focus, decenter and tilt of the secondary until the fringe pattern is largely free of coma, focus and tilt. Ideally alignment would be continued until the fringes were nominally straight and about 10 fringes filled the monitor screen.

10. Record and store 5 interferograms of the Hindle test wavefront in a file named _____.

11. Position a 0.50" steel ball at the vertex of the secondary mirror. Center the ball laterally by eye. Adjust longitudinally by using a piece of shim stock to determine the proximity of the ball to the vertex.

12. Without touching the ball, move the mirror assembly back away from the ball about 2".

13. Replace the protective Lexan cover on the mirror being careful not to touch the ball.

14. Attach the crane strap and remove the 2 securing bolts holding the secondary mirror assembly.

15. Use the crane to remove the mirror assembly and replace it in its storage box. Secure the lid on the box.

16. Using a pair of inside micrometers, measure the distance between the ball at the vertex of the secondary and the ball at the short conjugate. Use shim stock to determine the fit of the micrometers.

17. Verify with the point source microscope that the ball at the short conjugate has not moved.

18. Check the inside micrometer reading with the calibrated calipers. Remember to add in half the diameter of the ball (12.7 mm) to get the short conjugate distance. Record s as _____ mm.

19. As an intermediate step, calculate $R = 2(ss')/(s' - s)$ and $k = -((s + s')/(s' - s))2$.

20. In the computer, average the 5 interferograms of the Hindle test and store in a file named _____.

21. Subtract the Hindle sphere wavefront from the data in the file above and store in a file named _____.

22. Subtract the interferometer/diverger calibration wavefront from the data in the above file and store in a file named _____.

23. Using the residual first order (3 term fit) focus term, correct the R value found in step 19) and record $R' =$ _____.

24. Using the residual 3rd order spherical aberration coefficient from the above file, correct the value of k found in step 19) and record as k′ = _____.

25. Repeat the above procedure 2 more times to gather a complete data package for the test of the secondary mirror.

Appendix C

Error Budget for HST Secondary Testing

The errors associated with each step of the procedure are first determined. Then these total errors are associated with the parameters used to determine the secondary vertex radius and conic constant.

1. Place microscope at center of curvature of Hindle sphere.
   - Use a 10× microscope objective.
   - Actual cone angle limited by secondary mount to f/5
   - Depth of focus is $\lambda(f/\#)^2$ or 12.5 μm for λ = 0.5 μm (white light source)
   - Error for step 1) is plus or minus 12.5 μm
2. Position center of ball at microscope focus
   - Use same 10x microscope objective.
   - Cone now governed by NA of objective at 0.2
   - Depth of focus is $\lambda/(2(NA)^2)$ = 6.3 μm
   - Error for step 2) is plus or minus 6.3 μm
   - Total error in location of ball at short conjugate is $\pm$19 μm
3. Position fold mirror at 3343.92 mm from HS C of C
   - Calibration uncertainty for calipers = 25 μm
   - Reading error in each rod measurement = 25 μm
   - Uncompensated thermal error of 0.5° C = 18 μm
   - Positioning of fold mirror to rod = 12 μm
   - Error due to cement layer under ball = 12 μm
   - Total error in positioning mirror = 160 μm

4. Position a ball at 3343.92 mm from fold mirror

   - Same errors as in step 3) are present
   - Total error in this step = 160 μm

5. Adjust interferometer to ball set in step 4)

   - Assuming we can see 0.1 λ p-v error in focus with interferometer or delta sag of 0.03 μm
   - Interferometer objective f/# is 15
   - Detectable delta R is then 54 μm
   - (Error due to 1/10th fringe power in fold flat, i. e., an effective radius of 112,500 m, in the location of the long conjugate = 200 μm)
   - Total error in determining long conjugate position is $\pm$ 574 μm

6. Adjust the secondary mirror axially for "zero" focus error at interferometer, i. e., to less than 0.1λ p-v wavefront error in focus.

   - The shift in secondary position to produce a 0.1λ focus error is 3 μm

7. Position ball at vertex of secondary mirror

   - Error in positioning ball due to "touch" = 12 μm
   - Error in knowing height of vertex due to flat at vertex is 12 μm

8. Measure short conjugate distance with inside micrometer

   - Error in setting of micrometers due to "touch" = 12 μm

9. Calibration error of inside micrometer = 25 μm determined in cross check with calibrated calipers

   - Total error in location of secondary vertex = 64 μm

Application of errors in conjugate location to the determination of the vertex radius and conic constant of the secondary.

1. Total error in short conjugate ball location = 19 μm

2. Total error in secondary vertex location = 64 μm

3. Total error in long conjugate ball location = 574 μm so total error in short conjugate distance is 83 μm and 638 μm for the long conjugate distance.

Now from first order theory it is easy to show that

$$R = 2\frac{(ss')}{(s'-s)} \quad ,$$

where R = secondary mirror vertex radius;

s = the short conjugate distance; and

s' = the long conjugate distance.

Also we have

$$\kappa = -\left[\frac{s'+s}{s'-s}\right]^2 \quad .$$

Taking derivatives

$$\frac{\partial R}{\partial s} = 2\frac{s^2}{(s'-s)^2} = 2.47$$

$$\frac{\partial R}{\partial s'} = -2\frac{s^2}{(s'-s)^2} = -0.025$$

$$\frac{\partial \kappa}{\partial s} = -4\frac{s'(s'+s)}{(s'-s)^3} = -0.001/\text{mm}$$

$$\frac{\partial \kappa}{\partial s'} = 4\frac{s(s'+s)}{(s'-s)^3} = 0.0001/\text{mm}$$

The errors in the 2 conjugate measurements were

$$\Delta s' = 0.628 \text{ mm} \quad \text{and} \quad \Delta s = 0.104 \text{ mm}.$$

Thus the combined error in R is

$$\Delta R = \pm\sqrt{\left[\frac{\partial R}{\partial s}\right]^2(\Delta s)^2 + \left[\frac{\partial R}{\partial s'}\right]^2(\Delta s')^2}$$

$$= \pm\sqrt{(2.47)^2(0.104)^2 + (-0.025)^2(0.628)^2} \quad ;$$

$$= \pm 0.257\text{mm}$$

and the combined error in k is

$$\Delta\kappa = \pm\sqrt{\left[\frac{\partial \kappa}{\partial s}\right]^2(\Delta s)^2 + \left[\frac{\partial \kappa}{\partial s'}\right]^2(\Delta s')^2}$$

$$= \pm\sqrt{(-0.001)^2(0.104)^2 + (-0.0001)^2(0.628)^2} \quad .$$

$$= \pm 0.00012$$

Appendix D

Procedure for Calibrating the Interferometer/Diverger

Note: This procedure must be repeated for each diverger used (or each different f/# cone over which the same diverger is used). If divergers are changed, they do not have to be recalibrated if they are reinserted in the interferometer in the same azimuthal orientation as when they were calibrated and if they are used at the same f/# as when they were calibrated.

Principle of the calibration technique: A nominally spherical steel ball is placed so that its center is coincident with the focus of the diverger. It is assumed that both the figure of the ball and the residual error of the interferometer/diverger are small (less than $\lambda/4$) over the f/# cone of interest. Numerous interferograms are made as the ball is rotated about its center, the assumption being that the figure of the ball at each different position is uncorrelated with that at any other position.

Since the figure error due to the interferometer/diverger is common to all interferograms, when the interferograms are averaged, the result will be the signature of the interferometer/diverger plus a noise term equal to the average figure of the ball divided by the square root of the number of measurements. If the ball has an average error of less than $\lambda/4$, then there will be less than $\lambda/20$ noise in the calibration for 25 interferograms.

Procedure:

1. Insert the appropriate diverger in the interferometer for the test to be performed.

2. Rotate the diverger to a zero fiducial to locate the azimuthal position and finger tighten the lock screw.

3. After obtaining fringes off of the object under test (or a dummy object that defines the appropriate f/# cone for the test to be performed), set an aperture coincident with the edge of the object on the computer display.

4. Insert a steel ball concentric with the diverger focus. The ball should be supported in a mount such that it is easily and repeatably rotated. A hex socket wrench socket makes a good support.

5. Using either the interferometer or the ball mount, adjust tip, tilt and focus until the fringes are broken out to less than one.

6. Using the PMI option, take 25 interferograms of the ball, each in a different rotational position. Discard any data sets where the data is bad and keep taking data until there are 25 good sets. Readjust the fringes to less than one if any rotation misaligns the relative position of the ball and interferometer. Rotate the ball using something that will not contaminate the surface, a clean tissue would be good for this.

7. Average the data sets and store the average (under an appropriate file name) as the residual error for the interferometer/diverger pair at the f/# of the calibration.

8. Review the data to insure that all the interferograms going into the average were less than $\lambda/4$. This insures that the individual ball figure measurements are less than $\lambda/4$ and thus the noise will be less than $\lambda/20$.

9. Remove the ball from the diverger focus.

This completes the interferometer/diverger calibration.

Procedure for Calibrating the Figure of the Hindle Sphere

Note: This procedure need only be done once at the outset of testing as long as the sphere is not moved or readjusted in any way.

Procedure:

1. Calibrate the interferometer/diverger following the procedure for doing so.

2. Align the interferometer/diverger to the sphere using only adjustments on the interferometer.

3. Adjust the interferometer imaging focus so the CCD camera is conjugate to the Hindle sphere surface. Do this by placing an object near the sphere surface and adjusting the interferometer imaging lens until a sharp shadow is seen on the display.

4. Set the circular aperture on the display monitor to be coincident with the edge of the Hindle sphere.

5. Identify the top and left hand side of the sphere and record the locates as they appear on the monitor

6. Using the FAST option, capture and reduce 5 interferograms.

7. Average the 5 interferograms and store in a file labeled _____.

8. Subtract the interferometer calibration wavefront from the file just saved. Store the pure Hindle sphere wavefront in a file labeled _____.

This completes the calibration of the Hindle sphere.

Appendix E

Interferometric Data Reduction Work Sheet (First "Real" Test)

1. Hindle sphere surface error data (HSCAVE)

   C_4 -0.165 ± 0.052 C_5 0.123 ± 0.049 C_8 0.088 ± 0.009

2. Fast interferometer/diverger data (HGCAVE)

   C_4 -0.002 ± 0.038 C_5 0.030 ± 0.040 C_8 -0.010 ± 0.008

3. Line 1) minus line 2)

   C_4 -0.163 ± 0.090 C_5 0.093 ± 0.089 C_8 0.0098 ± 0.017

4. Hindle test data expressed as surface error (HTBCAVE)

   C_4 -0.192 ± 0.057 C_5 0.122 ± 0.066 C_8 0.106 ± 0.006

5. Slow interferometer/diverger data (HFCAVE)

   C_4 -0.012 ± 0.017 C_5 -0.012 ± 0.011 C_8 -0.008 ± 0.005

6. Line 4) minus line 5) - Pure Hindle test surface error

   C_4 -0.180 ± 0.074 C_5 0.134 ± 0.077 C_8 0.114 ± 0.011

7. Line 6) minus line 3) - Pure secondary wavefront error

   C_4 -0.017 ± 0.164 C_5 0.041 ± 0.166 C_8 0.016 ± 0.028

8. Line 7) divided by 2 - Secondary mirror surface error

   C_4 -0.008 ± 0.082 C_5 0.021 ± 0.083 C_8 0.008 ± 0.014

Interferometric Data Reduction Work Sheet (Second Real Test)

1. Hindle sphere surface error data (HSCAVE)

   C_4 -0.165 ± 0.052 C_5 0.123 ± 0.049 C_8 0.088 ± 0.009

2. Fast interferometer/diverger data (HGCAVE)

   C_4 -0.002 ± 0.038 C_5 0.030 ± 0.040 C_8 -0.010 ± 0.008

3. Line 1) minus line 2)

   C_4 -0.163 ± 0.090 C_5 0.093 ± 0.089 C_8 0.0098 ± 0.017

4. Hindle test data expressed as surface error (HTCCAVE)

   C_4 -0.215 ± 0.039 C_5 0.219 ± 0.056 C_8 0.0131 ± 0.020

5. Slow interferometer/diverger data (HFCAVE)

   C_4 -0.012 ± 0.017 C_5 -0.012 ± 0.011 C_8 -0.008 ± 0.005

6. Line 4) minus line 5) - Pure Hindle test surface error

   C_4 -0.203 ± 0.056 C_5 0.231 ± 0.067 C_8 0.139 ± 0.025

7. Line 6) minus line 3) - Pure secondary wavefront error

   C_4 -0.040 ± 0.146 C_5 0.138 ± 0.156 C_8 0.041 ± 0.042

8. Line 7) divided by 2 - Secondary mirror surface error

   C_4 -0.020 ± 0.073 C_5 0.069 ± 0.078 C_8 0.021 ± 0.021

Interferometric Data Reduction Work Sheet (Third Real Test)

1. Hindle sphere surface error data (HSCAVE)

   C_4 -0.165 ± 0.052 C_5 0.123 ± 0.049 C_8 0.088 ± 0.009

2. Fast interferometer/diverger data (HGCAVE)

   C_4 -0.002 ± 0.038 C_5 0.030 ± 0.040 C_8 -0.010 ± 0.008

3. Line 1) minus line 2)

   C_4 -0.163 ± 0.090 C_5 0.093 ± 0.089 C_8 0.0098 ± 0.017

4. Hindle test data expressed as surface error (HTDCAVE)

   C_4 -0.227 ± 0.054 C_5 0.154 ± 0.084 C_8 0.144 ± 0.012

5. Slow interferometer/diverger data (HFCAVE)

   C_4 -0.012 ± 0.017 C_5 -0.012 ± 0.011 C_8 -0.008 ± 0.005

6. Line 4) minus line 5) - Pure Hindle test surface error

   C_4 -0.215 ± 0.071 C_5 0.166 ± 0.095 C_8 0.152 ± 0.017

7. Line 6) minus line 3) - Pure secondary wavefront error

   C_4 -0.052 ± 0.161 C_5 0.073 ± 0.184 C_8 0.054 ± 0.034

8. Line 7) divided by 2 - Secondary mirror surface error

   C_4 -0.026 ± 0.081 C_5 0.037 ± 0.092 C_8 0.027 ± 0.017

Interferometric Data Reduction Work Sheet (Secondary Rotated 90°)

1. Hindle sphere surface error data (HSCAVE)

C_4	-0.165 ± 0.052	C_5	0.123 ± 0.049	C_8	0.088 ± 0.009

2. Fast interferometer/diverger data (HGCAVE)

C_4	-0.002 ± 0.038	C_5	0.030 ± 0.040	C_8	-0.010 ± 0.008

3. Line 1) minus line 2)

C_4	-0.163 ± 0.090	C_5	0.093 ± 0.089	C_8	0.0098 ± 0.017

4. Hindle test data expressed as surface error (HTECAVE)

C_4	-0.253 ± 0.046	C_5	0.130 ± 0.060	C_8	0.152 ± 0.028

5. Slow interferometer/diverger data (HFCAVE)

C_4	-0.012 ± 0.017	C_5	-0.012 ± 0.011	C_8	-0.008 ± 0.005

6. Line 4) minus line 5) - Pure Hindle test surface error

C_4	-0.241 ± 0.107	C_5	0.142 ± 0.071	C_8	0.160 ± 0.033

7. Line 6) minus line 3) - Pure secondary wavefront error

C_4	-0.078 ± 0.197	C_5	0.049 ± 0.160	C_8	0.062 ± 0.050

8. Line 7) divided by 2 - Secondary mirror surface error

C_4	-0.039 ± 0.098	C_5	0.025 ± 0.080	C_8	0.031 ± 0.025

Appendix F

Analysis of Interferometric Data Using rms Residual Errors

Rms error values are surface errors at $\lambda = 633$ nm after removal of tilt, focus, and coma and apply to the full circular aperture.

Hindle sphere rms surface error: 0.0998 ± 0.0189

Interferometer/fast diverger calibration error: 0.0290 ± 0.100

rss Hindle sphere error: 0.1039 ± 0.0214

Hindle test rms surface error (for each of the 3 test series)

HTBCAVE: 0.1165 ± 0.0092
HTCCAVE: 0.1472 ± 0.0156
HTDCAVE: 0.1430 ± 0.0280

Interferometer/slow diverger calibration error: 0.0110 ± 0.0048

rss Hindle test data:

HTBCAVE: 0.1170 ± 0.0104
HTCCAVE: 0.1476 ± 0.0163
HTDCAVE: 0.1434 ± 0.0284

rss Hindle test less Hindle sphere:

HTBCAVE: 0.0538 ± 0238
HTCCAVE: 0.1048 ± 0.0269
HTDCAVE: 0.0988 ± 0.0356

above divided by 2 to give rms secondary surface error

HTDCAVE: 0.0269 ± 0.0119
HTCCAVE: 0.0524 ± 0.0135
HTDCAVE: 0.0494 ± 0.0178

Average rms secondary surface error = $0.043 \pm 0.014\lambda$

DATE DUE
MAR 1 1 2006
MAY 1 3 2006

QC 385.2 .D47 F56 1991

Hubble Independent Optical Review Panel

Final report

NASA Headquarters Library
300 E St. SW Rm. 1J20
Washington, DC 20546

NASA HEADQUARTERS
3 1780 00046 9849